CHARACTERIZATION OF THE HYDROGEOLOGY AND SOLUTE TRANSPORT IN A GEOLOGICALLY COMPLEX, FRACTURED, LATE-CRETACEOUS SHALE, FORT À LA CORNE KIMBERLITE FIELD, SASKATCHEWAN, CANADA

A Thesis

Submitted to the College of Graduate Studies and Research

In Partial Fulfillment of the Requirements

For the Degree of Master of Science

In the Department of Geological Sciences

University of Saskatchewan

Saskatoon, Canada

By

Erin E. Schmeling

PERMISSION TO USE

In presenting this thesis in partial fulfillment of the requirements for a Postgraduate degree from the University of Saskatchewan, I agree that the Libraries of this University may make it freely available for inspection. I further agree that the permission for copying of this thesis in any manner, in whole or in part, for scholarly purposes may be granted by the professor or professors who supervised my thesis work or, in their absence, by the Head of the Department or the Dean of the College in which my thesis work was done. It is understood that any copying or publication or use of this thesis or parts thereof for financial gain shall not be allowed without my written permission. It is also understood that due recognition shall be given to me and the University of Saskatchewan in any scholarly use which may be made of any material in my thesis.

Requests for permission to copy or to make other use of material in this thesis in whole or part should be addressed to:

Head of the Department of Geological Sciences,

University of Saskatchewan

114 Science Place

Saskatoon, Saskatchewan S7N 5E2

Canada

ABSTRACT

Secondary structures (e.g., fractures, sand lenses, kimberlite intrusions) can compromise the ability of clay-rich bedrock aquitards to protect underlying aquifers from near-surface contamination. To date, the effects of secondary structures on water migration and solute transport in these deposits have been poorly characterized. This study characterized the water migration and solute transport mechanisms at both a geologically simple and a geologically complex late-Cretaceous shale aquitard, with the field sites located 5 km apart in central Saskatchewan, Canada. The geotechnical properties and hydrogeologic properties of the complex aquitard were altered by kimberlite volcanism and subsequent hydrothermal alteration during its deposition (99 to 112 Ma BP). High-resolution, 1-D vertical profiles of conservative δ^2H and Cl were collected from both sites (203 and 353 m deep, respectively) to define the vertical solute transport mechanisms. The shape of the 1-D tracer profiles and associated solute transport modeling from the geologically simple site suggest diffusion is the dominant transport mechanism through the entire thickness of the Lower Colorado shale aquitard (330 to 246 m above sea level, asl). Similarly, profiles through the complex, fractured, Cretaceous shale and associated modeling suggest diffusion is the dominant transport mechanism through the entire profile despite the presence of fractures; however, hydrothermal alteration during cooling of the kimberlite volcaniclastic material reduce the effective porosity (n_e) of the kimberlite material from 40% to 1-5%. Results also suggest that, despite kimberlite emplacement in the study area, water migration and solute transport in the overlying and underlying Cretaceous shale may be unaffected by kimberlite volcanism and associated fracturing and alteration.

ACKNOWLEDGEMENTS

I would like to thank my supervisor, Dr. M. Jim Hendry, for his guidance, wisdom, support, and, most importantly, patience, without which I would not have had the ability or desire to finish this degree.

I would also like to thank the remainder of my committee, Dr. S. Lee Barbour and Dr. Len Wassenaar, for their excellent teaching abilities, which helped me immensely.

I thank the fellow graduate students and technical support personnel (Virginia Chostner, Laura Smith, Fina Nelson, Keely Kulpa) who helped me along the way.

I thank Ethan Richardson, Chad Wilkinson, and Terry Burkholder of Shore Gold Inc., who provided guidance and support for the project and assisted in my field work.

I would like to thank Shore Gold Inc. and the Natural Sciences and Engineering Research Council (NSERC) of Canada for financial support.

I am grateful for my husband, my family, and my friends for their patience while I persevered through this degree.

TABLE OF CONTENTS

LIST OF TABLES

LIST OF FIGURES

CHAPTER 1. INTRODUCTION

1.1. Overview

Non-fractured clay-rich bedrock shale aquitards are important because they are effective barriers to fluid flow, thereby enabling the containment of waste in near surface environments and protection of underlying groundwater resources from contamination. Clay-rich aquitards are being considered as potential host rocks for geological disposal of radioactive waste as well as cap rocks for CO_2 sequestration, which requires that solute transport and groundwater flow processes be characterized over great distances (Croisé et al., 2004; Benson and Cole, 2008; Koroleva et al., 2011; Mazurek et al., 2011). In the development of fractured shale gas reservoirs, the degree of natural fracture development in an otherwise low-permeability environment is a controlling factor in gas production (Bowker, 2006; Curtis, 2002). The development of mines in complex aquitard settings also relies heavily on an understanding of groundwater movement for the design of dewatering systems (Booth and Spande, 1992; Rubio and Lorea, 1993) and the control of inflows to underground workings (Johnson and Wright, 2003; Wu and Wang, 2006). Clay-rich bedrock aquitards generally have low hydraulic conductivity (K; 10^{-8} to 10^{-14} m s^{-1}; Gautschi, 2001; Hart et al., 2006; Neuzil, 1986, 1994). Limited research has been conducted on the influence of secondary structures (e.g., fractures, sand layers, sand streaks) on solute transport and groundwater flow in more geologically complex aquitard systems (e.g., Hendry et al., 2004).

The hydrogeologic complexity of aquitards is often difficult to assess. In cases in which there is little or no evidence of hydraulically active fractures in recovered core, K must be inferred from laboratory testing or from an interpretation of field observations of hydraulic responses (Hendry et al., 2004). The presence of secondary structures (e.g., fractures, faults, sand layers, seams) can increase the bulk K of an aquitard by one to three orders of magnitude (Eaton and Bradbury, 2003; Hart et al., 2006; Hendry et al., 2004; Keller et al., 1986). The role of fractures on water migration and solute transport through clay-rich media, such as glacial tills and bedrock shales, has been studied to a limited extent (Eaton et al., 2007; Hart et al., 2006; Keller et al., 1986; Mazurek et al., 2011; Neuzil, 1993; Neuzil and Belitz, 1996; Vargas and Ortega-Guerrero, 2004). Some have concluded that the fracture systems are active and, as a result, influence the groundwater flow within adjacent aquifers (Capuano, 1993; Eaton and Bradbury, 2003; Hart et al., 2006; Mazurek et al., 1998; Williams and Paillet, 2002). In contrast,

other studies suggest that fractures are not hydraulically active (Gautschi, 2001; Mazurek et al., 2011).

Groundwater flow in most indurated bedrock shales is limited and occurs mainly in secondary structures such as faults and fractures, if at all (Mazurek et al., 1998). In a study of the hydraulic properties of the Opalinus clay at Mont Terri, Croisé et al. (2004) observed no significant variations in K among the different facies and no apparent enhancement of K in the vicinity of tectonic features. Diffusion is also the dominant transport mechanism through the shale at Mont Terri (Mazurek et al., 2011), despite the regional fault system in the Opalinus clay. At Mont Russelin, Switzerland, diffusion is the dominant transport mechanism despite a complex system of thrust faults. Similarly, in the Opalinus clay at Benken, Switzerland, advective flow is not evident and transport to the underlying aquifer can be explained by diffusion (Koroleva et al., 2011). Conversely, Patriarche et al. (2004) indicate that the δ^2H profile at Aveyron, France, cannot be explained by diffusion alone and that heterogeneity, such as fractures, has an important role in the tracer profile.

1.2. Description of the Problem

The Shore Gold Inc. Star Diamond operation is located in the Fort à la Corne forest, approximately 60 km east of Prince Albert, Saskatchewan, Canada (latitude 53°15"N, longitude 104°48" W; Figure 1.1). The Star Diamond Project encompasses the Star Kimberlite, which straddles a mineral disposition boundary between ground that is solely owned by Shore Gold Inc. and ground held by the Fort à la Corne Joint Venture between Kensington Resources Ltd., a wholly-owned subsidiary of Shore Gold Inc (67%), and Newmont Canada FN Holdings ULC (33%). The Star Diamond project is operated by Shore Gold Inc. (Ewert et al., 2009).

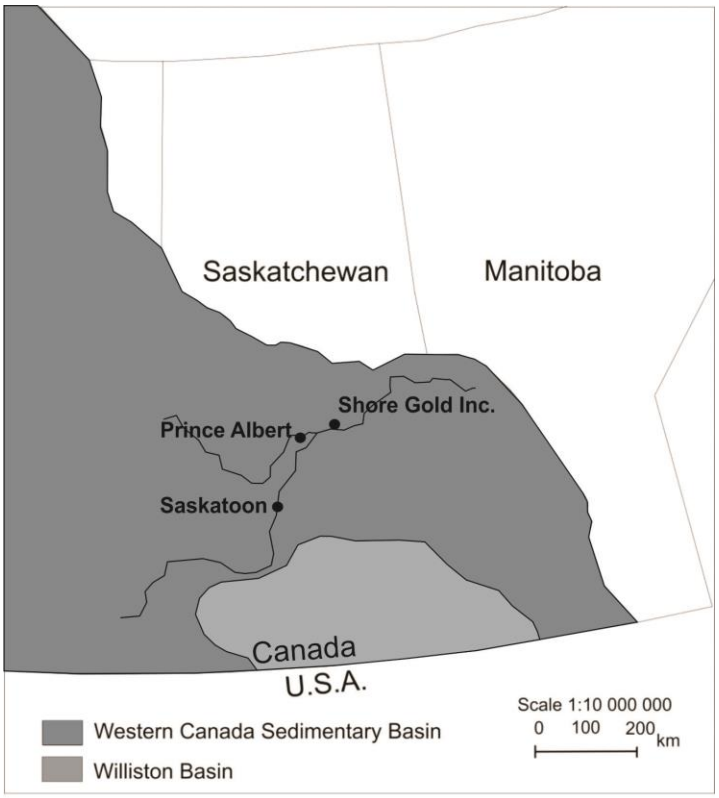

Figure 1.1. Map of the Shore Gold Inc. study area, Saskatchewan, and the distribution of the Western Canada Sedimentary Basin and the Williston Basin in west-central Canada (modified from Hendry et al., 2013).

Shore Gold's project consists of the Star and Orion South Kimberlites. The proposed Star and Orion South open pit mines are intended to be conventional open pit mining operations with 15 m high benches. There are concerns with pit wall stability due to high ground water levels in the shale and glacial sediments that will be slow to depressurize upon dewatering of the underlying Mannville aquifer and the existence of glacially sheared zones in the Colorado Group shales and near the glacial till-shale contact. It is estimated that 23 dewatering wells will be required to depressurize the Lower Colorado shale and Mannville sandstones around the Star Kimberlite open pit, and that an additional seven dewatering wells installed into the underlying Mannville aquifer will be required to depressurize the Lower Colorado and Mannville sediments around the Orion South open pit. During the dewatering process, there is concern that the drawdown of water levels in the underlying Mannville aquifer could result in drawdown of water levels in the aquifers that are present within the glacial till (through the Lower Colorado

aquitard), which are the major source of fresh water for the surrounding area (Ugorets and Pereira, 2010).

Aquifer pumping tests are commonly used to measure aquifer characteristics (K and specific storage (Ss)) and the characteristics of overlying and underlying confining units. Sedimentary sequences often consist of a series of aquifers separated by low hydraulic conductivity confining units (aquitards). Aquitard sediments are often more compressible than those in aquifers. As such, they can release large quantities of water from storage and increase the volumes of water available to the aquifer. This phenomena is termed leakage (Neuman and Witherspoon, 1972). Early methods to define leaky aquifer characteristics include that of Hantush (1956). This method assumed that all water flowing to a pumping well came from either elastic storage in the aquifer or leakage across the confining layer. No water was derived from elastic storage in the confining layer. Later, Hantush (1967) devised a method to incorporate the effect of leakage from confining units in the differential equation of groundwater motion as it occurs in the physical system, rather than being expressed as a boundary condition. This method, however, relied on the criteria that the aquifer be relatively thin and that a leakage factor (B) is <0.10, where B is equal to $\sqrt{T/(\frac{K'}{b'})}$ and T is the aquifer transmissivity, K' the aquitard hydraulic conductivity and b' is aquitard thickness. More recently, Wolff (1970) described a method for evaluating the hydraulic diffusivity of an aquitard using observation wells completed in the confining layer. In his analysis he assumed that drawdown can be represented in the pumped aquifer by a step function at any given radial distance from the pumping well and at a sufficiently large value of time. This approach, however, led to difficulties when applied to multiple aquifer systems. Also, drawdown in the pumped aquifer could not be reliably represented by a single step function unless a quasi-steady state was reached within a sufficiently short period of time and the observation wells were situated at relatively small radial distances from the pumping well (Neuman and Witherspoon, 1972). Situations in which these methods are not applicable include conditions in which there is a large contrast in hydraulic conductivity between the aquitard and aquifer, and B is > 0.10.

1.3. Research Objectives

The goal of the research was to determine if the Lower Colorado shale aquitard will restrict water flow from the overlying intertill aquifers to the lower Mannville aquifer during dewatering of the lower Mannville aquifer for open pit mining operations. The objectives of the study were to characterize both the hydrogeologic properties and solute transport mechanisms in the Lower Colorado shale aquitard as well as the impact of kimberlite volcanism and subsequent hydrothermal alteration and fractures on the hydraulic properties of the shales by investigating both a geologically simple aquitard site and a geologically complex aquitard site in the same study area. The simple site consists of undisturbed Cretaceous shale deposits. The complex site features Cretaceous shale deposits that are highly fractured and altered as a result of kimberlite volcanism during deposition.

The methodology followed in this investigation included the following:

1) characterizing the geotechnical parameters (i.e., dry bulk density [ρ_d] and gravimetric water content [ω]) of the aquitard and aquifer system;
2) estimating specific storage (Ss), hydraulic gradients (i), and groundwater flow direction from transducer data recorded in the shale aquitard and the underlying aquifer;
3) obtaining high-resolution vertical profiles of pore-water δ^2H and Cl through both the simple and complex aquitard systems;
4) identifying hydrogeological zones with depth in both systems using the high-resolution profiles;
5) measuring the groundwater age date of the dissolved inorganic carbon (DIC) in the underlying regional aquifer using ^{14}C-DIC analysis; and
6) mathematical modeling of the vertical δ^2H and Cl concentration profiles to define the dominant transport mechanism(s) and estimate the paleo-hydrogeologic evolution of the aquitard systems.

CHAPTER 2. STUDY AREA

2.1. Site Description/Geologic and Hydrogeologic Setting

The stratigraphy of the study area (from oldest to youngest) is as follows. The Cantuar Formation of the Mannville Group (Mannville), consisting of sandstone, siltstone, and shale, is overlain by the Joli Fou Formation shale of the Lower Colorado Group (Colorado). The Colorado shale is unconformably overlain by glacial sediments of the Dundurn Formation of the Sutherland Group, the Floral Formation of the Saskatoon Group, and surficial sand and lacustrine clay. The Mannville and Colorado sediments are of Late Cretaceous age and were deposited between 99 and 112 Ma (Zonneveld et al. 2004). Sutherland Group sediments are Pre-Illinoian in age (0.50-2.50 Ma) (Christiansen, 1992). The Saskatoon Group sediments were deposited more than 38 Ka BP and the surficial sand and clays were deposited during the late Wisconsin (95 to 20 ka BP) and Holocene (< 12 ka BP) (Christiansen, 1992; Christiansen and Sauer, 1993).

The Cretaceous kimberlite field was active over a time span of ~20 Ma during terrestrial (Mannville Group) and marine (Lower Colorado Group) background sedimentation (Zonneveld et al., 2004). More than 70 kimberlite pipes are located in the vicinity of the study area, most of which were deposited between 99 and 101 Ma BP (McNeil and Gilboy, 2000; Figure 2.1) during deposition of the Lower Colorado Group shales. The kimberlite pipes were deposited in a two stage process, beginning with excavation of shallow but wide craters that was followed by subsequent infilling by pyroclastic kimberlite (Berryman et al., 2004; Scott-Smith et al., 1998). The size and shape of the craters indicate the initial crater-forming explosions were powerful, causing country rock fragmentation and volcanically induced faulting in the form of ring faults and half grabens (Lefebvre and Kurszlaukis, 2008; Zonneveld et al., 2007). The kimberlite debris flow (KDF) deposits observed in the research area formed when walls of the kimberlite volcano, comprised of unconsolidated Colorado mudstone, became unstable, slumped, and were deposited on the crater floor, resulting in mixed, deformed, and brecciated kimberlite and shale (Pittari et al., 2006; Zonneveld et al., 2004). Further, Leckie et al. (1997) report the temperature of the kimberlite during deposition by pyroclastic airfall ranged from 418 to 434 °C.

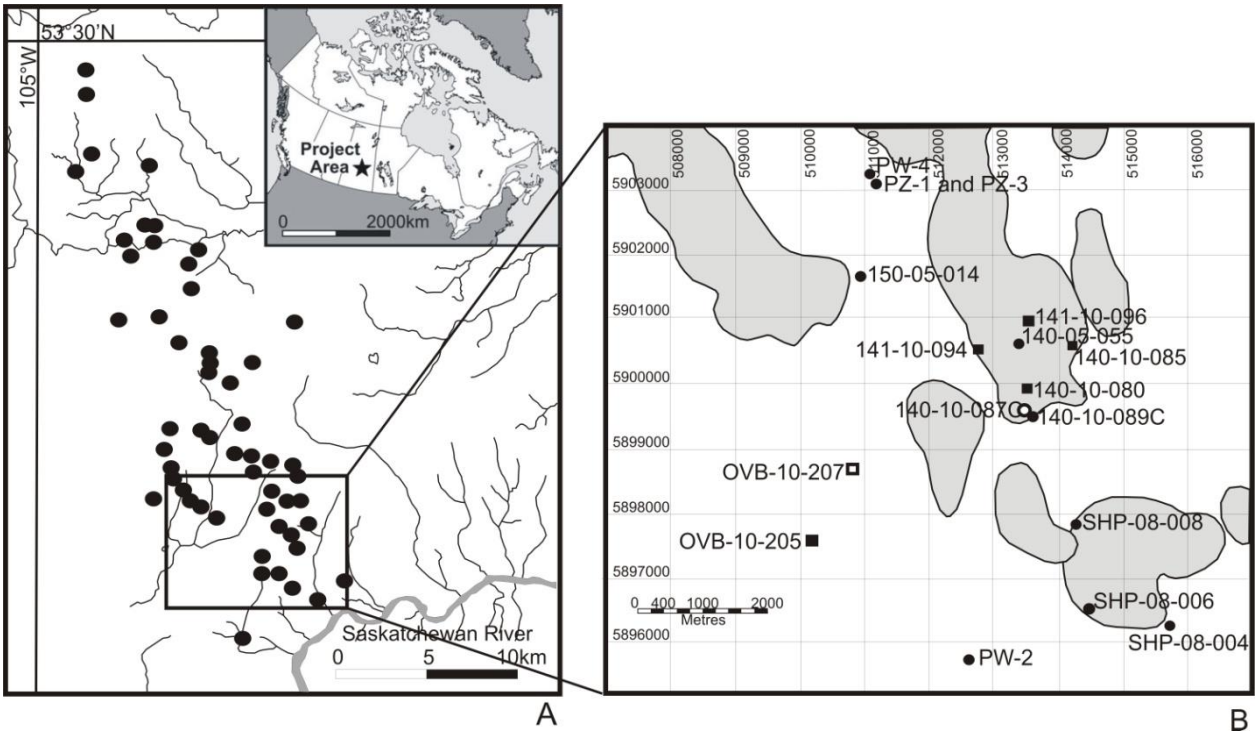

Figure 2.1. (A) Location of the study site and major surface water features. Kimberlite bodies are identified as black circles (modified from Berryman et al., 2004). (B) Location of drillhole locations and major geologic features. Kimberlite bodies are highlighted in grey. Drillhole locations for this study are identified with open symbols' borehole locations for data reported by Ugorets and Pereria (2011) are identified with closed symbols.

Recharge into the Mannville aquifer occurs in the western, northern, and eastern margins of the Williston Basin (Palombi, 2008). It has been suggested that Mannville Group water was recharged by an influx of glaciogenic water during the Pleistocene. Grasby and Betcher (2000) and Person et al. (2007) suggest low $\delta^{18}O$ (and $\delta^{2}H$) values of formation waters, collapse structures related to salt dissolution, hydrodynamic blowout structures, and biodegradation of oils all imply a significant influx of fresh water into the Basin along the outcrop belt in southern and central Manitoba during Pleistocene glaciation. The thickness of the continental ice sheet during the Pleistocene could have provided sufficient hydraulic head to reverse the hydraulic gradient and flow direction within the Williston Basin. Grasby et al. (2000) suggest a considerable influx of fresh water up to ~400 km beyond the outcrop limit in Manitoba as a result of this Pleistocene flow reversal.

A groundwater study of the Shore Gold Inc. study area (Ugorets and Pereira, 2011) provided K values estimated from slug and packer injection testing for the glacial till, Lower Colorado shale, and Kimberlite and Mannville sandstone, as well as water level data and groundwater flow direction (Table 2.1). This study identified three water-bearing units in the area: the first was the shallow surficial sands, silts, and clays (up to 50 m thick in the study area); the second was a basal boulder/gravel unit within the Saskatoon Group till; and the third was the deep sandstones of the Mannville Group. The two lower water-bearing units are separated by the Lower Colorado shale, an aquitard with a low K. Slug tests conducted in the surficial sand and surficial silt/clay yielded K_h and K_v values ranging from 6×10^{-7} to 1×10^{-4} m s^{-1} and 6×10^{-8} to 1×10^{-4} m s^{-1}, respectively. K_h and K_v values estimated from pump testing, airlifting, packer injecting, and falling head tests in the glacial till range from 7×10^{-8} to 6×10^{-7} m s^{-1} and 7×10^{-10} to 6×10^{-8} m s^{-1}, respectively. Packer injection tests conducted in the Lower Colorado shale on testholes at the Orion South and Star kimberlite bodies (Figure 2.1) estimated K_h and K_v values of 7×10^{-10} and 5×10^{-9} m s^{-1}, respectively. Average values for the K_h and K_v of the Mannville Formation were estimated at 2×10^{-5} and 2×10^{-6} m s^{-1}, respectively. Hydraulic testing of kimberlite material within the Orion South kimberlite yielded K_h and K_v values of 2×10^{-9} m s^{-1}. The vertical groundwater flow direction is downward through the glacial till to the intertill aquifer that exists within the Saskatoon Group till, and upward (to near hydrostatic gradients) from the Mannville aquifer through the Lower Colorado shale to the Saskatoon Group intertill aquifer (Ugorets and Pereira, 2011; Clifton Associates, 2011). A major river (the Saskatchewan River) and smaller creeks and ravines exist at the study area (Figure 2.1). Inflow from the Saskatchewan River through the glacial till and by recharge of the Mannville aquifer through the overlying Lower Colorado shale will likely be limited during mining conditions, when the hydraulic gradient would be reversed by the Mannville dewatering system (Ugorets and Pereira, 2011).

Table 2.1. Hydraulic conductivity (K) values measured in regionally located piezometers at the study area (Ugorets and Pereira, 2011; Clifton Associates, 2011).

Drillhole ID	Interval	K (m s^{-1})	Testing Method	Impacted by Kimberlite (Y/N)
150-05-014	Colorado	5.1×10^{-10}	Packer Injection	N
	Colorado	4.4×10^{-9}	Falling Head	N
SHP-08-004	Colorado	6.5×10^{-8}	Packer Injection	Y
SHP-08-006	Colorado	9.1×10^{-9}	Packer Injection	Y
	Colorado	1.7×10^{-7}	Packer Injection	Y
150-05-014	upper Mannville	4.6×10^{-8}	Falling Head	N
	upper Mannville	3.7×10^{-7}	Packer Injection	N
PW-2	lower Mannville	1.9×10^{-5}	Pumping Test	N
	lower Mannville	1.7×10^{-5}	Pumping Test	N
SHP-08-004	upper Mannville	1.2×10^{-9}	Packer Injection	N
	upper Mannville	9.3×10^{-9}	Packer Injection	N
SHP-08-006	upper Mannville	1.2×10^{-9}	Packer Injection	N

CHAPTER 3. LITERATURE REVIEW

3.1. Overview

The low K of aquitards makes it difficult to estimate their hydraulic properties using classical hydrogeological methods. Many methods for determining the bulk K of shallow clay aquitards are available; however, each has drawbacks and advantages and each is based on simplifying assumptions (i.e., slug tests, pumping tests, response of the aquitard to mechanical loading, and analysis of natural pore-pressure fluctuations). Many of the classical methods also require an independent measurement of specific storage (S_s) and, in many cases, laboratory methods for determining S_s are probably not representative of *in situ* conditions and may lead to overestimation of aquitard K (van der Kamp, 2001). For these reasons, the use of conservative tracers is playing an increasingly important role in defining aquitard K (Hendry and Wassenaar, 1999; Rübel et al., 2002).

3.2. Compressibility and Effective Stress

Total stress at a given plane in a saturated aquifer refers to the downward stress placed on the aquifer skeleton by the overlying rock and water. Fluid pressure causes an upward stress on the plane and will, in part, counteract the total stress. The resulting stress that is actually borne by the aquifer skeleton (the effective stress) is less than the total stress. Total stress can be defined as

$$\sigma_T = \sigma_e + P, \tag{3.1}$$

where σ_T is the total stress, σ_e is the effective stress, and P is the pressure. A change in total stress will result in a change in pressure and effective stress. There can be significant changes in pressure with very little change in actual thickness of the saturated water column and, as such, the total stress remains essentially constant and a change in pressure will result in a change in effective stress that is of equal magnitude but opposite in sign:

$$\partial P = \partial \sigma_e. \tag{3.2}$$

Aquifer pumping, for example, reduces the pressure head in a confined aquifer, and therefore the effective stress that acts on the aquifer skeleton will increase and cause the aquifer skeleton to

consolidate or compact. This consolidation or compaction occurs due to the shifting of mineral grains, thereby reducing the porosity. As such, aquifer compressibility can be defined as

$$\alpha = \frac{-\partial b/b}{\partial \sigma_e}, \tag{3.3}$$

where α is the aquifer compressibility (1 M^{-1} L^{-2}), ∂b is the change in aquifer thickness (L), b is the original aquifer thickness (L), and $\partial\sigma_e$ is the change in effective stress (M LT^{-2}). The negative sign indicates that the aquifer gets smaller with an increase in effective stress (Fetter, 1999).

The isothermal compressibility of water may be defined as

$$\beta = -\frac{1}{V_w}\left(\frac{\partial V_w}{\partial P}\right), \tag{3.4}$$

where β is the fluid compressibility (1 M^{-1} L^{-2}), V_w is the bulk fluid volume, and P is the pressure. The bulk fluid volume response to changes in fluid pressure at constant temperature and mass is defined as β. The minus sign is used because the fluid volume decreases and the pressure increases. The isothermal compressibility, β, can be taken as 4.8×10^{-10} m^2/N for ground water at 25 °C (Domenico and Schwartz, 1990).

The head creates pressure in the saturated zone, affecting the arrangement of mineral grains and the density of water in the voids. If the pressure increases, the mineral skeleton will expand; if the pressure drops, the mineral skeleton will contract. Similarly, water will contract with an increase in pressure and expand if the pressure drops. An aquifer skeleton will compress when the hydraulic head (h) declines, which reduces the effective porosity and expels water. Additional water is released as the pore water expands due to lower pressure. The S_s is defined as the amount of water per unit volume of a saturated formation that is stored or expelled from storage per unit change in head, and can be expressed as

$$S_s = \rho_w g(\alpha + n\beta), \tag{3.5}$$

where ρ_w is the density of the water (M L^{-3}), g is the acceleration of gravity (L T^{-3}), α is the compressibility of the aquifer skeleton (1 M^{-1} LT^{-2}), n is the porosity (L^3 L^{-3}), and β is the compressibility of water (1 M^{-1} LT^{-2}). Specific storage has dimensions of 1 L^{-1}.

When considering atmospheric loading, a portion of the barometric pressure transmitted through the underlying aquitard will be borne by the porewater and the remainder by the aquitard skeleton. The ratio of the pore pressure response to the applied load is Skempton's B-bar coefficient (B) or loading efficiency (γ) (Terzaghi, 1923; Skempton, 1954; Smith et al., 2013). If γ can be determined, then α can be determined using

$$\alpha = \frac{\gamma n \beta}{1-\gamma}. \tag{3.6}$$

The S_s for a saturated, compressible porous media can then be calculated using equation (3.5) (Smith et al., 2013).

3.3. Transport Processes

3.3.1. Diffusion in Porous Media

Transport in porous media is simulated by simultaneously considering advection, mechanical dispersion, and diffusion. At low flow velocities, transport may be diffusion dominated. In the case of low permeability media, a criterion based on a Péclet number (P_e) can relate the effectiveness of mass transport by advection to the effectiveness of mass transport by either dispersion or diffusion. The general form of the P_e is

$$P_e = \frac{vL}{D_e}, \tag{3.7}$$

where L is a reference length (e.g., the distance from the contaminant source) and v is the average linear groundwater velocity. Diffusion is considered the dominant transport process for P_e numbers smaller than 1 (Huysmans and Dassargues, 2005; Barbour et al., 2012).

In cases where advection and dispersion are negligible and diffusion is the dominant transport process, the mass flux of a solute through a porous media is described by

$$J = -n_e D_e \frac{\partial C}{\partial z}, \tag{3.8}$$

where J is the diffusive mass flux rate (M TL^{-2}) and n_e is the effective porosity. The negative sign indicates that the net mass flux of the solute is from areas of high concentration to areas of low concentration. The transient one-dimensional form of the diffusion equation for dissolved constituents through saturated, homogeneous, isotropic media is (Hendry and Wassenaar, 2011):

$$\frac{\partial C}{\partial t} = D_e \frac{\partial^2 C}{\partial z}. \quad (3.9)$$

3.3.2. Effective porosity

Several types of porosity can be distinguished in clay-rich rocks. Physical porosity, n_{phys}, is simply the ratio of the volume of voids to the total volume and can be defined as

$$n_{phys} = \frac{V_{void}}{V_{total}} = 1 - \frac{\rho_{bulk,dry}}{\rho_{grain}}, \quad (3.10)$$

where V_{void} is the volume of voids, V_{total} is the total volume of the sample, $\rho_{bulk,dry}$ is the bulk density of a dry sample, and ρ_{grain} is the grain density. Connected porosity is based on measurements of the water content of saturated rock and found from the relative masses of a sample when water saturated and when dry:

$$WC = 1 - \frac{m_{dry}}{m_{satd}}, \quad (3.11)$$

where WC is the water content, m_{dry} is the mass of the dry sample, and m_{satd} is the mass of the water saturated sample. Water content porosities or moisture contents (θ) are calculated from measured water contents and sample densities using

$$\theta = WC \frac{\rho_{bulk,satd}}{\rho_{water}}, \quad (3.12)$$

where θ is the moisture content of a sample at saturation, $\rho_{bulk,satd}$ is the bulk density of a water saturated sample, and ρ_{water} is the density of water (Pearson, 1999).

Transport porosity values are used to relate velocities of non-reactive tracers in a fluid to the flux of the fluid. Together with other variables, the transport porosity can relate the rates of diffusion of substances in a porous medium to their rates of diffusion in free water. Because transport occurs through pores, the maximum size of a substance being transported through a pore must be less than the minimum throat size of the pore. There are two types of transport porosity: (1) flow and advection porosity and (2) diffusion porosity. The average linear velocity of a fluid moving through a porous medium equals the velocity of a perfect tracer. As such, the Darcy flux, q, and average linear velocity, v, are related to a tracer by the advective transport porosity (n_{adv}) (Pearson, 1999):

$$n_{adv} = \frac{q}{v}. \tag{3.13}$$

The n_{adv} is the porosity through which flow can occur and does not include noninterconnected or dead end pores (Fetter, 1999). The porosity accessible to diffusion (diffusion porosity) may have a different value depending on foliation, grain size variations, and the solute used (i.e., ions with large hydration spheres vs. ions with small hydration spheres). The diffusive transport porosity of a tracer is described by equation (3.8). Pearson (1999) defines geochemical porosity as the species-specific transport porosity. The geochemical porosity is lower than the total porosity for most species because solutes do not have access to the entire water-filled connected pore space. This is due to (1) the species size and ionic charge, (2) the water associated with the diffusive double layers formed on charged mineral surfaces, and (3) the water associated with interlayer cations of clay minerals (Pearson, 1999; Waber and Smellie, 2008).

The effective porosity (advective, diffusive, and geochemical porosity) in clay-rich media has been determined using several methods. Van der Kamp et al. (1996) used the radial diffusion cell to simultaneously estimate the n_e and the D_e. Waber and Smellie (2008) and Koroleva et al. (2011) compare Cl concentrations determined using an aqueous extraction technique to concentrations obtained by mechanical squeezing to determine an n_e. Ratios of effective porosity to total porosity have been reported extensively in the literature and range from 0.3 in the Battleford Till in Saskatchewan, Canada (Hendry et al., 2000) to 0.75 in the Queenston Shale in Ontario, Canada (Barone et al., 1990). Ratios between 0.4 and 0.6 are widely reported for argillites in France, Belgium, and the UK (Mazurek et al., 2011).

3.3.3. Advection-Dispersion in Porous Media

The mass flux of a solute in a saturated porous medium under the combined effects of hydraulic and concentration gradients for one-dimensional transport is given by

$$J = n_e(vC - D_h \cdot \frac{\partial C}{\partial z}), \tag{3.14}$$

where J is the mass flux (M TL^{-2}), n is the porosity of the soil (dimensionless), v is the average linear groundwater velocity of the fluid (L T^{-1}), C is the mass concentration of the solute in the liquid phase in the soil (M L^{-3}), z is the direction of transport (L), and D_h is the coefficient of hydrodynamic dispersion (L^2 T^{-1}). In equation (3.13), $v = {}^{q}/_{n_e}$, where q is the Darcy velocity or

flux (L T^{-1}). The D_h accounts for both mechanical dispersion and diffusive dispersion of the solute during transport and is represented by

$$D_h = D_e + \alpha v, \tag{3.15}$$

where D_e is the effective diffusion coefficient (L^2 T^{-1}), α is dispersivity, and v is the average linear groundwater velocity (Fetter, 1999).

The transient one-dimensional form of the advection-dispersion equation for dissolved constituents through saturated, homogeneous, isotropic media is

$$\frac{\partial C}{\partial t} = \left(\frac{D_h}{R_d}\right) \cdot \frac{\partial^2 C}{\partial z^2} - \left(\frac{v}{R_d}\right) \cdot \frac{\partial C}{\partial z}, \tag{3.16}$$

where R_d is the dimensionless retardation factor that represents the relative rate of transport of a nonreactive solute (i.e., Cl) to that of a reactive solute. For non-reactive solutes, $R_d = 1$ (Shackelford and Daniel, 1991).

3.3.4. Solute Transport in Fractured Media

Due to the complexity of solute transport in fractured media, less research has been undertaken on this topic than on transport in porous media. In fractured media, fluid moves in the fractures as well as the rock matrix and can be considered at a number of different scales. A single fracture near the source would be at the very near scale. At the far field scale, the fracture network and porous media matrix would have separate, discernible impacts on flow. At a considerable distance from the source, at the very far field scale, the entire flow domain can be considered to be an equivalent porous medium, in which the repeating fractures can be considered large pores (Fetter, 1999). In fractured deposits, where advective transport may occur along the fractures, molecular diffusion acts as a mechanism of attenuation of solutes, which causes the transfer of contaminants from the fractures to the porous but relatively impervious matrix due to a concentration gradient between the fractures and the matrix (Gillham and Cherry, 1982). In this case, the transfer of solutes is complex and influenced by matrix porosity, the coefficient of matrix diffusion, and the parameters of the fracture network. Fractures are characterized by their dimensions (aperture, length, and width), orientation and spacing, and the nature of the fracture walls. The matrix is characterized by its porosity, diffusion coefficient, and

K. The fracture porosity (n_f) is defined as the ratio of the volume of fractures to the total volume of the soil. The total porosity is given by

$$n_T = n_f + n_m(1 - n_f), \tag{3.17}$$

where n_m is the matrix porosity (Cook, 2003).

Fractures may become filled with minerals or clay deposits; however, they can form channels for groundwater flow where they remain open. The velocity of water moving through a fracture will be greatest toward the middle of the fracture because frictional forces operate along the fracture walls. If the hydraulic gradient is constant, the mean velocity through a fracture will increase as the distance between the walls increases; it will also be greater if the fracture walls are flat and smooth rather than irregular and rough. Groundwater flow in fractured media occurs mainly through fractures; however, much of the water contained within these aquifers is stored within the matrix. This has a considerable effect on the movement of contaminants and other dissolved substances because diffusion will cause mixing of solutes in water flowing through the fractures with the solutes in the relatively immobile water in the rock matrix, even if the K of the matrix is very low. This phenomenon can cause dissolved substances to appear to travel more slowly than water.

A fracture can be represented as a planar void with two flat parallel surfaces. Its K can be defined as

$$K_f = (2b)^2 \frac{\rho g}{12\mu}, \tag{3.18}$$

where K_f is the fracture hydraulic conductivity (L T^{-1}), $2b$ is the fracture aperture, ρ is the density of water, g is the acceleration due to gravity, and μ is the viscosity of water. The mean groundwater velocity through a fracture, v_w, can be calculated using

$$v_w = K_f \frac{\partial i}{\partial z}, \tag{3.19}$$

where $\frac{\partial i}{\partial z}$ is the hydraulic gradient. When considering a system of evenly spaced, planar, parallel, identical fractures in a low permeability matrix, the K of the medium in the direction parallel to the fractures can be expressed as

$$K = \frac{(2b)^3}{2B}\frac{\rho g}{12\mu}, \tag{3.20}$$

where 2B is the fracture spacing. In any other direction, the K is equal to zero. This equation can also be referred to as the cubic law, because of the dependence of K on the fracture aperture (Cook, 2003).

When considering a low K rock matrix, solute transport is characterized by advection through the fractures with diffusion into the immobile water in the matrix. Three main approaches have been used to consider fracture transport, and can be summarized as (1) equivalent porous medium (EPM), (2) discrete fracture, and (3) double porous continuum (Leo et al., 1996). EPM conditions exist when there is complete equilibrium between fractured and unfractured blocks with regard to solute concentration. If a study can be treated as an EPM, then evaluation of solute transport can be straightforward (van der Kamp, 1992). A dimensionless number can be calculated to determine if the EPM approach can be used in formations with secondary fracture K,

$$F_s = \frac{t_e}{t_a} = \frac{L^2 K_b i}{znD_e} \ll 1 \tag{3.21}$$

$$t_a = \frac{z}{K_b \frac{i}{n_e}} \tag{3.22}$$

$$t_e = \frac{L^2}{D_e}, \tag{3.23}$$

where t_a is equal to the arrival time of the solute at distance z (L), t_e is equal to the time required for the solute concentration in the blocks to equilibrate with the concentration in the fractures by diffusion, L is the average fracture spacing (L), K_b is equal to the bulk hydraulic conductivity of the formation (L T^{-1}), i is the hydraulic gradient (dimensionless), n_e is the transport porosity (dimensionless), and D_e is equal to the effective diffusion coefficient (L^2 T^{-1}). When the value of F_s is less than 1, the system may be considered an EPM (van der Kamp, 1992). If the system can be considered an EPM, the L, b, and K_b can be related by

$$K_b = \frac{\rho g b^3}{12\mu L}, \tag{3.24}$$

where ρ and μ are the density and viscosity of water, respectively, and g is the acceleration due to gravity (Freeze and Cherry, 1979; van der Kamp, 1992). Transport under EPM conditions is dominated by molecular diffusion when K values are 10^{-10} m s^{-1} or less, in which case fractures have little effect on solute transport (van der Kamp, 1992).

3.4. Natural Tracers in Clay-Rich Aquitards

3.4.1. Overview

Slow groundwater velocities in aquitards, usually on the scale of 1 m 1 ka^{-1} to 1 m 10 ka^{-1}, suggest that diffusion is the dominant solute transport mechanism (Hendry and Wassenaar, 1999). For this reason, solute and isotopic depth profiles often exhibit diffusion gradient profiles. Natural tracer studies, commonly employing the stable isotopes of water and Cl, have provided information on groundwater flow, solute transport mechanisms, hydraulic conductivity, and the timing of climatic and geologic events (Remenda et al., 1996; Hendry and Wassenaar, 1999, 2011; Koroleva et al., 2011; Mazurek et al., 2011). Natural tracer profiles can be considered large-scale, long-term, natural experiments that can be used to constrain transport processes in pore water (Mazurek et al., 2011).

Early work on natural tracers in clay-rich aquitards focused on Quaternary deposits (Desaulniers et al., 1981; Hendry and Wassenaar, 1999; Hendry et al., 2000). More recent studies addressed thick glacial till and unfractured bedrock shale aquitards (Hendry and Wassenaar, 1999; Hendry et al., 2011) and deep, indurated, fractured shale deposits (Gautschi, 2001; Koroleva et al., 2011; Mazurek et al., 2011; Rübel et al., 2002). These studies used a variety of conservative and non-conservative tracers to explore long-term transport mechanisms and the hydrogeological evolution of the aquitard systems. In these cases, both the shape (curvilinear) of one-dimensional (1-D) vertical natural tracer profiles with depth and modeling were used to demonstrate that diffusion is the dominant transport mechanism, even in systems in which the aquitard is fractured (Gimmi et al., 2007; Koroleva et al., 2011; Mazurek et al., 2011; Patriarche et al., 2004). In contrast, vertically constant solute profiles may suggest advection is the dominant transport mechanism (Hendry et al., 2004; Kelln et al., 2001). Mathematical modeling of curvilinear depth tracer profiles also provides estimates of the timing of palaeo-hydrogeologic events, which have been used to test the effect of adding an advective component of transport to the modeled best-fit diffusion profiles (Hendry and Wassenaar, 1999; Hendry et al., 2000, 2011;

Koroleva et al., 2011; Mazurek et al., 2011). Interpretation of 1-D vertical profiles can also provide an increased level of confidence to physical hydrogeological studies (e.g., K, hydraulic gradients, porosities, recharge rates) of a groundwater system.

3.4.2. Stable Isotopes of Water (δ^2H and $\delta^{18}O$)

Environmental isotopes are naturally occurring isotopes of elements found in abundance in our environment (i.e., H, C, N, O, and S); these represent the principal elements of hydrological, geological, and biological systems. Environmental isotopes are used to trace groundwater provenance, subsurface processes, geochemical reactions, and reaction rates (Clark and Fritz, 1997).

Stable isotopes are measured in terms of the ratio of the two most abundant isotopes of an element. Isotopic concentrations are expressed as the difference between the measured ratios of the sample and reference over the measured ratio of the reference. They are expressed using delta (δ) notation. For example, for the ^{18}O stable isotope of oxygen,

$$\delta^{18}O_{sample} = \frac{m(^{18}O/^{16}O)_{sample} - (^{18}O/^{16}O)_{reference}}{m(^{18}O/^{16}O)_{reference}}. \quad (3.25)$$

Fractionation does not impart large variations in isotope concentrations, so δ values are expressed as the parts per thousand or permil (‰) difference from the reference, e.g.,

$$\delta^{18}O_{sample} = \left(\frac{(^{18}O/^{16}O)_{sample}}{(^{18}O/^{16}O)_{reference}} - 1\right) \cdot 1000‰\ VSMOW, \quad (3.26)$$

where Vienna Standard Mean Ocean Water (VSMOW) is the reference used (Clark and Fritz, 1997).

Climate changes are manifested by a shift in the stable isotope content of precipitation and are important tools in identifying paleogroundwaters. In temperate latitude climates, the dominant effect of climate change is the position of precipitation on the local meteoric water line (LMWL). Late Pleistocene paleogroundwaters from temperate regions (i.e., North America and Europe) are isotopically depleted with respect to modern waters and shifted along the global meteoric water line (GMWL) toward more negative values (Clark and Fritz, 1997; Person et al. 2007). In the glaciated regions of North America, the stable isotope content of old groundwater

can provide a record of pre-Holocene climate. Old groundwater is generally associated with large confined aquifers and long residence times and flow paths; however, mixing can dampen the climate signal. In thick, unfractured aquitards, old groundwater has long residence times but short travel paths and limited mixing, so may preserve the characteristic isotopic signature of water incorporated at the time of deposition (Remenda et al., 1994).

Many methods have been developed to determine the $\delta^{18}O$ and $\delta^{2}H$ values from core samples. In most cases, profiles are generated from measurements of porewater obtained either directly or by various extraction techniques, such as centrifugation, mechanical squeezing, or direct equilibration. All of these techniques have the potential to cause isotope fractionation during the extraction process. Centrifugation and mechanical squeezing can take up to 24 to 48 hours, during which time the sample is subject to evaporative effects (Edmunds and Bath, 1976; Patterson et al., 1978; Koehler et al., 2000). The radial diffusion method allows for the concurrent determination of n_e and groundwater isotope composition. The cores in these cells are also subject to evaporative effects and gas exchange with the atmosphere, require precisely measured physical and isotopic parameters for each diffusion cell, and require 40-60 days to complete; these factors render this method impractical when a large number of samples is involved (van der Kamp et al., 1996; Koehler et al., 2000). Water samples can also be taken directly from piezometers and evaluated for isotopes; however, it is not possible to develop detailed profiles of $\delta^{18}O$ and $\delta^{2}H$ as it is very costly and time consuming to install a large number of piezometers (Hendry et al., 2004). Koehler et al. (2000) developed a method in which the $\delta^{18}O$ and $\delta^{2}H$ values of core samples can be measured by equilibration with H_2 gas in the presence of a special Pt catalyst (Hokko beads) and CO_2 gas (Koehler et al., 2000; Kelln et al., 2001). Wassenaar et al. (2008) describe a method that can be used on either saturated or unsaturated geologic core samples and pore water $H_2O_{(liquid)}$-$H_2O_{(vapour)}$ equilibration, followed by a dual stable isotopic analysis using laser based off-axis integrated cavity output spectroscopy (OA-ICOS). This technique enables direct and rapid measurement of $\delta^{18}O$ and $\delta^{2}H$ of pore water on single core samples (Hendry et al., 2011, 2013). The major advantages of this method include measurements on pore water samples with minimal handling and exposure to evaporation and direct measurement of the isotopes of water with minimal complicating interferences from air or other gases (Wassenaar et al., 2008).

3.4.3. Chloride

Dissolved Cl is commonly used as a tracer in groundwater studies because it exhibits a lack of adsorption in its anionic form, exists at low concentrations in most rock-forming minerals, has high solubility in natural waters, and does not exhibit volatility in the subsurface (Feth, 1981; Hendry et al., 2000). The main sources of Cl in bedrock argillites are trapped seawaters and evaporate formations (Lavastre et al., 2005).

Pore water Cl concentrations can be measured directly from piezometers (Desaulniers et al., 1981, 1986; Hendry et al., 2000); however, these direct measurements can be difficult due to the long time periods required to collect sufficient volumes of water for analysis (Neuzil, 1986). Various extraction techniques are often used to determine pore water concentrations of Cl, including mechanical squeezing, centrifugation, and aqueous leaching. All of these methods are subject to alteration of pore water by dissolution, oxidation, temperature/pressure changes, and contamination through handling (Teasdale et al., 1995). When pore water is extracted, the applied energy needed can break the established bonds between water molecules and the cations, anions, organic matter, and clay minerals in the system. The extraction methods will not be uniform throughout the sample in most cases; therefore, new bonds between the components will be created and other strengthened while the water content decreases. The porosity can also be reduced in the system due to over-pressurization, which acts as a filter, enhancing and retarding the ions according to their radius and charge. The possibility of extracting not only free water, but also strongly bound water, is a potential problem. The impossibility of extracting all of the solution or controlling the relative amounts and composition does not allow for a true pore water composition to be derived (Sacci et al., 2001).

Aqueous leaching experiments are the most common method for developing Cl distribution profiles (Barone et al., 1990, 1992; Lavastre et al., 2005; Van Loon and Jacob, 2005; Van Loon et al., 2003, 2007). Aqueous leaching is done by placing a crushed sample in contact with deionized water at a given solid/liquid ratio. Once equilibrium between the two phases is established, the solid phase is separated and the liquid phase is analyzed. Aqueous leaching is the only method of extraction that is not subject to incomplete water extraction.

3.4.4. Groundwater Dating with $^{14}C_{DIC}$

Atmospheric $^{14}CO_2$ mixes with all living biomass through photosynthesis as well as with meteoric waters and oceans through CO_2 exchange reactions. Any carbon compound derived from atmospheric CO_2 since the late Pleistocene is potentially eligible for radiocarbon dating. ^{14}C is used to estimate the age of paleogroundwaters and is based on the incorporation of atmospherically derived ^{14}C from the decay of photosynthetically-fixed carbon in soil. Radiocarbon in soil can be taken into solution as dissolved inorganic carbon ($DIC=CO_{2(aq)}+HCO_3^-+CO_3^{2-}$) or as dissolved organic carbon (DOC). Radiocarbon dating is based on measuring the loss of the parent nucleotide (^{14}C), and the time is precisely measured by the exponential loss of the parent according to its half-life, represented by the decay equation

$$a_t = a_o \cdot e^{-\lambda t}, \tag{3.27}$$

where a_o is the initial activity of the parent nuclide and a_t is its activity after some time, *t.* The decay constant, λ, is equal to $\ln 2/t_{1/2}$. For ^{14}C, $t_{1/2}$ is 5730 years. Assuming the initial concentration of the parent is known and has remained constant in the past, and that the system is closed to subsequent gains or losses of the parent, dating with ^{14}C is a relatively simple calculation (Clark and Fritz, 1997). NETPATH-WIN (El-Kadi et al., 2011a,b) applies traditional adjustment models to $\delta^{13}C$ and C-14 concentrations defined in the model. When a single water sample is entered into the model, isotopic exchange is attributed to dissolution only; constraints and phases are ignored because their mass transfers are zero. By using the "run all C-14 models" option in the model, the radiocarbon ages are calculated from several traditional models, including Ingerson and Pearson (1964), Mook (1972), Tamers (1975), Fontes and Garnier (1979), and Eichinger (1983).

3.4.5. Transport Modeling of Natural Tracers

The shapes of 1-D vertical conservative tracer profiles are the most compelling evidence for determining the dominant transport mechanism in aquitards (Mazurek et al., 2011; Hendry et al., 2011). Where solute profiles are vertically constant, the dominant transport mechanism is inferred to be via advection (Hendry et al., 2004, 2011), whereas curvilinear concentration profiles suggest diffusive molecular transport is dominant (Desaulniers et al., 1981; Remenda et al., 1996; Hendry and Wassenaar, 1999; Hendry et al., 2000, 2011, 2013; Mazurek et al., 2011).

Curvilinear concentration profiles can be mathematically reproduced using reasonable hydrogeologic and solute transport properties and boundary conditions (Hendry et al., 2011, 2013).

Changes in the chemical or isotopic composition in surrounding aquifer waters can affect the composition of pore water in aquitards by transport across the boundaries. Due to the slow solute transport within the sequences, the resulting chemical or isotopic gradients can persist over geological time scales and be characterized by analyzing the spatial distribution of tracer concentrations. Independent constraints must be characterized with respect to the evolution of ground water composition in bounding aquifers over the time periods of interest, so the observed tracer profiles in the aquitard sequences can be simulated by transport modeling to constrain relevant transport processes and their given sets of transport parameters (Mazurek et al., 2011). Initial conditions and starting points (t=0) for models are set at a stage of post-depositional evolution such that reasonable assumptions about water composition and hydrogeological evolution up to the present can be made (i.e., when a bounding aquifer has been exposed to meteoric water recharge). Generally, transport parameters are independently derived from laboratory or field experiments (Hendry et al., 1999, 2011; Mazurek et al., 2011). Uncertainty in transport parameters and in initial and boundary conditions is considered by varying the conditions and parameters. Based on palaeo-hydrogeological information, initial conditions are sometimes difficult to constrain so an iterative modeling approach is used. A good match between data and simulations is generally taken as evidence that the processes and input parameters are appropriate (Mazurek et al., 2011).

Traditionally, the approach to determine the time to generate tracer profiles from aquifer activation (i.e., flushing with meteoric water) was to assign a constant concentration in the aquifer at the present day measured values. This would force the profile to propagate into or out of the aquitard for a simulated period of time (Hendry et al., 1999, 2000; Mazurek et al., 2011). Recently, Hendry et al. (2013) used the complex glacial history of the Williston Basin to define aquifer boundary conditions by assuming flushing of the aquifer with water during glaciations. The latter method should be employed at any study site with a complex paleo-hydrogeologic history.

CHAPTER 4. MATERIALS AND METHODS

4.1. Drilling, Sampling, and Installation of Piezometers and Transducers

Two boreholes were continuously cored between March 23 and May 1, 2010 using a Boart Longyear diamond drill rig with an HQ sized core barrel (63 mm). The first hole, OVB-10-207, was located approximately 3 km northwest of the Star Kimberlite deposit (UTM coordinates 5898783 and 0510627; Figure 2.1) and was cored to 204 m below ground (BG; 238.9 m asl). The second hole, 140-10-087, was located approximately 300 m north of the electromagnetic (EM) boundary of the Orion South Kimberlite (UTM coordinates 5899783 and 0513536; Figure 2.1) and was cored to 353 m BG (92.6 m asl). Borehole OVB-10-207 did not intersect kimberlite whereas 140-10-087 intersected kimberlite in the Lower Colorado shale. Overall, core recovery varied from 68-100% in the Saskatoon Group Till (mean 92%), 0-17% in the Saskatoon Group intertill aquifer (mean 4%), 33-100% in the Sutherland Group tills (mean 50%), 0-100% in the Lower Colorado shale (mean 75%), 37-100% in the upper Mannville silt and shale (mean 44%), and 0-96% in the lower Mannville sand (mean 27%). The rotary drill mud was spiked with 99% D_2O to a value of up to -30‰. Drill mud and fluid samples were collected every 6 hours during drilling to assess the extent of core contamination by the drilling fluid. These samples (n=32) were collected and stored at room temperature in 250 mL high-density polyethylene (HDPE) bottles for stable isotope (δ^2H and $\delta^{18}O$) analyses.

Geological and geotechnical logging of core samples was performed immediately after coring. Samples 7.5 cm in diameter and 10-20 cm long were collected every 3 m from both core holes for determination of ρ_d, ρ, and ω. These samples were placed in 17.7 × 19.5 cm Ziploc® freezer bags, which were then placed in 26.8 × 27.3 cm Ziploc® freezer bags to minimize vapour loss. The samples were stored in coolers to maintain moisture and temperature stability until analyses could be performed. Eleven samples were collected from the two holes for laboratory testing of K: five from OVB-10-207 at depths of 316.9, 305.9, 284.9, 274.9, and 263.9 m asl; and six from 140-10-087 at depths of 320.6, 300.6, 280.6, 266.8, 259.3, and 249.6 m asl. These samples were wrapped in Saran® wrap and masking tape and coated in paraffin wax in the field before being stored in coolers to maintain moisture and temperature stability.

Samples (7.5 cm in diam. × 10-20 cm long; n =303) were collected every 1 m (where core recovery permitted), trimmed to remove the outer 2-5 mm of core (to minimize

contamination of the surface of the core), and placed in 17.7 × 19.5 cm Ziploc® freezer bags within 26.8 × 27.3 cm Ziploc® freezer bags (to minimize vapour loss). Samples were stored in coolers to maintain moisture and temperature stability until analyses of isotopes of water could be performed.

Core samples (7.5 cm in diam. × 10-20 cm long) were also collected every 3 m (where core recovery permitted) for determination of n_t (n = 110) and analysis of extractable Cl concentrations (n = 93). Additional core samples (7.5 cm in diam. × 10-20 cm long) (two samples from the glacial till at 399 and 372 m asl and six from the Lower Colorado and KDF at 326, 314, 296, 281, 271, and 261.6 m asl) were collected from corehole 140-10-087 for mechanical squeezing and subsequent measurement of Cl concentration. These core samples were wrapped in plastic wrap and masking tape and coated in paraffin wax in the field before being stored in coolers to maintain moisture and temperature stability until tested.

Absolute pressure vibrating wire piezometers (VWPs) were installed in each borehole immediately after coring to measure fluid pressure. Four RST VW2100 VWPs were installed at OVB-10-207 and four Geokon 4500 vibrating wire pressure transducers were installed at 140-10-087. The VWPs at OVB-10-207 were installed in the surficial sand (406.1 m asl), in the Saskatoon and Sutherland Group till units (367.9 and 329.2 m asl), and at the top of the Colorado Group shale (324.2 m asl). The VWPs at 140-10-087 were installed in the Lower Colorado shale (301.4 and 280.8 m BG) and in the Mannville Group sediments (242.2 and 174.6 m BG). In both boreholes, the transducers were attached to a polyvinyl chloride (PVC) pipe, lowered into the hole to the assigned depths, then grouted in place. The grout (1:3 ratio by mass of bentonite powder to Portland type cement) was mixed at a dry solids to water ratio of 2.5:1, then pumped into the PVC pipe until the grout returned to surface through the annular space. Pressure head measurements were obtained in June 2010 from VWPs installed in OVB-10-207 using an RST VW2106 single channel readout unit. Measurements of pressure head from the VWP installed in 140-10-087 were recorded in 5 min increments on a Geokon Model LC-2x4, 4 channel datalogger from September 30, 2010 to January 18, 2011 and in 6 h increments from January 18 to March 22, 2011.

4.2. Laboratory Testing

4.2.1. Porosity

The value of n_t was calculated from ρ_d and ω measurements made on saturated core samples collected every 3 m from both core holes (where core recovery permitted). The ω was measured on core samples using the method outlined in ASTM D2216-10 (ASTM 2010a). Determination of ρ and calculation of n_t were performed in accordance with ASTM D7263-09 (ASTM 2009).

4.2.2. Laboratory Hydraulic Conductivity

Triaxial testing of hydraulic conductivity of core samples was performed by MDH Engineering Solutions Ltd. in accordance with ASTM D5084-10 (ASTM 2010b) within 45 d of sampling. Samples were consolidated to effective stress levels of 17-24 kPa, with a back pressure of 215 kPa (a confining pressure of about 240 kPa). The hydraulic head across a given test specimen was maintained at about 7 kPa and the gradient at about 11 kPa. The effective stress applied to the samples was less than in situ effective stress, potentially resulting in swelling of the core samples within the triaxial cell, which could result in a one to two order of magnitude overestimation of K (Mitchell, 1993).

4.3. Field Measurements of Hydraulic Head and Specific Storage

Transducer data from 140-10-087 were recorded every 5 min from September 30 to January 18, 2010 and every 6 h from January 18 to March 22, 2010. The absolute pressure records obtained from the pressure transducers were converted to “gauge pressure” by subtracting the atmospheric pressure (B_0) at the site of the time of installation (T=0; September 30, 2010). These data were corrected for barometric and temperature effects following the methods outlined by Smith et al. (2013). These corrected data, as well as data recorded every 5 min from October 24 to December 17, 2010 from additional standpipe and vibrating wire piezometers (150-05-014, PZ-3, and PZ-1; Figure 2.1; Table 4.1; Ugorets and Pereira, 2011), were used to determine the total hydraulic head (h_t) distribution as well as the vertical hydraulic gradients (i) through the Colorado and Mannville sediments.

Table 4.1. Depths of piezometers and corresponding geological units and total head (h_t) values for OVB-10-207, 140-10-087 as well as regional piezometers identified in Figure 2.1 (Ugorets and Pereira, 2011).

Drillhole ID #	Geological Unit	Piezometer Depth (m)	Total Head (m)	Drillhole ID #	Geological Unit	Piezometer Depth (m)	Total Head (m)
OVB-10-207	Surficial Sand	409.01	425.83	OVB-10-205	Surficial Sand	410.08	420.90
	Saskatoon Group	372.61	394.96		Saskatoon Group	369.38	404.82
	Sutherland Group	332.11	387.66		Sutherland Group	334.58	387.10
	Lower Colorado Group	327.11	388.70		Lower Colorado Group	324.38	388.07
140-10-080	Surficial Sand	407.67	429.28	140-10-087	Lower Colorado Group	301.10	387.51
	Saskatoon Group	365.57	401.39		Lower Colorado Group	280.50	388.00
	Sutherland Group	336.97	385.52		upper Mannville	241.90	390.50
	Lower Colorado Group	325.67	386.12		lower Mannville	174.30	391.90
141-10-094	Surficial Sand	408.09	425.21	150-05-014	Lower Colorado Group	325.58	403.20
	Saskatoon Group	363.09	387.79		upper Mannville	222.94	409.00

	Sutherland Group	339.79	388.48	PZ-3	upper Mannville	176.66	397.50
	Lower Colorado Group	328.79	400.14		lower Mannville	119.51	396.90
141-10-096	Surficial Sand	409.47	429.41	PZ-1	Lower Colorado Group	302.00	390.00
	Saskatoon Group	375.27	410.96		Lower Colorado Group	272.00	388.30
	Sutherland Group	334.57	391.53		lower Mannville	170.00	390.30
	Lower Colorado Group	328.47	389.73		lower Mannville	117.00	393.90
140-10-085	Surficial Sand	402.96	419.37				
	Saskatoon Group	364.56	394.74				
	Sutherland Group	336.46	386.29				
	Lower Colorado Group	328.46	385.49				

Barometric pressure data were collected from a Solinst Barologger model 3001 with an accuracy of 0.05% every 30 min from September 30 to March 22, 2011 by G. van der Kamp (Environment Canada) at the White Gull Lake research site, 70 km north of the study site. These data were used to correct the transducer data from 140-10-087 for barometric pressure and to estimate the loading efficiency (γ), compressibility (α), and, ultimately, specific storage (S_s) of the Colorado shale. The ratio of the pore-pressure response to applied load (i.e., barometric pressure) is often referred to as Skempton's coefficient ($\bar{B}$) or, in hydrogeology, as loading efficiency (γ) (Skempton, 1954; Wang, 2000). The γ can be used to estimate α and S_s using equation (3.6) and S_s for a saturated, compressible porous media can be calculated using equation (3.5).

Pressure head measurements were recorded in June 2010 using a single channel RST VW2106 unit at OVB-10-207. Additional pressure head data from regionally located piezometers (140-10-080, 141-10-094, 141-10-095, 140-10-085, and OVB-10-205; Ugorets and Pereira, 2011; Figure 2.1; Table 4.1) were used to determine the distribution of hydraulic head through the surficial sand, Saskatoon Group, Sutherland Group, and upper Colorado shale and compared to the data collected in the current study.

4.4. Mannville Aquifer Pumping Test

Two pumping tests were conducted by SRK Consulting Ltd. in a well completed in the Mannville aquifer at 140-10-089 (75 m north and 69 m west of 140-10-087; October 22 to November 14, 2010; Figure 2.1). The intake screen of the pumping well extended from 254.1 to 162.6 m asl and consisted of stainless steel water well Johnson screen with a 3 mm slot size and an outside diameter of 0.30 m. Pumping tests 1 and 2 were conducted for 3 hours and 22 days, respectively. Pumping test 1 was conducted at a constant rate of Q=0.056 m^3 s^{-1} and pumping test 2 was conducted at a variable rate (Table 4.2). Finite element modeling of transient flow within the aquifer/aquitard sequence to estimate K_v of the Lower Colorado shale was performed using the commercial finite element model SEEP/W (GEO-SLOPE International Ltd., 2007). However, the pumping test data could not be used to accurately estimate K_v in the Lower Colorado aquitard due to the lack of response in the transducers in the Lower Colorado at 140-10-087 during both pumping tests 1 and 2, the lack of transducer data at OVB-10-207 during both pumping tests, and the fact that the transducers had not fully recovered from installation

before pumping was initiated; as such, these data are not presented here. Details of the numerical simulations of pump test data are presented in Appendix A.

Table 4.2. Pumping rate (Q) recorded during pump test 2 conducted at 140-10-089 between October 25 and November 14, 2010.

Time (days)		Time (s)	Q ($m^3 s^{-1}$)
October 25, 2010	10:00 am	0	-0.056
October 26, 2010	12:00 pm	93600	0
October 26, 2010	3:00 pm	104400	-0.056
October 31, 2010	7:00 pm	550800	0
November 1, 2010	3:00 am	579600	-0.056
November 14, 2010	10:00 am	1731600	0

Three water samples were collected from the 22-day pumping test conducted at 140-10-089 (Figure 2.1). The first was collected on October 25, 2010 after 7.6×10^2 m^3 of water was pumped, the second on October 26, 2010 after 7.3×10^3 m^3, and the last on November 9, 2010 after 7.2×10^4 m^3. These samples were stored in 100 mL HDPE bottles at room temperature for stable isotope and Cl analyses. An additional water sample was collected from the pumping well on the final sampling date for $^{14}C_{DIC}$ analysis at room temperature in 250 mL HDPE bottles. Sample collection was performed in accordance with the national groundwater sampling protocol developed by GNS Science in collaboration with the Ministry for the Environment, Greater Wellington Regional Council, and Environment Canterbury (GNS Science, 2010). This sample was submitted to Beta Analytic in Miami, Florida, for $^{14}C_{DIC}$ and $\delta^{13}C$ (‰) analyses.

4.5. Natural Tracers

4.5.1. Squeezing of Porewater from Core Samples

The core samples from 140-10-087 were squeezed in a high-pressure mechanical squeezer using a method similar to Patterson et al. (1978) and Bangsund et al. (2012) to obtain

pore water samples for Cl analyses. Samples were chipped and immediately packed into the squeeze cylinder (316 L stainless steel; 50 mm diam. × 80 mm long). The piston was inserted into the cylinder, placed in a hydraulic press, and the pressure increased to 50 MPa and maintained for 3-5 days. This pressure was selected because testing by Bangsund et al. (2012) suggested no measurable effects on the pore water Cl concentration at this pressure. The porewater passed through a 0.45 μm stainless steel filter before exiting the squeezer through a port located at the base of the cylinder, where it was collected in a clean 60 cm^3 syringe then transferred to a 20 mL scintillation vial and stored at room temperature for analysis.

4.5.2. Aqueous Extractions from Core Samples for Cl Analyses

Core samples were dried in an oven for 48 hours at 90 °C and pulverized using a titanium carbide swing mill. To determine the optimum leaching time and water:rock ratio for aqueous extraction of Cl, batch testing was performed on three samples (from 305, 290, and 249 m asl) from OVB-10-207. Based on leaching times of 1, 5, 10, and 100 hours and water:rock ratios of 2:1, 3:1, 4:1, and 5:1, an optimum extraction technique was devised (Appendix B), where 10 g of ground core sample was mixed with 30 mL of nanopure water, then shaken with a Burrell Scientific Model 75 wrist action shaker, centrifuged at 3000 rpm for 1 hour in an IEC Centra-4B centrifuge, and filtered through 0.45 μm nitrate membrane filter paper. The resulting aqueous phases were collected in 20 mL scintillation vials and stored at room temperature for Cl analyses. Details of the batch testing are presented in Appendix B.

Pore water Cl concentrations were determined for core samples using the aqueous extract data and a method similar to Van Loon et al. (2007). The pore water Cl concentration for each extract sample (C_{pw}; n=94) was calculated from the analyte Cl concentration using

$$C_{pw} = C_R \cdot \rho_d \cdot \frac{V_L}{M_R} \cdot \frac{1}{n_e}, \tag{4.1}$$

where C_R is the mass of Cl per volume of pore fluid in the extract (mg L^{-1}), M_R is the mass of solute per mass of leached bulk sample, ρ_d is the dry density, V_L is the volume of leach solution per mass of bulk sample leached (the water to rock ratio used in the extraction), and n_e is the effective porosity (Pearson, 1999; Waber and Smellie, 2008). Mazurek et al. (2011) and Koroleva et al. (2011) compare anion concentrations from aqueous leaching tests to squeezed waters from the same rocks to determine the n_e in equation (4.1). The n_e of the Saskatoon Group

till and Lower Colorado shale were estimated by multiplying the n_T (calculated from ρ_d and ω) by the ratio of anion to water accessible porosity, such that the extracted Cl concentrations matched the limited squeezed Cl concentrations. To determine the n_e of the lower Mannville, the Mannville groundwater samples collected during the pump test were used to approximate the pore water Cl concentration. Chloride analyses were performed on the samples from the mechanically squeezed porewaters, the pump discharge samples, and the core extract samples using a Dionex IC25 ion chromatograph (IC) and AS50 autosampler with an accuracy and precision of <5% and a detection limit of 1.0 mg L^{-1}.

4.5.3. Stable Isotopes of Water Analysis (δ^2H and $\delta^{18}O$)

The δ^2H and $\delta^{18}O$ of the porewater in core samples (n=303) were determined using $H_2O_{(liquid)}$-$H_2O_{(vapour)}$ pore water equilibration and laser spectroscopy on a Picarro cavity ringdown spectrometer L1102-i (Wassenaar et al., 2008). The medium sized Ziploc™ bags containing the core samples were inflated with H_2O-free dry air and resealed. The samples were then replaced in the large Ziploc™ bag in which they were stored and the air removed. The samples were allowed to equilibrate to 100% relative humidity at room temperature for 3 days prior to analysis. To correct for instrumental drift and to normalize the results to the VSMOW scale, two water standards with $\delta^{18}O$ and δ^2H values that bracketed that of the porewaters in the core samples were prepared and run after every four samples. The accuracy and precision of this method is better than ±0.3‰ for $\delta^{18}O$ and ±0.8‰ for δ^2H relative to the Vienna Standard Mean Ocean Water (VSMOW) reference (Hendry et al., 2011; Wassenaar et al., 2008). The drill mud was spiked with 99% D_2O to values of δ^2H up to -30‰ at 140-10-087 and OVB-10-207 in order to detect contamination of the core subsamples by drilling fluid. Spiked drill fluids and water samples collected from the pumping well were analyzed for δ^2H and $\delta^{18}O$ using a Los Gatos liquid isotope analyzer, with accuracies of ± 0.8‰ for δ^2H and ± 0.1‰ for $\delta^{18}O$ (Lis et al., 2008) relative to VSMOW.

Additional vapour equilibration analyses were run to determine the length of time core samples can be stored without compromising data quality. The same core samples were analyzed immediately after collection, then again 5 months and 1 year after collection. These tests suggested vapour isotope analyses should be conducted soon after the samples are collected to

avoid evaporative effects. Details of the time series vapour equilibration tests are presented in Appendix C.

The water sample from the pumping well for $^{14}C_{DIC}$ and $\delta^{13}C$ (‰) analyses was analyzed by reducing the sample carbon to graphite (100% C), which was in turn analyzed for ^{14}C in an accelerated mass spectrometer (AMS). The ^{14}C content was reported as fraction of modern day carbon (Fmdn) with an accuracy of ±0.0008. The corrected age of the DIC was calculated using NETPATH geochemical modeling software (Plummer et al., 1994) using a method of El-Kadi et al. (2011a,b). NETPATH applies traditional correction models, including those of Tamers (1975), Ingerson and Pearson (1964), Mook (1972), Eichinger (1983), and Fontes and Garnier (1979).

CHAPTER 5. RESULTS AND DISCUSSION

5.1. Geology of Coreholes

Stratigraphic logging was conducted in drillholes 140-10-087 and OVB-10-207 (Figure 5.1), and photographs taken of selected core samples from the bedrock units (Figure 5.2). Photographs include samples from drillhole 140-10-087, which was drilled to 353 m BG (92.6 m asl). The geology of corehole 140-10-087 consisted of 45 m of surficial sand and silt underlain by 50 m of Saskatoon Group glacial till and sand (Floral Formation), 12 m of Saskatoon Group gravels and sands (Saskatoon Group intertill aquifer), and 9 m of Sutherland Group glacial till (Christiansen and Sauer, 1993). Glacial sediments were underlain by 13 m of Colorado shale (Figure 5.2a), 32 m of KDF (Figure 5.2b-d), 24 m of Lower Colorado Shale (Figure 5.2e), 7 m of Pense volcaniclastic kimberlite (PVK) (Figure 5.2f), and 158 m of Mannville sand, silt, and shale (Figure 5.2g-i). Unlike 140-10-087, the effects of kimberlite volcanism were not evident at OVB-10-207. It was drilled to 204 m BG (238.9 m asl) and intersected 9 m of Mannville sand, silt, and shale, 82 m of Colorado shale (Figure 5.2j-k; Zonneveld et al., 2004), 5 m of Sutherland Group till, 59 m of Saskatoon Group till, and 39 m of surficial sand and lacustrine clay (Christiansen and Sauer, 1993).

The Lower Colorado shale at 140-10-087 was considered highly fractured. Fracture frequency per metre was mapped through the Lower Colorado by identifying fractures and their orientations to core axis immediately after coring (Ugorets and Pereira, 2011). Fracture frequency ranged from 0.3 to 1.7 m^{-1} in the Lower Colorado shale from 326.6 and 312.6 m asl (mean 0.7), to 0.3 to 1.7 m^{-1} in the KDF from 312.6 to 281.6 m asl (mean 0.7), 0.3 to 0.4 m^{-1} in the Lower Colorado from 281.6 to 257.1 m asl (mean 0.3), and 0.3 m^{-1} throughout the PVK from 257.1 to 250.6 m asl. Fractures within the shale were smooth and displayed no mineral infill on the surfaces (Figure 5.2a). Fractures within the KDF unit were commonly infilled with calcite (Figure 5.2b) or had slickensided fracture surfaces. Fractures were estimated to be at high inclinations from 10 and 60 degrees to core axis.

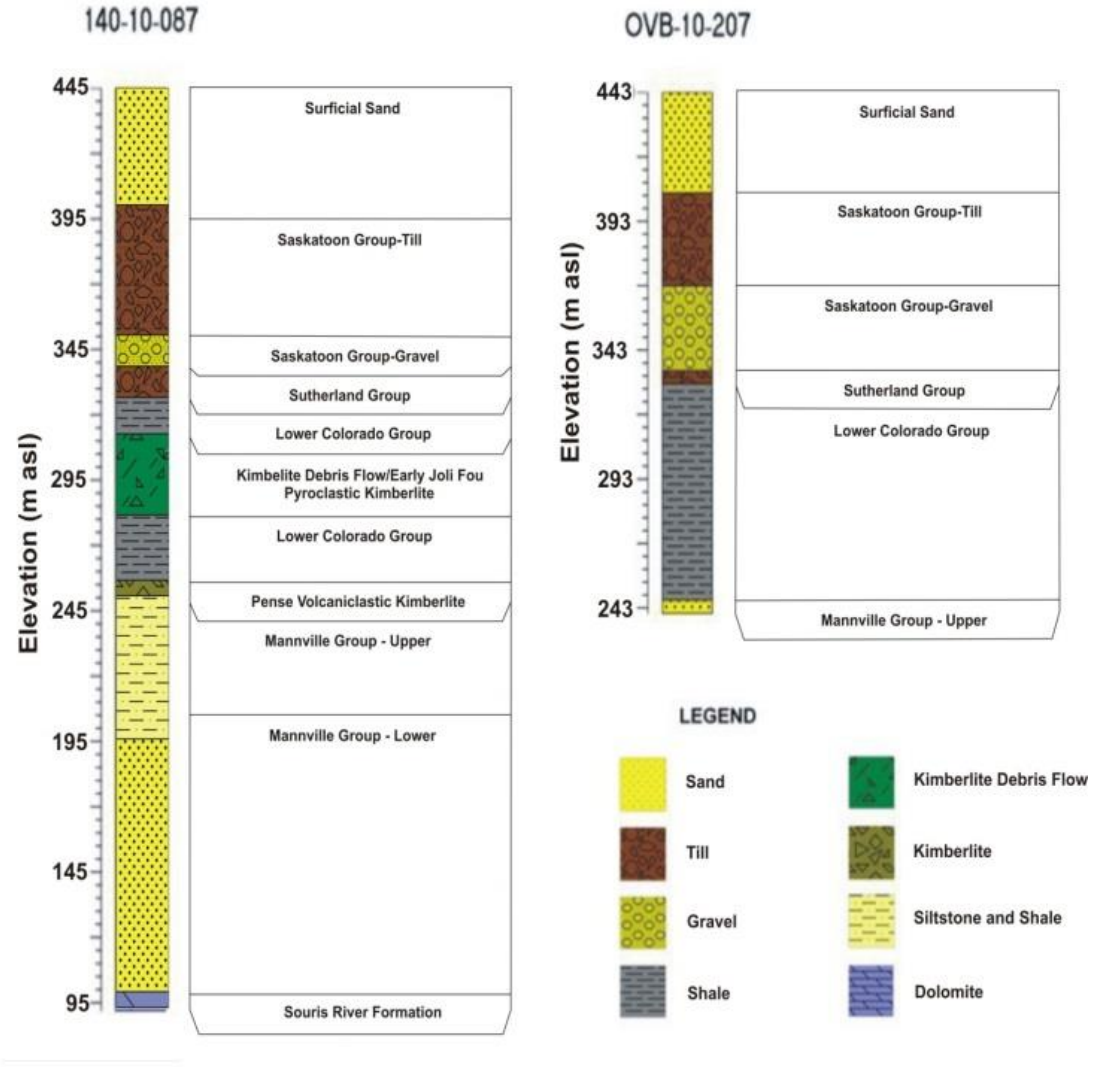

Figure 5.1. Stratigraphic logs from coreholes 140-10-087 and OVB-10-207.

Figure 5.2. Core photographs from 140-10-087 (a-i) of fractured Colorado shale (a), fractured kimberlite with calcite infill (b), KDF (c), kimberlite with calcite veins within KDF (d), typical Colorado shale with sand lenses (e), PVK (f), laminated siltstone and clay of the upper Mannville group (g), mudstone of the upper Mannville (h), and typical sandstone of the lower Mannville (i). Photographs j and k were taken at OVB-10-207 and were characteristic of undisturbed Colorado shales in which no kimberlite was observed.

Two aquifers were identified in the study area: the Saskatoon Group intertill aquifer and the Mannville sand and silt (Figure 5.1). The Saskatoon Group intertill gravel aquifer was observed in both drillholes, from 350.6 to 338.6 m asl in 140-10-087 and from 367.9 to 333.9 m asl in OVB-10-207. The Mannville sand and silt, which formed the base of this investigation, was sub-divided into the upper and lower Mannville based on the geologic and hydrogeologic properties in this formation. In general, the upper 60 m of the Mannville is dominated by unconsolidated silt, very fine grained sand, and laminated silt and clay (Figure 5.2g-h) while the lower 90 m consists of a greater portion of unconsolidated fine to medium-grained sand with lesser amounts of laminated siltstone, clay, and small amounts of coal (Figure 5.2i).

5.2. Laboratory Testing

5.2.1. Total Porosity

The n_T values were calculated for individual core samples from both boreholes (Figure 5.3). The n_T values and associated ρ_d and ω values were also calculated for each geologic unit (Table 5.1; Appendix D). The consistent values of n_t through the Saskatoon Group and Sutherland Group tills reflect their geologically homogeneous character with depth. Mean n_T values at OVB-10-207 were 0.60±0.02 (n=3) in the surficial sand/lacustrine clay and 0.24±0.04 (n=13) in the Saskatoon Group till. Because the surficial sand and clay were unconsolidated and difficult to keep intact during testing, the n_T values measured for these samples are likely overestimates. At 140-10-087, mean n_T values were 0.24±0.06 (n=15) and 0.34±0.04 (n=4) in the Saskatoon and Sutherland Group tills, respectively. No n_T values were determined for the Saskatoon Group gravel aquifer due to 100% core loss for this unit in both drillholes; however, Keller et al. (1986) estimated an n_T of 0.25 through the Saskatoon Group glacial till near Saskatoon, Saskatchewan.

Table 5.1. Mean, standard deviation (σ), and maximum and minimum values of total porosity (n_T), dry bulk density (ρ_d), and gravimetric water content (ω) determined from core samples of each geologic unit collected from drillholes 140-10-087 and OVB-10-207.

	n_T					ρ_d (kg m^{-3})				ω			
Group	n	mean	st dev	max	min	mean	st dev	max	min	mean	st dev	max	min
140-10-087													
Saskatoon	15	0.22	0.02	0.27	0.18	2.06	0.06	2.17	1.98	0.07	0.01	0.09	0.06
Sutherland	4	0.34	0.04	0.39	0.30	1.76	0.11	1.86	1.61	0.12	0.03	0.15	0.08
KDF	8	0.46	0.06	0.58	0.41	1.44	0.16	1.56	1.30	0.21	0.09	0.38	0.11
Lower Colorado	10	0.40	0.05	0.52	0.33	1.58	0.14	1.68	1.28	0.18	0.02	0.20	0.16
upper Mannville	16	0.36	0.03	0.42	0.30	1.69	0.07	1.87	1.54	0.14	0.02	0.16	0.12
lower Mannville	11	0.36	0.09	0.49	0.25	1.70	0.24	1.99	1.35	0.15	0.06	0.25	0.09
OVB-10-207													
Surficial Sand/clay	3	0.60	0.02	0.58	0.62	1.09	0.05	1.13	1.04	0.33	0.02	0.34	0.31

Saskatoon	13	0.24	0.04	0.32	0.19	2.06	0.10	2.12	1.83	0.08	0.02	0.12	0.06
Sutherland	0	n/a	n/a										
Lower Colorado	26	0.45	0.05	0.55	0.38	1.47	0.13	1.65	1.21	0.18	0.08	0.22	0.14
lower Mannville	4	0.37	0.08	0.44	0.28	1.69	0.22	1.95	1.50	0.14	0.04	0.18	0.10

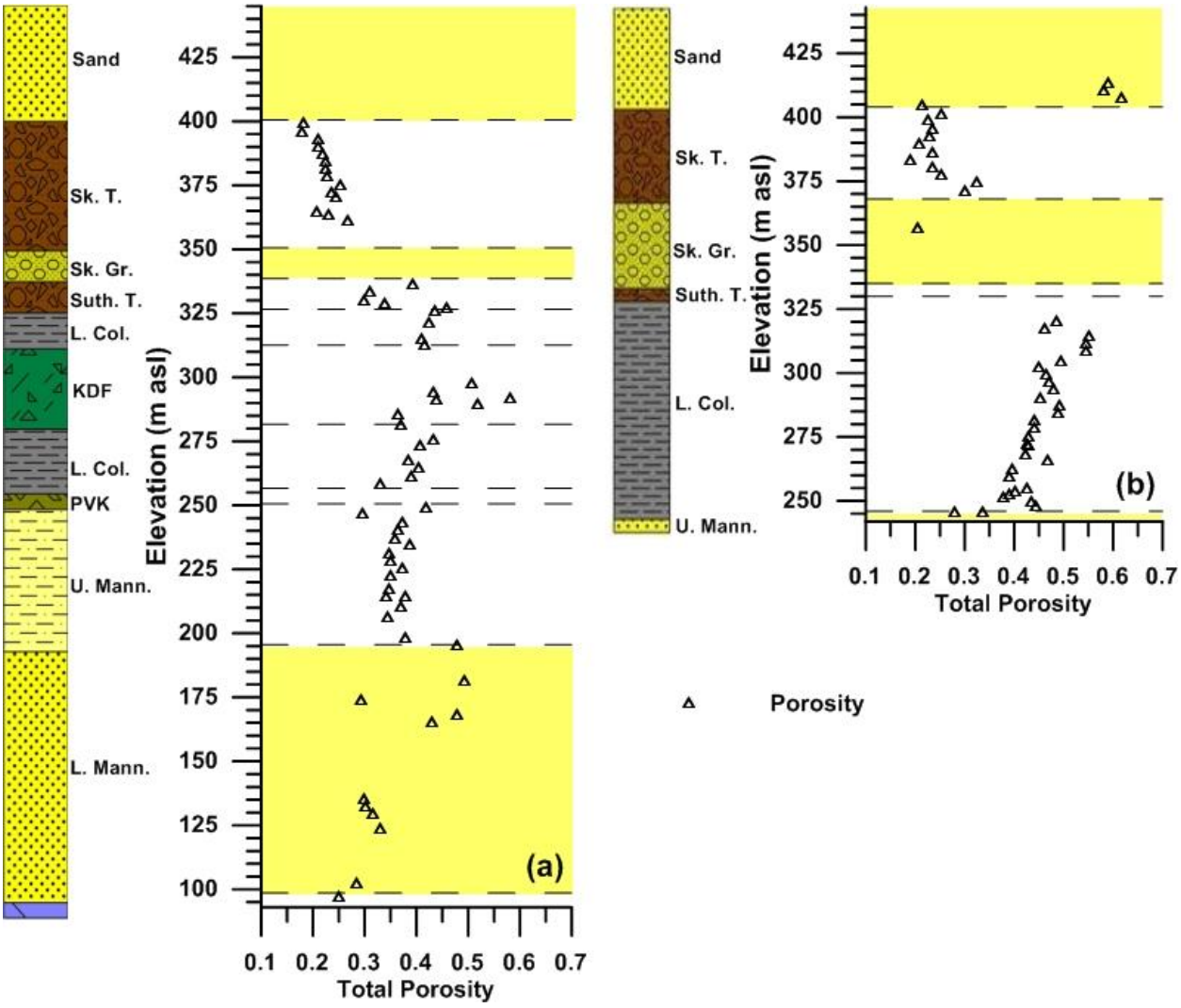

Figure 5.3. Total porosity (nT) determined for core samples collected from coreholes 140-10-087 (a) and OVB-10-207 (b).

The mean n_T of the Colorado shale was determined to be 0.40±0.05 (n=10) and 0.45±0.05 (n=26) at boreholes 140-10-087 and OVB-10-207, respectively. Mean n_T of the KDF at 140-10-087 was determined to be 0.46±0.06 (n=8). Similar n_T values are reported for Cretaceous-aged shale throughout the Williston Basin. Shaw and Hendry (1998) report mean n_T values of 0.37 to 0.44 in the Cretaceous-aged Snakebite Member of the Bearpaw formation. Nichols et al. (1986) report n_T values of up to 0.35 in the Pierre shale near Hayes, South Dakota, and Neuzil (1994) reports n_t values for the Pierre shale of between 0.1 and 0.4. Smith et al.

(2013) report n_T values of the Pierre, 1st and 2nd speckled, and Belle Fourche shales between 0.30 and 0.45.

Porosity values in the Colorado shale decrease with depth, from 0.49 at 329.9 m asl to 0.37 at 247.9 m asl in OVB-10-207. These data suggest decreases in porosity with depth may be associated with consolidation following deposition, consistent with the findings of Hendry et al. (2011) and Shaw and Hendry (1998) for 20 Ma younger Cretaceous-aged Bearpaw shale. Porosity values determined through the KDF at 140-10-087 show no distinct trend with depth and range from 0.41 to 0.58 with a high standard deviation (0.06). These data suggest that kimberlite emplacement altered the n_T distribution at this site. KDF, by its nature, is highly altered and variable in lithology. As a result, variations in geotechnical properties are expected. The n_T of the shale both above and below the KDF at 140-10-087 (from 326.6 to 312.6 m asl and 281.6 to 250.6 m asl) is more uniform with depth (ranging from 0.33 to 0.52) and similar to values at similar depths in OVB-10-207.

Mannville sediments were only sampled at 140-10-087. The n_T decreases with depth in the upper 55 m (250.6 to 190.6 m asl), where the sediments are fine-grained with a mean n_T of 0.36±0.03 (n=16; Figure 5.3, Table 5.1). Between 190.6 and 145.6 m asl, the average n_T increases to 0.49±0.07 (n=5) and exhibits no trend with depth. From 145.6 to 95.6 m asl, the n_T decreases with depth and has an average value of 0.32±0.02 (n=6). The n_T of the Mannville, in general, decreases from 0.33 at the base of the Colorado shale to 0.25 at the top of the Souris River dolomite. Similarly, Jessop and Vigrass (1989) present average n_T values of 0.25 for the Mannville sand near Regina, Saskatchewan and Bachu (1985) presents average n_T values of 0.33 to 0.34 for the upper and lower Mannville sands, respectively, near Cold Lake, Alberta.

5.2.2. Laboratory Hydraulic Conductivity

Laboratory testing of samples at OVB-10-207 yielded K results (2×10^{-10} to 2×10^{-11} m s^{-1}) within the same order of magnitude as those determined by laboratory testing at 140-10-087 (2×10-10 to 2×10^{-11} m s^{-1}), suggesting that the hydraulic properties of the shale across the site are spatially consistent when no kimberlite is present. The increase in Kv at 305.9 m asl at OVB-10-207 (2×10^{-10} m s^{-1}) and 280 to 266.8 m asl at 140-10-087 (1×10^{-10} to 2.0×10^{-10} m s^{-1}) suggests the presence of sand layers within the Lower Colorado shale. Low core recovery in the Lower

Colorado shale (0-100%; mean 75%) could bias the results to lower K values because the fractured zones are likely not represented due to poor core recovery. X-ray diffraction (XRD) analysis indicates that the clay mineralogy at both locations is similar (Appendix E). The regional groundwater study at the site conducted by Ugorets and Pereira (2011) reports similar Kv trends measured by falling head tests (FHT) and packer injection tests (PIT) (Table 5.2; Figure 5.4) for the Lower Colorado shale at 150-05-014, which was not influenced by kimberlite (4.4×10^{-9} to 5.1×10^{-10} m s^{-1}), as well as SHP-08-006 (1.7×10^{-7} to 9.1×10^{-9} m s^{-1}) and SHP-08-004 (6.5×10^{-9} m s^{-1}), which were affected by kimberlite emplacement (Figure 2.1). Drillholes SHP-08-006 and SHP-08-004 were influenced by kimberlite volcanism to a greater extent than 140-10-087 (this study), and yielded greater field measured K values (Figure 5.4; Table 5.2) than the drillholes with no kimberlite units observed. This may be attributed to the presence of a greater number of transmissive fractures in the kimberlite and shale units in these drillholes. Results of the triaxial tests also suggested that because the effective stress applied to the samples was considerably less than in situ effective stress swelling of the core samples may have occurred within the triaxial cell. Mithcell (1993) suggested that this could result in an overestimation of K up to two orders of magnitude.

Table 5.2. Hydraulic conductivity (K) values determined at drillholes 140-10-087 and OVB-10-207 and data obtained from piezometers installed proximal to these coreholes for comparison.

Colorado Group				**Mannville Group**			
Drillhole ID	**Interval**	**K (m s^{-1})**	**Testing Method**	**Drillhole ID**	**Interval**	**K (m s^{-1})**	**Testing Method**
140-10-087	Colorado†	2.0×10^{-11}	Triaxial	150-05-014*	upper Mannville	4.6×10^{-8}	FHT
	KDF†	2.0×10^{-11}	Triaxial		upper Mannville	3.7×10^{-7}	PIT
	KDF†	2.0×10^{-10}	Triaxial	PW-2*	Mannville	1.9×10^{-5}	7 Day Pump Test
	Colorado†	1.0×10^{-10}	Triaxial	PW-4*	Mannville	1.7×10^{-5}	7 Day Pump Test
	Colorado†	4.0×10^{-11}	Triaxial	SHP-08-004*	upper Mannville	1.2×10^{-9}	PIT
	PVK†	5.0×10^{-11}	Triaxial		upper Mannville	9.3×10^{-9}	PIT
OVB-10-207	Colorado	3.0×10^{-11}	Triaxial	SHP-08-006*	upper Mannville	1.2×10^{-9}	PIT
	Colorado	2.0×10^{-10}	Triaxial				
	Colorado	4.0×10^{-11}	Triaxial				
	Colorado	2.0×10^{-11}	Triaxial				
	Colorado	4.0×10^{-11}	Triaxial				
150-05-014*	Colorado	5.1×10^{-10}	PIT				
	Colorado	4.4×10^{-9}	FHT				

SHP-08-004*	Colorado†	6.5×10^{-8}	PIT
SHP-08-006	Colorado†	9.1×10^{-9}	PIT
	Colorado†	1.7×10^{-7}	PIT

† Indicates units impacted by kimberlite volcanism

*Indicates supplementary data from Ugorets and Pereira (2011)

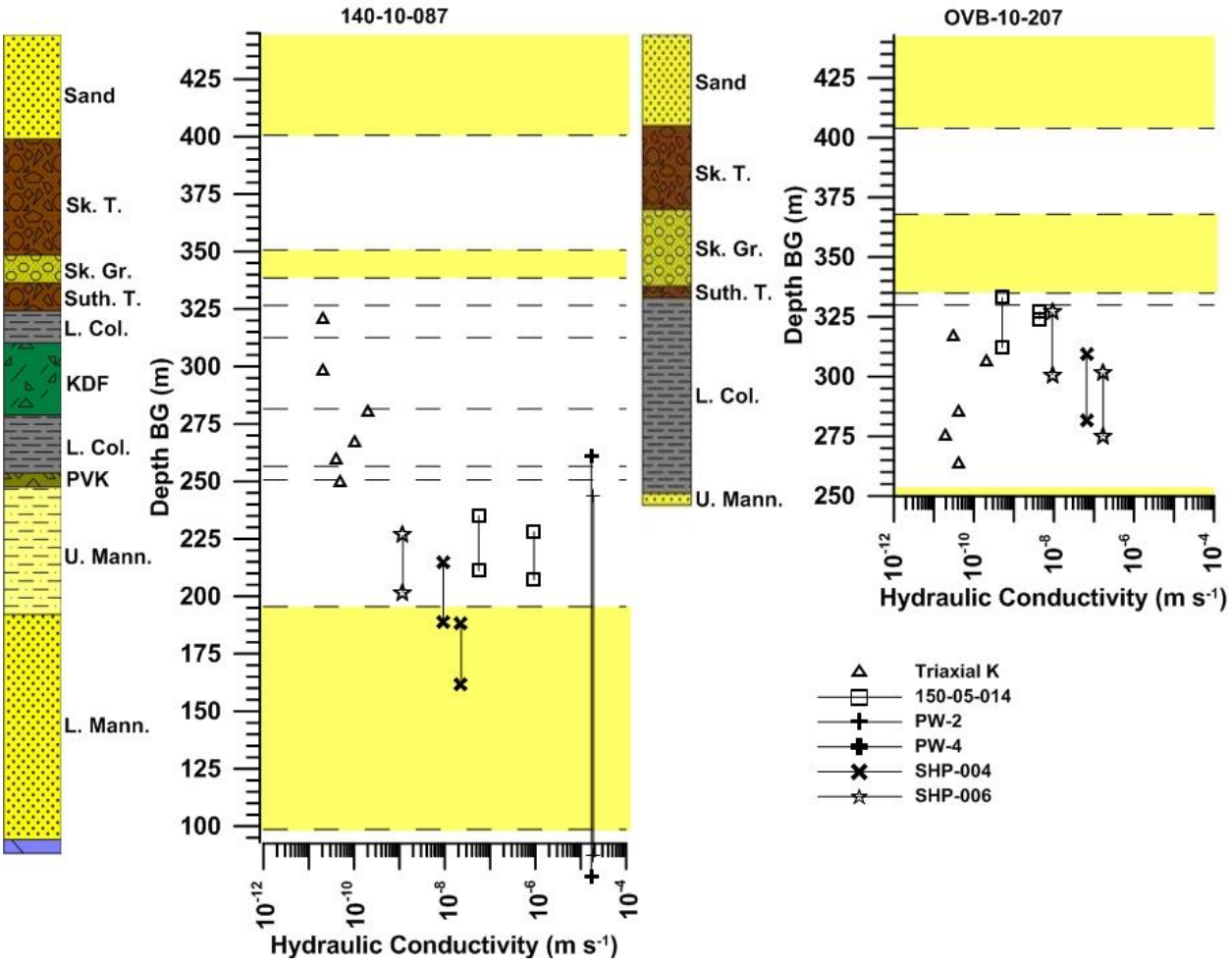

Figure 5.4. Summary of vertical hydraulic conductivity (Kv) measurements on core samples from triaxial hydraulic conductivity (K) testing at coreholes 140-10-087 and OVB-10-207 as well as K data obtained using FHT, PIT, and a 7-day pumping test at regionally located piezometers 150-05-014, PW-2, PW-4, SHP-08-004, and SHP-08-006 for the same geologic units (from Ugorets and Pereira, 2011).

5.3. Hydraulic Gradient, Specific Storage and Pumping Test Simulations

Total hydraulic head and gradients in the glacial sediments were determined using total head data from piezometers installed in OVB-10-207 and 140-10-087 and total head data from piezometers and vibrating wire piezometers (VWP) installed at 140-10-080, 141-10-094, 141-10-096, 140-10-085, and OVB-10-205 (Figures 2.1 and 5.5; Ugorets and Pereira, 2011). The initial static total head at the transducers located at 301.1, 280.5, and 241.9 m asl were estimated using the mean h_t of the final 22 days of recorded VWP total head data (March 1 to March 22, 2011); early time data between October 4 and 22, 2010 (when the pumping test began) suggested that water levels in VWPs installed at 140-10-087 did not attain steady state prior to the onset of pumping (Appendix A). Total head data from supplementary piezometers at 150-05-014, PZ-1, and PZ-3 (Table 5.3; Figure 5.5) were also used to estimate horizontal gradients in the Mannville as well as the direction of groundwater flow after steady state was attained. Gradients and groundwater flow direction in the Mannville should be estimated using more than the two wells described here but such data were not available at the study site.

Table 5.3. Depths of piezometers, corresponding geological units, and total head (h_t) values for regional piezometers identified in Figure 2.1 (Ugorets and Pereira, 2011).

Drillhole ID #	Geological Unit	Piezometer Elevation (m asl)	Total Head (m)	Drillhole ID #	Geological Unit	Piezometer Elevation (m asl)	Total Head (m)
OVB-10-207	Surficial Sand	409.01	425.83	OVB-10-205	Surficial Sand	410.08	420.90
	Saskatoon Group	372.61	394.96		Saskatoon Group	369.38	404.82
	Sutherland Group	332.11	387.66		Sutherland Group	334.58	387.10
	Lower Colorado Group	327.11	388.70		Lower Colorado Group	324.38	388.07
140-10-080	Surficial Sand	407.67	429.28	140-10-087	Lower Colorado Group	301.10	387.51
	Saskatoon Group	365.57	401.39		Lower Colorado Group	280.50	388.00
	Sutherland Group	336.97	385.52		upper Mannville	241.90	390.50
	Lower Colorado Group	325.67	386.12		lower Mannville	174.30	391.90

141-10-094	Surficial Sand	408.09	425.21	150-05-014	Lower Colorado Group	325.58	403.20
	Saskatoon Group	363.09	387.79		upper Mannville	222.94	409.00
	Sutherland Group	339.79	388.48	PZ-3	upper Mannville	176.66	397.50
	Lower Colorado Group	328.79	400.14		lower Mannville	119.51	396.90
141-10-096	Surficial Sand	409.47	429.41	PZ-1	lower Colorado Group	302.00	390.00
	Saskatoon Group	375.27	410.96		lower Colorado Group	272.00	388.30
	Sutherland Group	334.57	391.53		lower Mannville	170.00	390.30
	Lower Colorado Group	328.47	389.73		lower Mannville	117.00	393.90
140-10-085	Surficial Sand	402.96	419.37				
	Saskatoon Group	364.56	394.74				
	Sutherland Group	336.46	386.29				
	Lower Colorado Group	328.46	385.49				

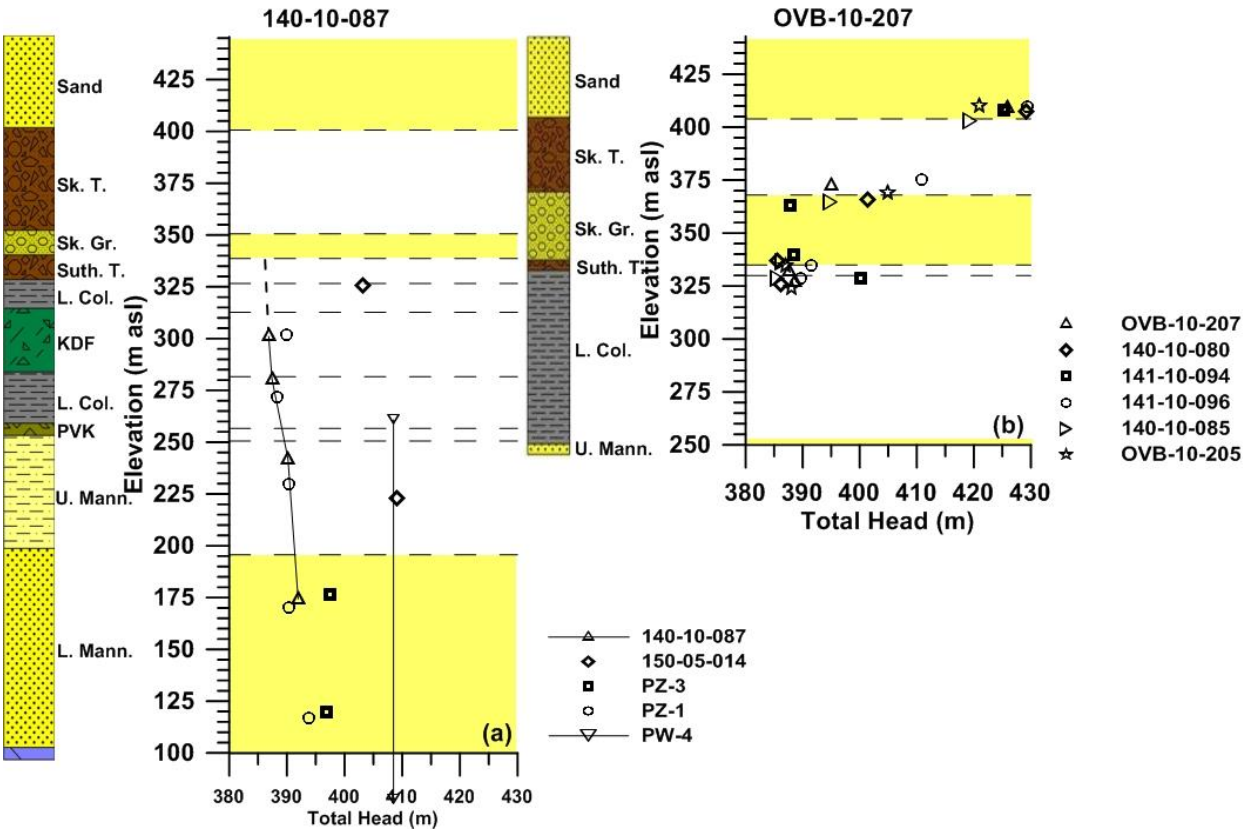

Figure 5.5. Total head distributions of vibrating wire piezometers installed in the Joli Fou and Mannville shale (a; 140-10-087) and the surficial sand and glacial till (b; OVB-0-207). The total head profile at 140-10-087 is extrapolated to the Saskatoon Group intertill aquifer (dashed line in a). Total head data were corrected for density effects. Data obtained from piezometers installed proximal to boreholes 140-10-087 and OVB-10-207 (Ugorets and Pereira, 2011) are plotted for comparison.

The hydraulic gradient across the Saskatoon Group till indicates groundwater flow is downward from ground surface to the Saskatoon Group intertill aquifer, with an average gradient of 0.32 through the Saskatoon Group till. Hydraulic gradients through the formations below the intertill aquifer (i.e., Sutherland Group glacial sediments and Colorado shale) were upward or near hydrostatic. The average vertical gradient through the Sutherland Group till was estimated to be 0.32, while the average vertical gradient through the Colorado shale and Mannville sediments ranged from 0.03 to 0.07. The vertical gradients from ground surface to the Saskatoon Group intertill aquifer are oriented downward. The lowest heads in the Lower Colorado shale and KDF at 140-10-087 have h_T values similar to those observed in the intertill aquifer (h_T=386

m), which differ from those observed at the top of the Lower Colorado shale at 150-10-014 (403.2 m) and 141-10-094 (400.14 m). This suggests that these low h_T values may be controlled by lateral connection to the Saskatchewan River.

The α was determined for the Lower Colorado shale and Mannville shale, silt, and sand based on the barometric loading efficiency as evaluated from static pressure head values recorded by transducers installed at 301.1, 280.5, 241.9, and 174.3 m asl in 140-10-087. The loading efficiency was estimated using the method described by Smith et al. (2013). The values of α at elevations of 301.1 and 280.5 m asl were determined to be 3.2×10^{-7} and 2.8×10^{-7} kPa^{-1}, respectively. The value of α at elevations of 241.9 and 174.3 m asl was 1.7×10^{-7} kPa^{-1}. The α of the Lower Colorado shale decreases slightly with depth, suggesting increasing stiffness with depth; this is consistent with the decreasing n_t values with increasing depth (Figure 5.1) at 140-10-087 and OVB-10-207. Smith et al. (2013) document decreasing α values with depth through the Pierre, 1st and 2nd Speckled, and Belle Fourche shales (3.1×10^{-6} to 4.1×10^{-7} kPa^{-1}). They attribute the decrease to increasing consolidation with depth, with values of the same order of magnitude as those determined in transducers installed at 301.4 and 280.8 m asl at 140-10-087 (3.2×10^{-7} and 2.8×10^{-7} m^{-1}, respectively). Because of greater overburden thickness due to both ice from past glaciations (up to 2 km thick) and sediments (1-3 km thick) that were deposited and later eroded during the middle to late Tertiary, the Cretaceous shales in the Williston Basin are generally considered to be overconsolidated with depth (Dawson et al., 1994; Smith et al., 2013).

S_s values at transducers installed at 140-10-087 were estimated using equation (3.5) and α values determined from loading efficiencies. S_s values were estimated to be 5.2×10^{-6} and 4.6×10^{-6} m^{-1} at elevations of 301.1 and 280.5 m asl, respectively, and 3.2×10-6 m^{-1} at elevations of 241.9 and 174.3 m asl.

K_h values were estimated from two-dimensional transient flow modeling and K_v values from one-dimensional steady-state flow modeling (Appendix A; Table A.2.; Figure A.7). While the simulations of the pumping tests could to provide an accurate estimate of K in the aquifer and aquitard units, the simulations demonstrated that the effect of pumping were not observed in the aquitard for estimated K_v values of less than 3×10^{-9} and 5×10^{-9} m s^{-1} in the KDF (301.1 to 280.5 m asl), 9×10^{-10} and 2×10^{-9} m s^{-1} in the Lower Colorado and PVK (280.5 to 250.6 m asl) and 2×10^{-10} and 4×10^{-10} m s^{-1} in the upper Mannville. K_h values estimated from the pumping tests in

the lower Mannville were estimated to be between 2.5×10^{-10} and 2.75×10^{-5} m s^{-1} (Figure A.7). K_v values in the KDF and Lower Colorado were one to two orders of magnitude greater than K_v estimated from triaxial testing in the same units and from values estimated from solute transport modeling (described below). The overestimation of K_v through the aquitard units from pumping test simulations may be the result of heterogeneities within the aquitard and aquifer units not addressed in the laboratory testing (Neuzil, 1994). The pumping test performed at this site could not provide an accurate estimate of K_v in the aquitard units, because the aquitard units were not stressed and showed no drawdown during the pumping test. Hantush (1967) described a method to describe leakage from confining units into the solution of the well equation, provided it fit the criteria that B is less than 0.10. At the study site, B was calculated to be 13,000, suggesting the thickness of the aquifer and its transmissivity were too large compared to the confining unit to yield drawdown in the aquitard during the pumping test. Results of the pumping tests suggested that the limitations of 2-D axisymmetric modeling to estimate larger scale lateral heterogeneity (i.e. kimberlite bodies) as well as lateral boundary conditions (Saskatchewan River) rendered it inadequate to estimate hydraulic parameters. Also, the lack of response in the Lower Colorado shale to the pumping tests in the lower aquifer suggested an inability to sufficiently stress the system and induce leakage, likely due to the thickness and regional extent of the aquifer being pumped in comparison to the thickness of the overlying Lower Colorado aquitard (Hantush, 1967).

5.4. Anion Accessible Porosity and Chloride Profiles

The n_e for Cl was initially constrained by comparing Cl concentrations obtained by aqueous leaching with pore water Cl concentrations from mechanical squeezing and from Mannville groundwater samples collected during the 22-day pump test (Koroleva et al., 2011). The calculated n_e values in the glacial till using this method were determined to range from 0.18 to 0.27 and the ratio of n_e to n_t was determined to be 100%, suggesting that all of the connected pore space was accessible to anions. These results are not consistent with the ratio of $n_e=0.8n_T$ calculated for the Battleford Glacial Till in Saskatchewan (Hendry et al., 2000). The contrast may be due to the fact that their study area consisted exclusively of Battleford Formation while the Shore Gold Inc. study area consisted of glacial sediments deposited prior to the deposition of the Battleford Formation in Saskatchewan. The glacial sediments at the study area may have had a greater sand content than those described by Hendry and Wassenaar (1999), thereby decreasing

the effect of anion exclusion through negatively charged clay particles in the glacial till. The ratio of n_e to n_T was estimated to be 30% in the upper part of the Lower Colorado (327 to 313 m asl) and in the KDF (313 to 291 m asl), the Lower Colorado, and the Pense kimberlite. The length of storage time of the squeezed samples before analyses could be performed (6 months), and evidence of isotopic fractionation when compared to samples analyzed using the vapour method (data not presented), led to the assumption that the squeezed Cl concentrations may be concentrated due to water loss, thus rendering them inadequate to accurately calculate n_e values in the shale. As a result, n_e values were estimated to be between 0.4 and 0.6 n_e/n_T. These values were chosen to be consistent with reported values for other clay-rich aquitards. Mazurek et al. (2011) report ratios of n_e to n_T of 0.43 in the Boom Clay in Belgium and 0.5 in the Callovo-Oxfordian Clay in France. Similarly, Hendry et al. (2000) report ratios of 0.30 in the Battleford till and 0.38 in the snakebite clay in Saskatchewan, Canada. Van der Kamp et al. (1996) report ratios of n_e to n_T of 0.43 to 0.63 in clay-rich tills collected near Warman, Saskatchewan.

The estimated n_e/n_T of 0.4 and 0.6 resulted in n_e values of 0.16 to 0.24, respectively, in the Lower Colorado Shale at 140-10-087. This ratio suggested that only 40 to 60% of the interconnected pore space in this media was accessible to anions. Similarly, the estimated n_e/n_T ratios of 0.4 and 0.6 in the Lower Colorado shale at OVB-10-207 yielded n_e values of 0.18 and 0.27, respectively. The ratio of n_e to n_T applied to the upper and lower Mannville sand, silt, and clays was estimated at 100%, based on transport simulations described below.

XRD and clay content analysis of Lower Colorado shale core samples suggested that the mineralogy and clay content of the Lower Colorado shale (not including KDF) in both 140-10-087 and OVB-10-207 were similar (Appendix E). As such, the n_e estimated at 140-10-087 (n_e=0.40 to 0.60n_T) was applied to the Cl concentrations of core samples from aqueous leaching in the Lower Colorado shale at OVB-10-207.

The vertical distribution of calculated pore water Cl concentrations (equation 4.1) with depth at 140-10-087 and OVB-10-207 are presented in Figure 5.6. At 140-10-087, the Cl concentrations in the glacial till and KDF (399 to 270 m asl) were vertically constant and ranged from 130 to 840 mg L^{-1}. The pore water Cl concentration increases from 840 mg L^{-1} at the base of the KDF (270 m asl) to 1,670 and 2,500 mg L^{-1} (calculated using n_e/n_T of 0.6 and 0.4, respectively) at the boundary between the Lower Colorado and upper Mannville (247 m asl),

then decreased again to 910 and 1,370 mg L^{-1} (calculated using an n_e/n_T ratio of 1) at 225 m asl. Below 225 m asl, the concentration ranged from 740 to 1,110 with an average of 1,020 mg L^{-1} (calculated using an n_e/n_T ratio of 1) to the base of the Mannville at 99 m asl.

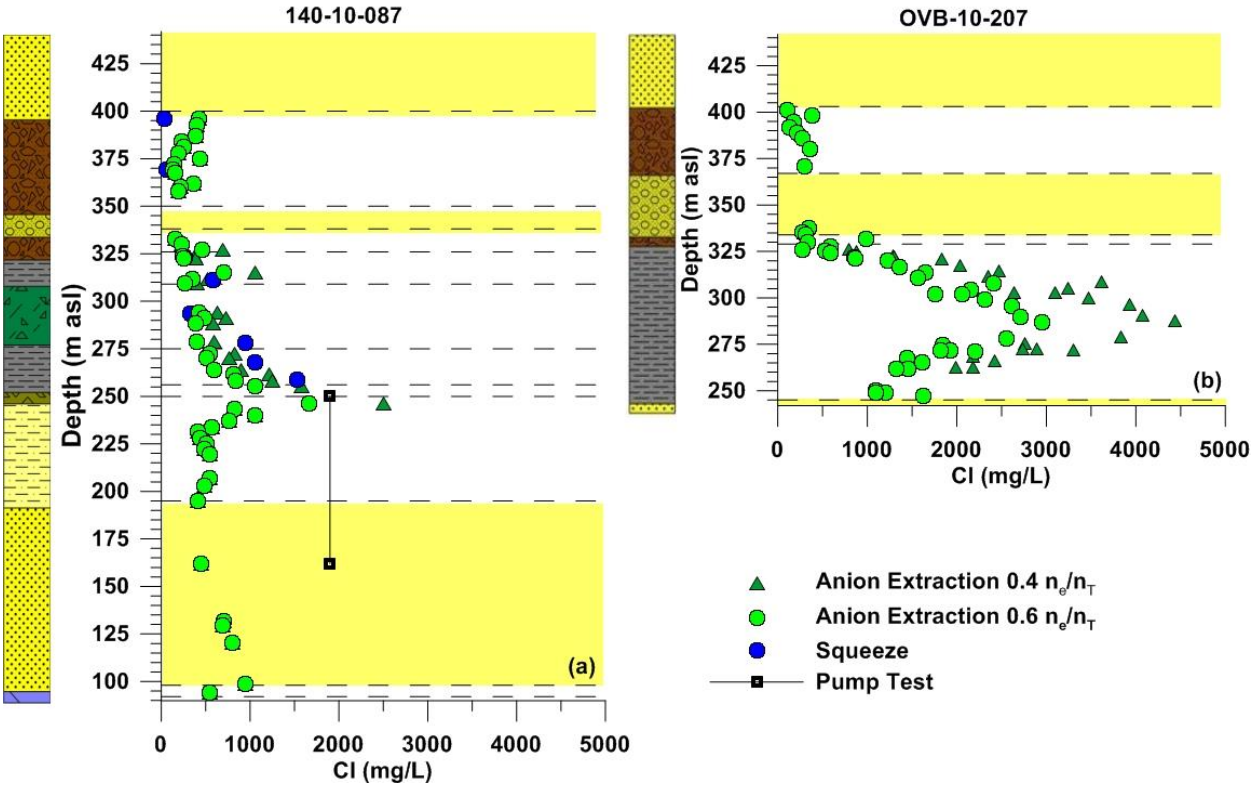

Figure 5.6. Cl concentrations determined from aqueous extractions, mechanical squeezing, and pump test waters for borehole 140-10-087 (a) and OVB-10-207 (b). Pore water Cl concentrations were corrected from aqueous extraction data by estimating n_e/n_T values of 0.4 and 0.6 in (a) and (b), respectively. The vertical dashed line in (a) represents the average Cl concentration of pump test water collected from a well screened from 250.6 to 162.6 m asl.

At OVB-10-207, the lack of variability in Cl concentration with depth in the glacial till, as observed at 140-10-087, was attributed to low variability of Cl concentration in the till during deposition that resulted in an initially uniform vertical Cl profile (Hendry et al., 2000). The Cl concentration in the glacial till ranged from 110 to 1,000 mg L^{-1} with depth (410 to 330 m asl; Figure 5.6b). A symmetrical, well-defined diffusion-like trend was observed in the Lower Colorado shale between the base of the glacial till (330 m asl) and the top of the upper Mannville (248 m asl), increasing from 1,290 and 860 mg L^{-1} (using n_e/n_T ratios of 0.4 and 0.6, respectively) at the top of the Lower Colorado shale (329 m asl) to 5,300 and 3,500 mg L^{-1}

(using n_e/n_T ratios of 0.4 and 0.6, respectively) in the middle of the Lower Colorado (284 m asl), then decreasing again with depth to 2,740 and 1,830 mg L^{-1} (using ratios of 0.4 and 0.6, respectively) at the top of the upper Mannville (248 m asl). The Cl concentration in the pumping test water (1,940 mg L^{-1}) was considerably greater in the leach extract through the upper and lower Mannville. This may be attributed to the pumping test well (140-10-089) being located approximately 200 m from 140-10-087. The Cl concentration in the Lower Colorado and upper Mannville may be greater at 140-10-089, thus increasing the Cl concentration in the water drawn from those formations during pumping. As was the case with δ^2H and $\delta^{18}O$ (see discussion below), the Cl concentration may be a mixture of water from the bottom of the Lower Colorado shale, the upper Mannville, and the lower Mannville, as 140-10-089 was screened from the base of the Lower Colorado shale through the upper Mannville and 30 m into the lower Mannville.

5.5. δ^2H and $\delta^{18}O$ Profiles

Pore-water δ^2H and $\delta^{18}O$ values for all core samples at 140-10-087 and OVB-10-207, as well as Mannville groundwater collected during the pump test, were cross plotted in Figure 5.7. The δ^2H and $\delta^{18}O$ values of the three Mannville groundwater samples collected during the pump test lie on the LMWL and ranged from -143 to -145‰ and -18.3 to -18.6‰, respectively (Figure 5.7). The data sets for 140-10-087 and OVB-10-207 yielded linear trends (δ^2H = 5.87, $\delta^{18}O$-52.12, R^2 = 0.82 and δ^2H = 6.50, $\delta^{18}O$-27.45, R^2 = 0.80, respectively). The shallow slope of the lines with respect to the local meteoric water line for Saskatoon (LMWL; δ^2H = 7.73, $\delta^{18}O$-1.72, R^2 = 0.96; Hendry et al., 2011, 2013) suggests that the core samples may have been subject to evaporation after sampling (Hendry et al., 2011; Kelln et al., 2001). The δ^2H and $\delta^{18}O$ values of the rotary drill fluid spiked during coring for each corehole plot above the LMWL, with δ^2H and $\delta^{18}O$ values ranging from -28 to -150‰ and from -14 to -19‰ at 140-10-087 and from -48 to -111‰ and from -15 to -16‰ at OVB-10-207, respectively (Figure 5.7; Hendry et al., 2013). The few core samples from each corehole that plot above the LMWL (n=18) are consistent with the values for the spiked drill fluids. As such, these samples were considered contaminated and are not discussed further.

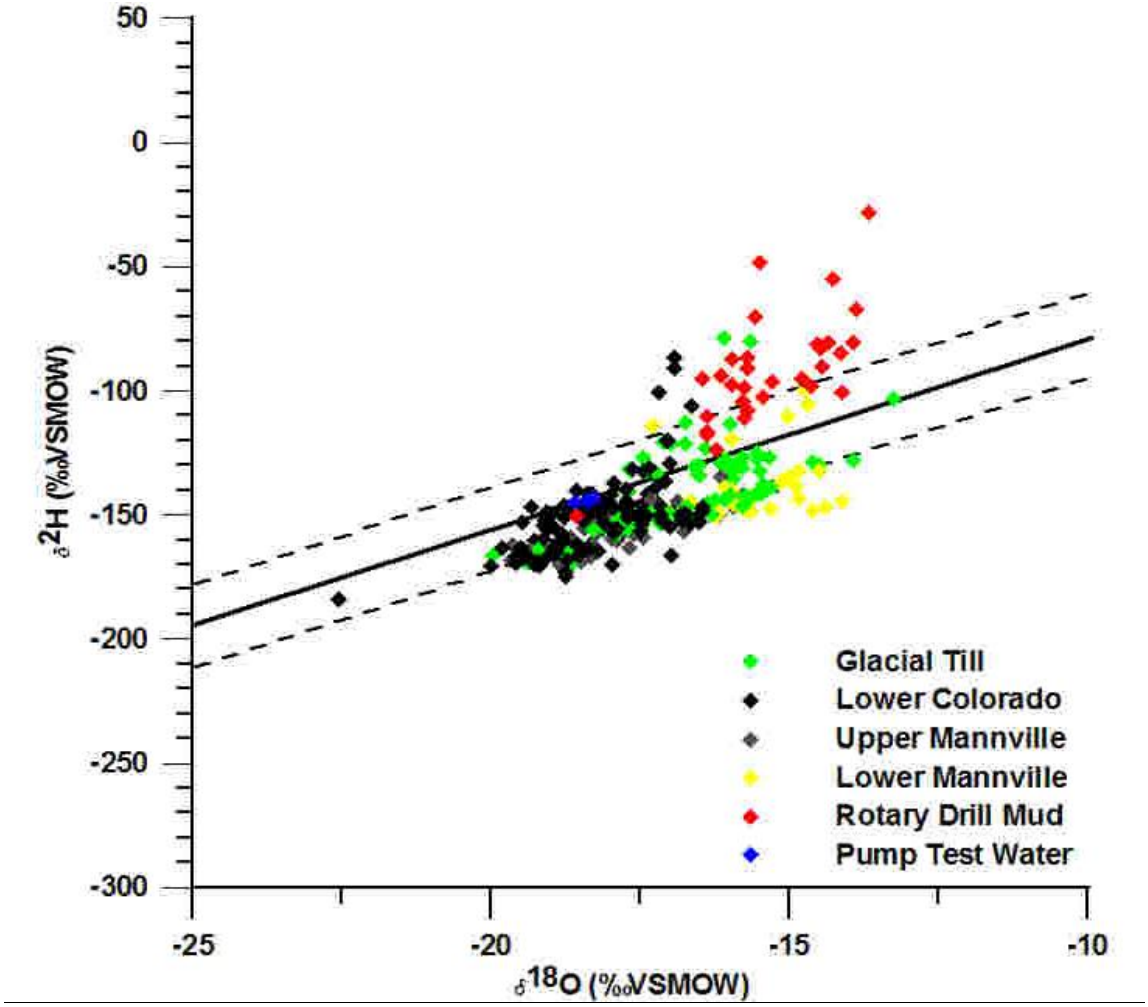

Figure 5.7. Plot of δ^2H versus $\delta^{18}O$ for porewater collected from core samples at OVB-10-207 and 140-10-087 and drilling fluid used to core at both drillholes. The solid line represents the Saskatoon local meteoric water line and the dashed lines represent the 95% confidence interval of precipitation data.

Pore-water δ^2H vs. $\delta^{18}O$ were plotted for all core samples collected from both drillholes, as well as Mannville groundwater collected during the pump test (Figure 5.7). Core samples collected from the glacial till range from -138 and -15‰ to -171 and -19‰ for δ^2H and $\delta^{18}O$, respectively, representing a transition from modern meteoric water at the surface to glaciogenic water at the base of the glacial till. Core samples collected from the Lower Colorado and upper Mannville are isotopically different than core samples collected from the lower Mannville. Lower Colorado and upper Mannville core samples range from -168 and -19‰ to -147 and -16‰ for δ^2H and $\delta^{18}O$, respectively, reflecting a glaciogenic origin of the pore water (Hendry and Wassenaar, 1999; Remenda et al., 1996). Core samples collected from the lower Mannville

range from -132 and -15‰ to -151 and -16‰ for δ^2H and $\delta^{18}O$, respectively, and suggest the presence of meteoric waters (-132 and -15‰, respectively; Figure 4).

Because δ^2H and $\delta^{18}O$ are linearly correlated, δ^2H was used to describe the transport of the stable isotopes of water at the Shore Gold study site. The δ^2H vapour values at 140-10-087 are presented in Figure 5.8a. These data show a well-defined trend with depth from ground surface through the glacial till, Lower Colorado shale, and upper and lower Mannville. The δ^2H values decrease from -137‰ at 400.6 m asl to -175‰ at the contact between the glacial till and shale contact (327 m asl). The δ^2H values then increase from -175 to -147‰ in the Lower Colorado shale (between 327 and 251 m asl) and decrease again from -147‰ at the contact between the Lower Colorado and upper Mannville to -171‰ in the middle of the upper Mannville (211 m asl). Vapour δ^2H values increase again from -171‰ at 211 m asl to -145‰ at the contact between the upper and lower Mannville, where the δ^2H trend with depth remains vertically constant to the contact between the lower Mannville and the Souris River dolomite (99 m asl; Figure 5.8a). The scattered values observed between 327 and 300.6 m asl in the lower Colorado shale and Sutherland till could be a result of D_2O spiked drill fluid contamination of the core, resulting in greater δ^2H values in this zone. Between 191 and 99 m asl in the lower Mannville aquifer, the vertical trend with depth suggests this zone is dominated by advection.

Similar vertical profiles have been observed by Hendry and Wassenaar (2004) in the Quaternary till and Pierre shale at the Lanigan site and Kelln et al. (2001) in Battleford and Floral till, and have been identified as zones dominated by advective transport. The pump test water δ^2H values (-144‰) were consistent with values determined on lower Mannville core samples at 140-10-087 located between 191 and 99 m asl (Figure 5.8a); however, the $\delta^{18}O$ values collected from pumping test water (-18.4‰) were consistent with core samples collected in both the upper and lower Mannville formations (Appendix D). This suggests the pumping test water originated from both the upper and lower Mannville formations.

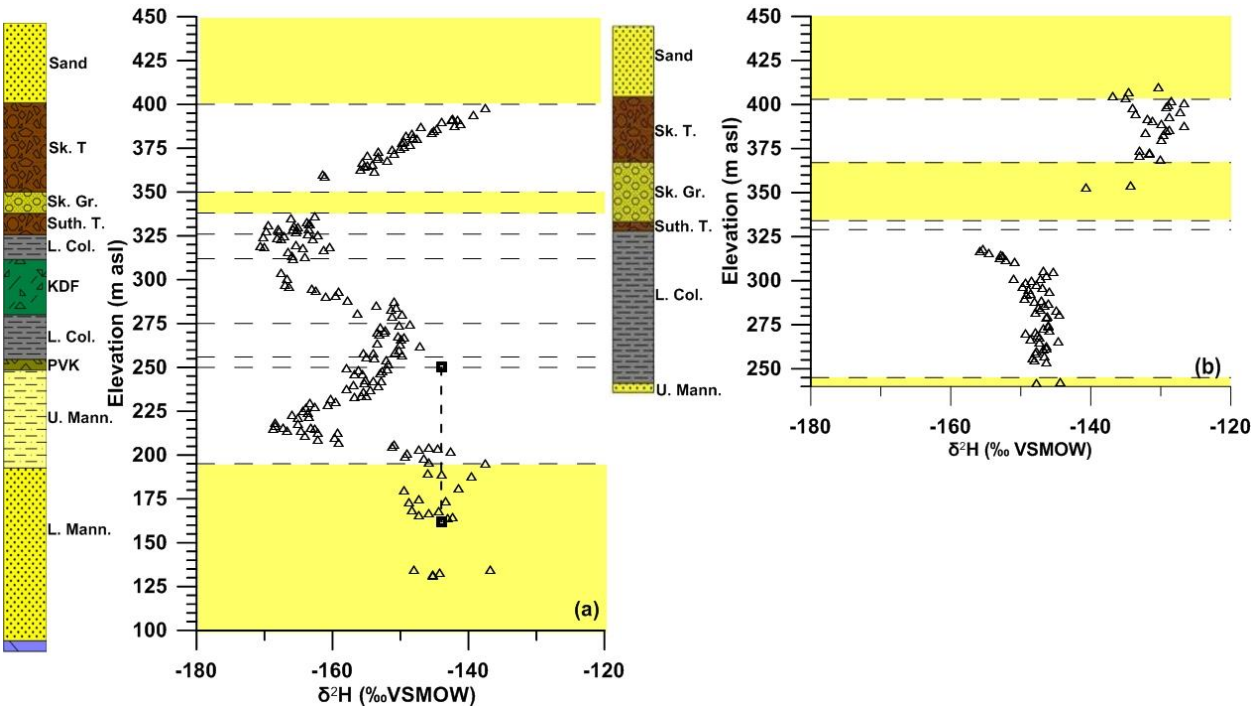

Figure 5.8. δ^2H values versus depth through the till and shale aquitard systems and sand aquifer system at 140-10-087 (a) and δ^2H values versus depth through the till and shale aquitard at OVB-10-207 (b). The vertical dashed line in (a) represents the average δ^2H value of pump test water collected from a well screened from 250.6 to 162.6 m asl. Aquifers are represented by yellow squares on (a) and (b).

The δ^2H depth-trend at OVB-10-207 (Figure 5.8b) was less complex than that observed at 140-10-087. For example, unlike the δ^2H trend in the glacial sediments at 140-10-087, the δ^2H trend in the glacial sediments at OVB-10-207 was vertically constant with depth (412.6 to 355.6 m asl) and ranged from -127 to -141‰. This trend may be the result of transport dominated by advection, either vertically through fractures or laterally through sand lenses in the glacial sediments, but was more likely a result of contamination with drilling fluid during drilling. The glacial till at this site proved difficult to retrieve with the core barrel, resulting in the core either being stuck inside the core barrel or at the bottom of the hole for many hours and becoming contaminated with spiked drilling fluid. The trend in the Lower Colorado shale at this site ranged from -156‰ at 318 m asl and increased with depth to -144‰ at the top of the upper Mannville at 248 m asl. The gap in the δ^2H profile between 353 and 318 m asl prevents comment on the dominant transport mechanisms or pore water age and origin in this zone (Figure 5.8). The

curvilinear Cl concentration profile over the same depth suggests the δ^2H trend of this profile, between the base of the intertill aquifer (326 m asl) and the top of the Mannville aquifer (248 m asl), may be curvilinear and diffusion could be the dominant transport mechanism.

No samples were collected in the surficial sands, silts, and lacustrine clays at either site; however, the δ^2H profiles at both sites, from ground surface to the top of the Saskatoon Group glacial till (approx. 445 to 400 m BG), suggests δ^2H values of -138 and -130‰ may have existed in the unconfined aquifer at 140-10-087 and OVB-10-207, respectively. These δ^2H values are typical of modern δ^2H values in Saskatchewan (Hendry et al., 2004, 2011). Where the Saskatoon Group glacial till shows a well-defined mixing trend at 140-10-087 (400-350 m BG), a uniform vertical δ^2H profile was observed in the same unit (406-370 m BG) at OVB-10-207. This difference could be attributed to either the presence of groundwater flow in vertical fractures and lateral flow in sand layers and streaks, the increased thickness of the Saskatoon Group intertill aquifer at OVB-10-207 compared to the thickness at 140-10-087 (33 and 12 m thick, respectively), or, more likely, contamination of the core with spiked drill fluid at OVB-10-207. A curved mixing trend in the glacial till is observed in the δ^2H profile with depth (400-350 m BG) at 140-10-087; conversely, a vertically uniform profile is observed in the Cl concentration profile at the same depth. This may suggest a uniform Cl concentration during deposition throughout both glacial and interglacial periods (Hendry et al., 2000). A vertical Cl and δ^2H profile in the glacial till at OVB-10-207 could suggest either uniform Cl concentration during deposition, groundwater flow in sand layers and lenses at this site, or contamination due to difficulties during coring.

5.6. $^{14}C_{DIC}$ Age Dating of Mannville Groundwater Samples

The apparent $^{14}C_{DIC}$ age of the pump test Mannville groundwater sample was estimated to be 22,330±100 a BP, as calculated from the fraction of modern (Fmdn) of 0.0621±0.0008 and a $\delta^{13}C$ value of -12‰. The corrected radiocarbon age of the Mannville groundwater was estimated to be between 15,700 and 22,000±100 a BP. Table 5.4 presents a summary of ages of the Mannville groundwater determined using the correction models. These results are consistent with the Mannville Group water being recharged by an influx of glaciogenic water during the Pleistocene (Grasby and Betcher, 2000). Grasby et al. (2000) suggest a considerable influx of fresh water up to ~400 km beyond the outcrop limit in Manitoba as a result of Pleistocene flow

reversal in the Mannville aquifer. More local injection of melt water may have occurred through collapse features (Wittrup and Kyser, 1990; Hendry et al., 2013), as inflow from the Saskatchewan River or as leakage through kimberlite pipes in the study area.

Table 5.4. Summary of corrected Mannville groundwater ages estimated using $\delta^{13}C$ and ^{14}C values from pumping test water.

Model	Age (years)
Vogel	21630
Tamers	17885
Ingerson and Pearson	18420
Mook	15698
Fontes and Garnier	18876
Eichinger	17996

5.7. Defining Initial and Boundary Conditions for 1-D Transport Modeling of δ^2H and Cl Profiles in the Cretaceous

Transport modeling of 1-D vertical tracer profiles (δ^2H and Cl) requires knowledge of the timing and initial conditions for the tracer profiles. This information can be estimated from geologic and paleo-hydrogeological history of the region. Because the δ^2H profile at 140-10-087 was more completely defined than that at OVB-10-207 (i.e., it included glacial till and the upper and lower Mannville profile), it was used to define the hydrogeological evolution of the study area and the initial and boundary conditions for transport modeling. As such, the δ^2H profile at 140-10-087 was simulated first to define the timing of evolution of the δ^2H profile through the shale. This evolution timing was then applied to the Cl concentration profile with depth at 140-10-087. The presence of higher δ^2H values, indicative of the Holocene warming period (10 Ka BP), and the $^{14}C_{DIC}$ age date of the Mannville Groundwater (15-22 Ka BP) at 140-10-087 also provided time constraints for transport modeling.

5.7.1. Hydrogeological Evolution of the Study Area and its Impact on Initial and Boundary Conditions

Based on the hydrogeologic history of the region, the δ^2H and pore water Cl concentration profiles at 140-10-087 and OVB-10-207 were hypothesized to be the result of the following sequence of events. The upper and lower Mannville shale, silt, and sand were deposited between 104 and 112 Ma BP in a terrestrial environment, which transitioned into a marine setting when the Lower Colorado shale was deposited between 99 and 104 Ma BP (Zonneveld et al., 2004). The kimberlites in the study area were emplaced between 99 and 112 Ma BP during deposition of the Mannville Group sand, silt, and clay and the Lower Colorado shale. Because the shale was deposited by an epi-continental sea, which covered North America during the Cretaceous and much of the Tertiary, a modern seawater δ^2H value and Cl concentration (0‰ and 20,000 mg L^{-1}, respectively) were assumed for the initial concentration of the porewater in the shale. This assumption is consistent with Mazurek et al. (2011) and Hendry et al. (2013) for other shales. Seven interglacial and glacial cycles occurred during the Late Pleistocene (650 ka BP to present), beginning with the Nebraska glacial (650 to 625 ka BP), Aftonian I interglacial (625 to 540 ka BP), and Kansan I glacial (540 to 510 ka BP) that were responsible for depositing the Sutherland Group glacial sediments and the basal Saskatoon Group aquifer in the study area. The Saskatoon Group glacial sediments were deposited during the Kansan II (460 to 430 ka BP), III (370 to 335 ka BP), and IV (290 to 240 ka BP) and their equivalent interglacial periods (Mindel-Riss Interglacial I (430 to 370 ka BP), II (335 to 290 ka BP), and III (240 to 195 ka BP), followed by the Illinois glacial (195 to 135 ka BP) and Sangamon interglacial (135 to 95 ka BP; Table 5.5). At the study area, deposition of the Fort à la Corne delta sands, silts, and clays and subsequent melt water flow into glacial Lake Saskatchewan occurred during the latter part of the Wisconsin glacial period (95 to 20 ka) and the Holocene warming period (10 to 20 ka) (Christiansen et al., 1995). Glacial sediments were hypothesized to have been deposited with pore water δ^2H values of -180‰ (Remenda et al., 1996; Hendry and Wassenaar, 1999; Hendry et al., 2011, 2013); however, during periods of non-deposition, glacial sediments were considered to have been exposed at the water table to meteoric δ^2H values ranging from -110 to -135‰ (Hendry and Wassenaar, 1999). In contrast, Cl concentrations in the glacial sediments likely remained relatively constant during both glacial and interglacial periods. Prior to the initial influx of glaciogenic water into the Mannville aquifer during Pleistocene glaciation, the aquifer may have

had δ^2H and Cl concentrations of 0‰ and 21,000 mg L^{-1} consistent with modern seawater (Mazurek et al. 2011; Hendry et al., 2013). lower Mannville groundwater at the study site had a present day δ^2H value of -145‰ and Cl concentration of 1,900 mg L^{-1}. These values were assumed to be the result of mixing between an influx of glacial water into the aquifer (-180‰ and 100-1,500 mg L^{-1}) during the Pleistocene and pre-Pleistocene-aged water of the Mannville aquifer (0‰ and 21,000 mg L^{-1}). Modern groundwater flow in the Basin is topographically driven from recharge areas in the southwest (Black Hills, South Dakota) to discharge areas in the northeast (Manitoba Escarpment). Loading of ice sheets (up to 3 km thick) during Pleistocene glaciations is believed to have reversed regional-scale groundwater flow and recharged glacial meltwaters into Paleozoic brines and Devonian carbonates (Person et al. 2007) as well as the Mannville group aquifer (Hendry et al., 2013). Grasby and Betcher (2002) and Grasby and Chen (2005) suggest that depleted meteoric water was introduced into the Mannville at the outcrop area in Manitoba and migrated as far as 400 km downgradient during the Pleistocene glaciations as subglacial meltwater (Hendry et al., 2013). Intrusion of subglacial meltwater may also have occurred by infiltration through collapse structures (Wittrup and Kyser, 1990), infiltration though the kimberlite pipes in the study area, or as inflow from the Saskatchewan River.

Table 5.5. Summary of Late Pleistocene glacial and interglacial cycles at the study area.

Name	**Timing (ka BP)**	**Glacial/Interglacial**
Nebraska	>650 to 625	glacial
Aftonian I	625 to 540	interglacial
Kansan I	540 to 510	glacial
Aftonian II	510 to 460	interglacial
Kansan II	460 to 430	glacial
Mindel-Riss I	430 to 370	interglacial
Kansan III	370 to 335	glacial
Mindel-Riss II	335 to 290	interglacial
Kansan IV	290 to 240	glacial
Mindel-Riss III	240 to 195	interglacial
Illinois	195 to 135	glacial

Sangamon	135 to 95	interglacial
Wisconsin	95 to 20	glacial
Holocene	20 to present	interglacial

5.8. Characterizing the Evolution of the δ^2H and Cl at 140-10-087 and OVB-10-207 after Activation of the Mannville and Glacial Intertill Aquifers

5.8.1. Characterizing the Evolution of the δ^2H and Cl in the Cretaceous Sediments at 140-10-087

Values of n_e are equal to n_T for stable isotopes of water (Hendry and Wassenaar, 1999); therefore, the n_e for each geologic unit was estimated based on results of laboratory experiments (Figure 5.3). The n_e values of the Saskatoon and Sutherland glacial till, shale, and Mannville sediments were assigned the mean measured n_T values of 0.22, 0.34, 0.40, and 0.36, respectively. The kimberlite at 140-10-087 (312-275 m asl) was assigned n_e values of 0.01 and 0.05 based on studies by Katsube and Kjarsgaard (1996) and Stripp et al. (2006). These studies suggest lithification of the initially porous volcaniclastic kimberlite into a massive dense rock was the result of post emplacement sub-solidus hydrothermal metamorphism (<400 °C) during cooling, resulting in a very small interconnected effective porosity.

The 1-D model was set up as a column of elements 1 m wide, 350 m high, and 1 m into the third dimension (assumed because it is a 2D analysis), with a mesh size of 0.5 m. Time steps increased linearly every 10 ka. The same column of elements, mesh size, and time steps were used for all analyses discussed in this thesis. The D_e values for the δ^2H in the glacial till, Cretaceous shale, and Mannville sands, silts, and clays were assumed to be 2.3×10^{-10} m^2s^{-1}, consistent with D_e measurements for δ^2H in till and Cretaceous shale by Hendry and Wassenaar (1999), Hendry et al. (2011), and Hendry et al. (2013). Effective diffusion coefficients of 1.5×10^{-10} m^2 s^{-1} and 1.7×10^{-10} m^2 s^{-1} were assigned to the $n_e=0.4n_T$ and $n_e=0.6n_T$ simulations of Cl concentration with depth, respectively, and a D_e value of 7×10^{-11} m^2s^{-1} was assigned to the KDF. D_e values for Cl and KDF were calculated from empirical relationships between D_e and n_e (Boudreau, 1996; Boudreau and Meysman, 2006; Hendry et al., 2013). The δ^2H of glaciogenic water (-180‰) measured by Hendry and Wassenaar (1999) at the King Site near Birsay, Saskatchewan and a Cl concentration of 40 mg L^{-1} were used as the initial conditions in the glacial sediments. The lower boundary (applied as a region to the Lower Mannville aquifer) alternated between δ^2H values of

-180‰ and Cl concentrations ranging from 100 to 1,500 mg L^{-1} during glacial periods and a zero mass flux boundary during interglacial periods, respectively. The lower boundary applied to the lower Mannville aquifer implied that a sufficient amount of glaciogenic water was introduced into the Mannville during the first glacial period in the Pleistocene. This influx of glaciogenic water could have resulted in the water in the Mannville flowing northeast toward the discharge area in Manitoba during interglacial periods and southwest toward the recharge area in South Dakota during glacial periods with minimal alteration of the δ^2H and Cl values in the Mannville.

Initial conditions in the Cretaceous sediments were assumed to be that of present-day seawater (δ^2H=0‰, Cl=20,000 mg L^{-1}) because the shales were deposited in a marine environment (Mazurek et al., 2011; Hendry et al., 2013).

In the simulation of δ^2H with depth, one steady-state model was created that included all sediments observed from ground surface to 98 m asl (Figure 5.9). This implied that all of the glacial sediments were deposited at the onset of glaciation. Three subsequent analyses were run for a total of 730, 750, and 770 ka, consistent with the onset of the Late Pleistocene glaciations in the study area. The first analysis was run for 460 ka. In this analysis, the upper boundary applied to the surficial sand was given a constant δ^2H value of -180‰ (Figure 5.9) and a constant Cl concentration of 40 mg L^{-1} (Figure 5.10) to simulate a constant source of glaciogenic water during glacial and interglacial periods. The lower Mannville sediments were also given a constant δ^2H value of -180‰ and a range in Cl values from 100 to 1,500 mg L^{-1} to simulate constant flushing of the Mannville Group sediments during glacial and interglacial periods. This range in Cl concentration during flushing of the lower Mannville Group aquifer was used because of the variability of Cl concentrations measured in the lower Mannville at this site. The second analysis was run for an additional 260, 280, and 300 ka to simulate the end of deposition of glacial till at the study area and the infiltration of meteoric water at the water table. In this analysis, the upper boundary applied to the surficial sand was given a constant δ^2H value of -138‰ and Cl concentration of 40 mg L^{-1}. The lower Mannville boundary was again assigned a constant δ^2H value of -180‰ and a range of Cl values from 100 to 1,500 mg L^{-1} to simulate continued constant flushing of the Lower Mannville during glaciation. The third analysis was run for 10 ka to simulate the Holocene warming period at the study area. In this analysis, the upper

boundary in the surficial sand was assigned a value representative of modern meteoric water (-138‰ and 40 mg L^{-1} for δ^2H and Cl, respectively) and the Lower Mannville was assigned a δ^2H value of -144‰ and a range in Cl values between 100 to 1,500 mg L^{-1} to simulate mixing between glaciogenic and pre-Pleistocene aged water in the Mannville aquifer during this time period. Evolution timings for the Cl simulation were consistent with those applied to the δ^2H model at 140-10-087.

Good fits were determined qualitatively by visual inspection similar to Mazurek et al. (2011) and Hendry et al. (2013). Good fits between the simulated and measured δ^2H values at 140-10-087 were obtained for the range in elapsed times (730 to 770 ka BP) (Figure 5.9). The onset of infiltration of meteoric water into the glacial sediments ranged from 260 to 300 ka BP, which suggests that no glacial sediments were deposited in the study area after the Kansan IV glaciation (290 to 240 ka BP). A δ^2H value of -144‰ was applied to the lower Mannville at the onset of the Holocene, which was assumed to be 10 ka BP in these simulations. This timing was based on the literature and was consistent with ^{14}C DIC dates measured from pumping test water.

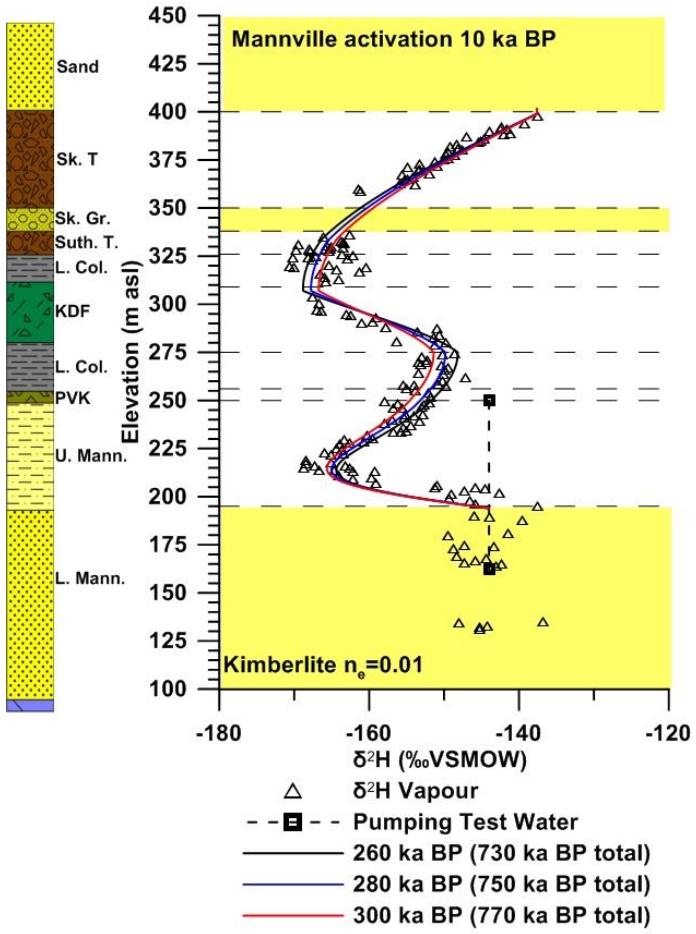

Figure 5.9. Geologic profile of the 140-10-087 site and measured and simulated pore water δ^2H values versus elevation (m asl) from ground surface to the base of the Lower Mannville aquifer. Simulations of the diffusive evolution of the profile after recharge of the Mannville with glacial water during the late Pleistocene are presented. Simulations assume $n_e=n_T$ through the Cretaceous shale and 0.01 through the kimberlite. Simulations are presented for evolution timings of 460, 260, and 10 ka; 460, 280, and 10 ka; and 460, 300, and 10 ka for analysis 1 (glaciogenic water (-180‰) on upper and lower boundaries), analysis 2 (glaciogenic water on lower boundary and modern water (-135‰) on upper boundary), and analysis 3 (modern water on upper and lower boundaries) in the Holocene as presented in the text.

Results of the simulations of Cl concentration with depth at 140-10-087 are shown in Figure 5.10. The same evolution timings that were used to simulate δ^2H with depth at this site were applied to this simulation. Reasonable fits to the measured data could not be produced using an n_e of $0.40n_T$ or $0.6n_T$ in the upper Mannville. As such, the upper Mannville was assigned n_e values equal to the n_T values measured in the lab (Figure 5.10c,d). This was

considered reasonable because the upper Mannville was dominated by silt and very fine-grained sand with less common zones of laminated silts and clay. As such, anion exclusion effects would not be expected in silts and sands containing a lack of negatively charged surfaces (Rowe and Badv, 1996). In these simulations, the best fits to the measured data were observed when the measured Cl values were simulated with $n_e=0.4n_T$ in the Cretaceous sediments and $n_e=n_T$ in the upper Mannville sediments; the lower boundary condition was set between 100 and 1,500 mg L^{-1} (Figure 5.10c).

Although the simulations of δ^2H and Cl concentration with depth provided good overall fits to the measured δ^2H and Cl profiles, it was unrealistic to assume that all glacial sediments were deposited at the same time, that there was no effect of infiltration of meteoric water into the glacial sediments between glacial periods, or that the Mannville aquifer could be represented by a constant boundary condition for 770 ka with no increasing concentration during interglacial periods (when the aquifer is not being recharged with glaciogenic water). A more realistic approach to the simulations could be represented by a more complex modeling approach (discussed later in the text).

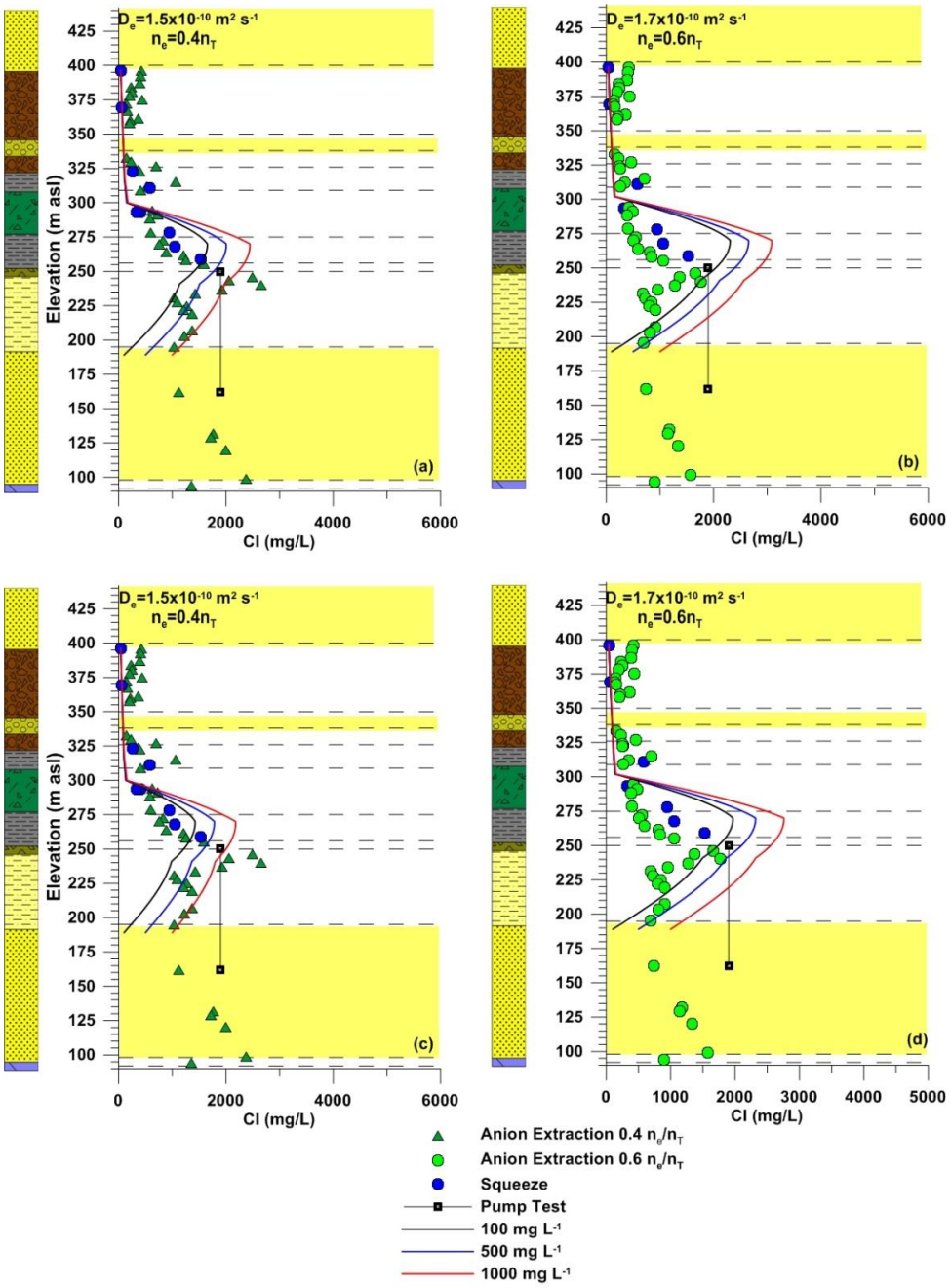

Figure 5.10. Geologic profile of 140-10-087 and measured and simulated Cl concentration profiles through the glacial till and Cretaceous sediments versus elevation (m asl). Simulation timings and boundaries are the same as those presented for δ^2H with elevation in Figure 5.9 (770 ka total evolution time), where glaciogenic and modern water were given Cl values of 40 mg L^{-1}. Simulations assume uniform effective porosities of $n_e=0.4n_T$ in the Cretaceous shale and upper Mannville (a), $n_e=0.4n_T$ in the Cretaceous shale and $n_e=n_T$ in the upper Mannville (b), $n_e=0.6n_T$ in the Cretaceous shale and upper Mannville (c), and $n_e=0.6n_T$ in the Cretaceous shale and $n_e=n_T$ in the upper Mannville (d). All simulations assume $n_e=0.01$ in the kimberlite. Details of the initial and boundary conditions are presented in the text.

5.8.2. Characterization of the Evolution of δ^2H and Cl at OVB-10-207

The D_e values used for the δ^2H profile at 140-10-087 were applied to the δ^2H in the glacial till, Cretaceous shale, and Mannville sands, silts, and clays at OVB-10-207 (2.3×10^{-10} m^2 s^{-1}) in this simulation. Initial conditions in the Cretaceous sediments were also assumed to be that of present-day seawater (0‰ and 20,000 mg L^{-1} for δ^2H and Cl, respectively) because the shales were deposited in a marine environment (Mazurek et al., 2011; Hendry et al., 2013). The n_T values for each geologic unit were again estimated based on results of laboratory experiments (Figure 5.3) and, as such, the n_e values for Saskatoon and Sutherland glacial till, shale, and Mannville sediments were assigned the mean measured values of 0.24, 0.34, 0.45, and 0.37, respectively, in the simulation of δ^2H with depth. As was the case with the Cl simulations at 140-10-087, ratios of n_e/n_T of 0.4 and 0.6 were used to calculate the Cl concentration in the leach extract with depth and were applied to the simulations (Figure 5.12a-d). Based on empirical relationships, D_e values of 1.6×10^{-10} and 1.9×10^{-10} m^2 s^{-1} were applied to the simulations of $n_e=0.4n_T$ and $n_e=0.6n_T$, respectively. Because no samples existed below the base of the Lower Colorado shale at this site, the depth of the upper-lower Mannville boundary as well as δ^2H values and Cl concentrations were assumed to be the same as those measured at 140-10-087.

Consistent with the simulations of δ^2H and Cl with depth at 140-10-087, the entire sequence of glacial sediments were included in one initial steady-state analysis, again with the assumption that all of the till in the study area was deposited at the onset of glaciation. Three subsequent analyses were added to the model. The first analysis was run for 460 to 540 ka BP, consistent with the simulations conducted at 140-10-087. In this analysis, the glacial till was assigned initial δ^2H and Cl values of -180‰ and 40 mg L^{-1}, respectively; the upper boundary was set at constant values of -180‰ and 40 mg L^{-1} for δ^2H and Cl, respectively, to simulate glaciogenic water entering the glacial sediments during deposition. The lower boundary assigned to the Mannville aquifer as a region was set constant at -180‰ and 100 to 1,500 mg L^{-1} for δ^2H and Cl, respectively, to simulate constant flushing of the Mannville aquifer during glaciation. In the second analysis (210 to 290 ka BP), the upper boundary was changed to a δ^2H value of -130‰ (the average δ^2H value measured near the surficial sand at this site) to simulate infiltration of meteoric water after the glacial sediments were deposited in the study area; the upper boundary in the Cl simulation remained at 40 mg L^{-1}. The lower boundary also remained constant at -180‰ and 100-1,500 mg L^{-1} for δ^2H and Cl, respectively. The lower boundary in the

Mannville aquifer was changed to -135‰ for the last 15 ka of the simulation (analysis 3) to simulate influx of pre-Pleistocene-aged water into the Mannville at this site during the Holocene warming period, while the Cl concentration remained set at 100 to 1,500 mg L^{-1}.

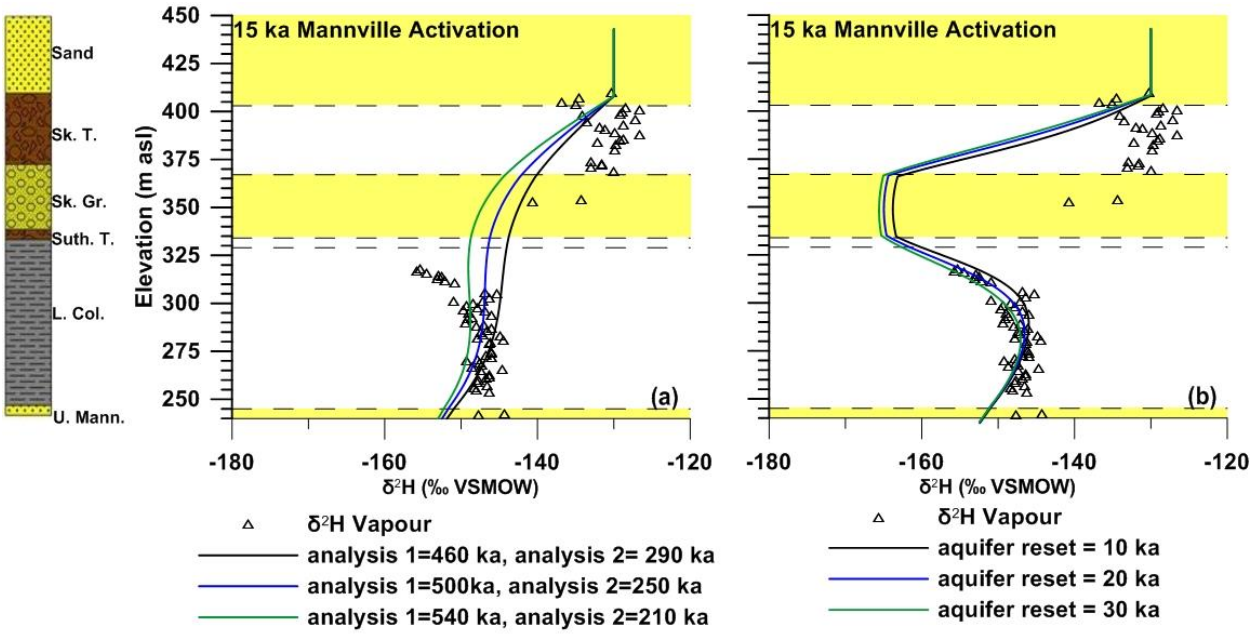

Figure 5.11. Geologic profile of OVB-10-207 and measured and simulated pore water δ^2H versus elevation (m asl) from ground surface to the base of the Cretaceous shale. Simulations assume $n_e=n_T$ through the Cretaceous shale. Simulations are presented for evolution timings of 460, 290, and 15 ka; 500, 250, and 15 ka; and 540, 210, and 15 ka for analysis 1 (glaciogenic water (-180‰) on upper and lower boundaries, analysis 2 (glaciogenic water on lower boundary and modern water (-125‰) on upper boundary, and analysis 3 (modern water on upper and lower boundaries) in the Holocene. Simulated profiles in (b) were conducted with the same evolution timing as in (a) with an additional analysis added to flush the intertill aquifer at the end of the Wisconsin Glaciation for 10 to 30 ka (25 to 45 ka BP). Boundary conditions and transport parameters used in the modeling are presented in the text.

While the shape of the simulated δ^2H profile resembled the shape of the measured data, no good fits to the data were observed (Figure 5.11a). As a result, an additional analysis was added before the Holocene. In this analysis, the Saskatoon Group intertill aquifer was assigned constant values of -135‰ and 40 mg L^{-1} for δ^2H and Cl, respectively, for 10-30 ka at the end of the Wisconsin Glaciation (25 to 45 ka BP) to simulate influx of recharge water into the aquifer during deposition of the Fort à la Corne delta in the study area (Christiansen, 1992); the upper and lower boundaries remained the same as those applied in the previous analysis. Timing of

analyses 1 and 2 were 460 ka and 260 ka BP, respectively. Good fits to the measured data were observed for 10 to 30 ka of flushing prior to the onset of the Holocene (25 to 45 ka BP) (Figure 5.11b).

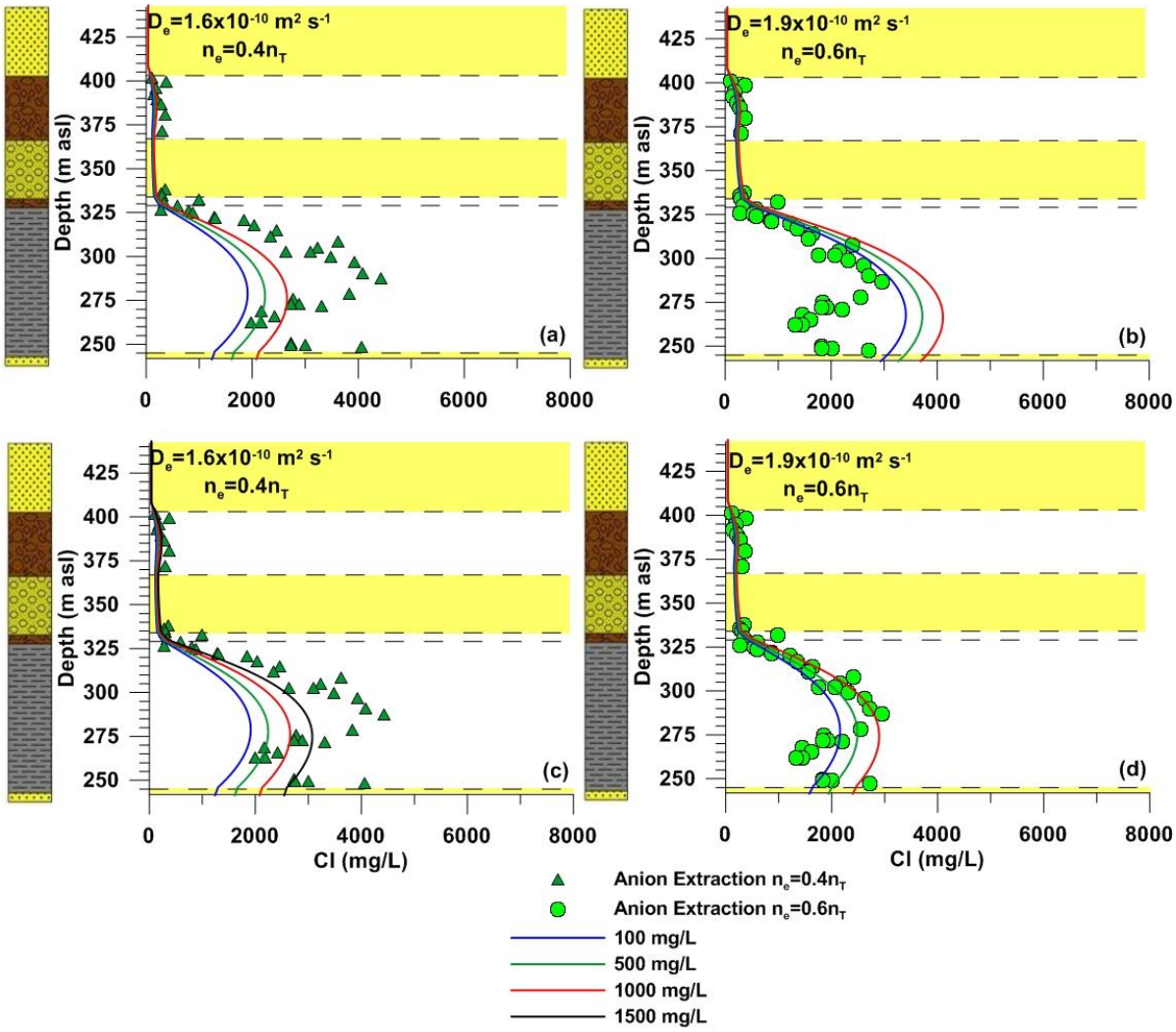

Figure 5.12. Geologic profile of OVB-10-207 and measured and simulated Cl concentration versus elevation (m asl) from ground surface to the base of the Cretaceous shale. Simulation timings and boundaries are the same as those presented for δ^2H with elevation in Figure 5.11 (765 ka total evolution time), where glaciogenic and modern water were assigned values of 40 mg L^{-1}. Simulations assume uniform effective porosities of $n_e=0.4n_T$ in the Cretaceous shale and upper Mannville (a), $n_e=0.4n_T$ in the Cretaceous shale and $n_e=n_T$ in the upper Mannville (b), $n_e=0.6n_T$ in the Cretaceous shale and upper Mannville (c), and $n_e=0.6n_T$ in the Cretaceous shale and $n_e=n_T$ in the upper Mannville (d). Details of the initial and boundary conditions are presented in the text.

Good fits between the simulated and measured δ^2H (Figure 5.11) and Cl (Figure 5.12) values at OVB-10-207 were obtained for an evolution time of 765 ka BP. Best fits to the measured Cl concentration with depth at OVB-10-207 were observed when the profile was simulated with an $n_e=0.6n_T$ in the Cretaceous shale and an $n_e=n_t$ in the upper Mannville sediments. Consistent with the observation at 140-10-087, the simplified simulations provide good fits to the measured data but are unrealistic when compared to the paleo-hydrogeologic history of the study area. The assumption that the lower Mannville aquifer was constantly flushed for the whole 765 ka of the simulation was unrealistic, as was the assumption that no meteoric water infiltrated the glacial till during interglacial periods for the simulation time. As such, a more complex approach to the simulation of the δ^2H and Cl with depth based on the complex glacial history of the study area at both 140-10-087 and OVB-10-207 was warranted.

5.8.3. Characterizing the Evolution of δ^2H in the Cretaceous Sediments at 140-10-087 using the Complex Glacial History of the Study Area

The n_e values applied to the Saskatoon and Sutherland glacial till, shale, and Mannville sediments were the same as those applied in the simple model in Section 5.8.1. The kimberlite at 140-10-087 (312-275 m asl) was assigned n_e values of 0.01 and 0.05 based on studies by Katsube and Kjarsgaard (1996) and Stripp et al. (2006). D_e values for the δ^2H in the glacial till, Cretaceous shale, and Mannville sands, silts, and clays remained at 2.3×10^{-10} m^2s^{-1}, consistent with D_e measurements for δ^2H in till and Cretaceous shale by Hendry and Wassenaar (1990), Hendry et al. (2011), and Hendry et al. (2013). A D_e value of 7×10^{-11} m^2s^{-1} was assigned to the KDF and was calculated from empirical relationships between D_e and n_e (Boudreau, 1996; Boudreau and Meysman, 2006; Hendry et al., 2013). The δ^2H value of glaciogenic water (-180‰) measured by Hendry and Wassenaar (1999) at the King Site near Birsay, Saskatchewan, was used as the initial condition in the glacial sediments. The lower boundary, applied as a region to the lower Mannville aquifer, alternated between δ^2H values of -180‰ during glacial periods and a zero mass flux boundary during interglacial periods to allow the concentration in the aquifer to increase with time. Initial conditions in the Cretaceous sediments were assumed to be that of present-day seawater (0‰) because the shales were deposited in a marine environment (Mazurek et al., 2011; Hendry et al., 2013).

Because of the complex paleo-hydrogeologic history of the study area, the δ^2H profile in the Quaternary and Cretaceous sediments was simulated by considering all seven glacial/interglacial cycles during the Late Pleistocene (Table 5.6). For these simulations, the Mannville was reset to glacial values after deposition of the Sutherland Group glacial till. The onset of Mannville activation in the simulations was estimated to be 800 ka BP because no early-mid Pleistocene Sutherland Group glacial sediments were deposited in the study area (i.e., Mennon Formation or Empress Group sediments); there was also an interglacial hiatus of unknown duration between deposition of the Sutherland and Saskatoon Group glacial tills in the study area (Christiansen, 1968).

The simulation of the δ^2H profile with depth at 140-10-087 was conducted as a series of 14 analyses generated for each glacial and interglacial period (Table 5.6). Because the Sutherland Group glacial till was hypothesized to have been deposited prior to the start of the simulation, the initial steady state hydraulic model included only Sutherland group till and Cretaceous sediments. This steady state analysis was defined as the parent steady state model from the Nebraska glaciation to the onset of the 2nd Kansan glaciation (800 to 460 ka). The Sutherland Group till was assigned an initial δ^2H value of -180‰. A zero mass flux boundary was assigned to the top of the model during the Nebraska period. The Saskatoon Group intertill aquifer may have been deposited between the end of the Nebraska period and the Aftonian II interglacial (625-460 ka) (Christiansen, 1992). As such, a constant δ^2H value of -180‰ was applied to the top of the profile to simulate the recharge of this aquifer with glaciogenic water and glaciogenic meltwater until the overlying Saskatoon Group till was deposited, after which the recharge area for the aquifer may have been covered with low K material. The Saskatoon Group till (400-338 m asl) was added to the top of the Sutherland Group till in the model during the 2nd Kansan glaciation by adding a second steady state analysis at 460 ka BP. This steady state analysis was defined as the parent hydraulic model for subsequent analyses. Again, the Saskatoon Group till was given an initial δ^2H value of -180‰ and a zero mass flux boundary was applied to the top of the model. To simulate the end of deposition of glacial sediments and the subsequent onset of infiltration of meteoric water from ground surface, the model was assigned a constant upper boundary of -135‰. To best fit the simulated data to the measured data, the onset of the upper boundary was simulated at three time periods—the Mindel-Riss III interglacial (240-195 ka BP; simulation 1), the Illinois glacial (195-135 ka BP; simulation 2), and the

Sangamon interglacial (135-95 ka BP; simulation 3)—and remained constant until the end of the simulation. Because there is no evidence that Battleford till was deposited in the study area and, as such, no isotopically depleted pore water was deposited within this unit of glacial sediments, these timings were considered reasonable (Christiansen, 1992). The lower boundary was applied as a region to the lower Mannville (195 m asl) at a constant δ^2H value of -180‰ during glacial periods and a zero mass flux boundary was applied during interglacial periods, whereby the δ^2H value in the aquifer gradually increased as diffusion into the aquifer from the overlying formation occurred (Table 5.6). To simulate the onset of the Holocene warming period, the lower boundary was assigned a δ^2H value of -144‰ for the last 10-20 ka of the simulation, which coincided with the measured δ^2H value and the ^{14}C age date estimated from water collected during the pumping test at 140-10-089 (Figure 5.13a-d).

Table 5.6. Summary of analysis of the timing and upper and lower boundaries used to simulate the δ^2H and Cl profiles at 140-10-087 and OVB-10-207 in Figures 5.13 and 5.15-5.20, respectively.

Analysis	Name	Timing (ka BP)	Glacial/ Interglacial	Lower Boundary (Lower Mannville)	Timing of Glacial Till Deposition	Upper Boundary (top of glacial till)
Steady State 1		800			Sutherland	
Ctran 1	Nebraska	>650 to 625	glacial	-180‰/100-1000mg/L		
Ctran 2	Aftonian I	625 to 540	interglacial			-180‰/40mg/L
Ctran 3	Kansan I	540 to 510	glacial	-180‰/100-1000mg/L		-180‰/40mg/L
Ctran 4	Aftonian II	510 to 460	interglacial			-180‰/40mg/L
Steady State 2		460			Saskatoon	
Ctran 5	Kansan II	460 to 430	glacial	-180‰/100-1000mg/L		
Ctran 6	Mindel-Riss I	430 to 370	interglacial			
Ctran 7	Kansan III	370 to 335	glacial	-180‰/100-1000mg/L		
Ctran 8	Mindel-Riss II	335 to 290	interglacial			
Ctran 9	Kansan IV	290 to 240	glacial	-180‰/100-1000mg/L		
Ctran 10	Mindel-Riss III	240 to 195	interglacial			Simulation 1 -135‰/40mg/L*
Ctran 11	Illinois	195 to 135	glacial	-180‰/100-1000mg/L		Simulation 2 -135‰/40mg/L*
Ctran 12	Sangamon	135 to 95	interglacial			Simulation 3 -135‰/40mg/L*
Ctran 13	Wisconsin	95 to 20	glacial	-180‰/100-1000mg/L	Delta sand and silt	
Ctran 14	Holocene	20 to present	interglacial	-144‰/100-1000 mg/L		

* The upper boundary was applied during this time period and remained constant until the end of the simulation.

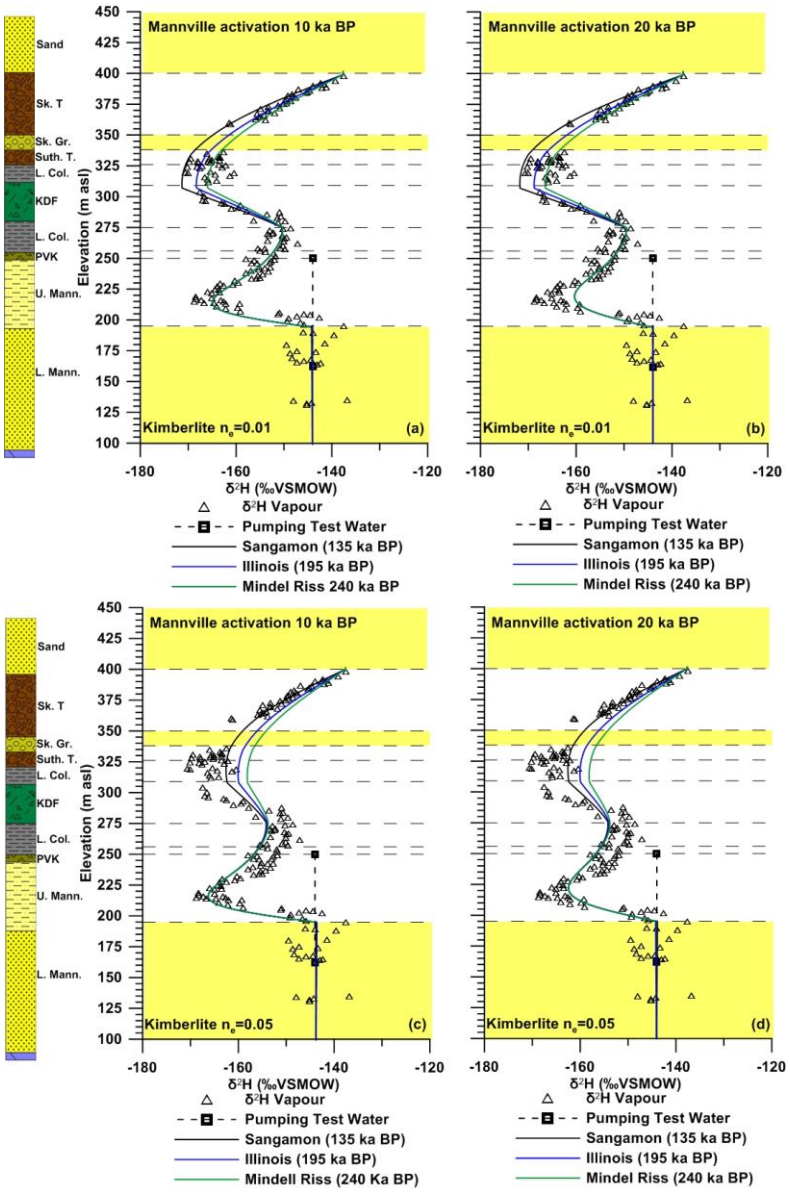

Figure 5.13. Measured and simulated δ^2H profiles with elevation (m asl) at 140-10-087 through the glacial till and Cretaceous sediments. Simulations assume constant recharge of glaciogenic water (-180‰) during glaciations, no mass flux during interglacial periods in the lower Mannville aquifer, and constant influx of glaciogenic water in the intertill aquifer from the onset of the Nebraska glacial (800 ka) to the end of the Aftonian II interglacial (460 ka). The upper boundary applied to the surficial sand was changed from no mass flux to modern water (-135‰) during the Sangamon (135 ka BP), the Illinois (195 ka BP), and the Mindell Riss III (240 ka BP). Simulations were conducted assuming a constant $n_e=n_T$ through the Cretaceous sediments and $n_e=0.01$ in the kimberlite in (a) and (b) and $n_e=n_T$ through the Cretaceous sedients and $n_e=0.05$ in the kimberlite in (c) and (d). The influx of Holocene water into the lower Mannville ranged from 10 ka BP in (a) and (c) to 20 ka BP in (b) and (d).

The best fit to the measured profile (determined visually) was obtained when n_e=0.01 was applied to the kimberlite material (312-275 m asl; Figure 5.9a-b). The Saskatoon Group intertill aquifer was given a constant δ^2H value equal to that of glaciogenic water from the end of the Nebraska period to the onset of the Aftonian II interglacial (625-460 ka), and the Saskatoon Group Glacial Till was deposited at the onset of the 2nd Kansan glaciation (460 ka) in the simulation. Results also suggest deposition of the Saskatoon Group till was complete between the end of the 4th Kansan glaciation (240 ka) and the onset of the Wisconsin interglacial period (95 ka) and that there was an influx of Holocene-aged meteoric water into the Mannville aquifer between 10-20 ka BP. Christiansen (1968) suggests that the glacier that deposited the Floral Formation till (Saskatoon Group) at the study area retreated more than 34 ka BP based on radiocarbon dating of wood found between Floral and Battleford Formation glacial till near Prince Albert (60 km west of the study area); however, no suggestion was made as to the onset of deposition in the study area. Christiansen (1992) suggests that the lower member of the Floral Formation (Saskatoon Group) was deposited at the end of the early to mid-Pleistocene (625 to 560 ka BP), the Riddell member (aquifer) was deposited as early as 560 ka BP, and the upper members of the Floral Formations (Saskatoon Group) were deposited in the Late Pleistocene (560 and 38 ka BP). The Battleford Formation of the Saskatoon Group tills was thought to be deposited during the end of the Wisconsin glaciation (38-20 ka; Christiansen, 1968), so the absence of Battleford till and presence of the Riddell (aquifer) and upper members of the Floral Formation of the Saskatoon Group at the study area suggest that the simulation timings presented here provide a reasonable estimate of the paleo-hydrogeologic history of the study area.

Additional simulations were conducted to explore the timing of deposition of the Saskatoon and Sutherland Group glacial tills; however, only the depositional history described above could reasonably approximate the measured δ^2H profile. In all other instances, the simulated δ^2H values in the Sutherland Group till and the Lower Colorado shale above the kimberlite (338-312 m asl) were greater than those that were measured; for example, by assigning a boundary condition to the Saskatoon Group aquifer only during glaciations, the simulated value in the Sutherland till and Lower Colorado shale (338-312 m asl) was greater than that observed in the measured profile (Figure 5.14a). Further simulations were conducted to

investigate whether an increased thickness of the Sutherland Group glacial sediments from the onset of the Nebraska Glaciation (800 ka BP) to the end of the Mindel Riss II interglacial period (290 ka BP) would better approximate the measured data. In this simulation, the thickness of the Sutherland group was increased from 12 to 77 m (i.e., the top of the Floral Formation glacial till that was deposited later) and a no mass flux boundary was applied to the top of the glacial till (Figure 5.14b). In subsequent analyses, the Sutherland Group glacial sediments were "eroded" from the model to present day thicknesses and the Saskatoon Group members were "deposited" between 460 to 260 ka BP. No good fit to the measured data was observed when the thickness of the Sutherland glacial till was increased so this was not explored further. The simulations presented in Figures 5.14a and b suggest that the Saskatoon Group intertill aquifer may have been a constant source of glaciogenic water (δ^2H = -180‰) during the Aftonian I, Kansan I, and Aftonian II time periods, as no other combination of depositional histories could reasonably reproduce the measured data.

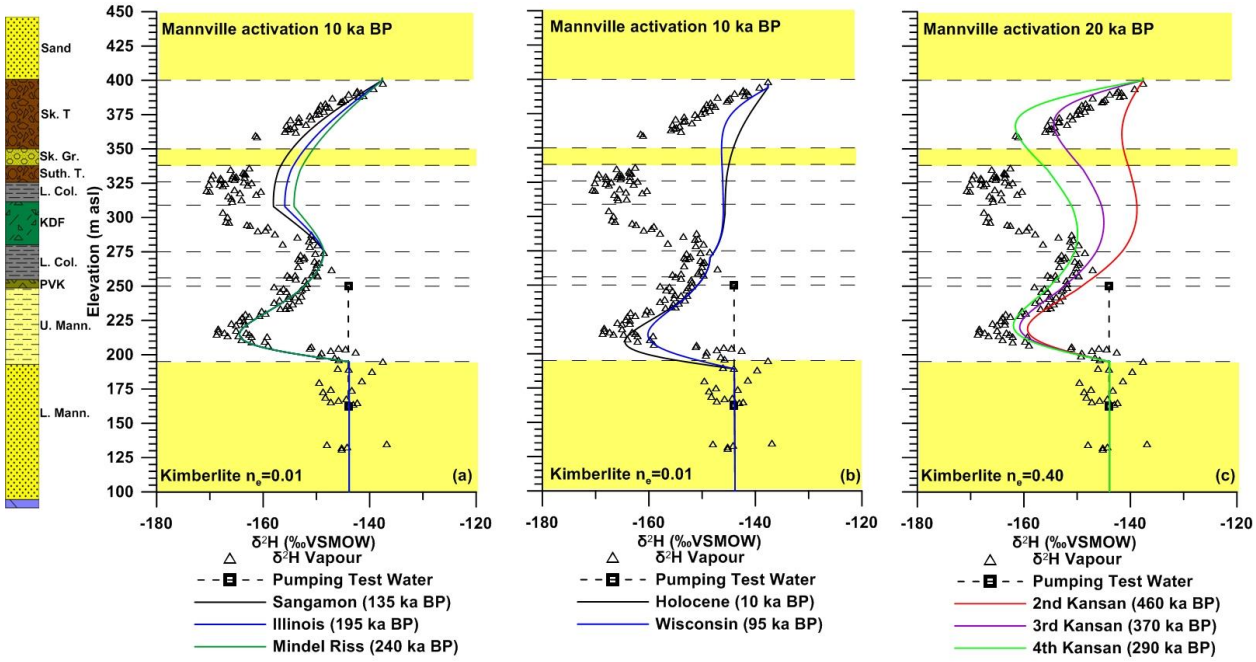

Figure 5.14. Measured and simulated δ^2H profiles with elevation (m asl) at 140-10-087 through the glacial till and Cretaceous sediments. All simulations assume a constant recharge of glaciogenic water (-180‰) during glaciations and no mass flux during interglacial periods in the lower Mannville aquifer. Simulations in (a) assume a constant influx of glaciogenic water in the intertill aquifer from the onset of the Nebraska glacial (800 ka) to the Aftonian II interglacial (625-460 ka) during glacial periods only and no mass flux during interglacial periods. The upper boundary applied to the surficial sand was changed from no mass flux to modern water (-135‰) duing the Sangamon (135 ka BP), the Illinois (195 ka BP), and the Mindell Riss (240 ka BP). Simulations in (b) were conducted by increasing the thickness of the Sutherland group sediments to the base of the surficial sand until the onset of the Kansan II (460 ka BP). Simulations in (a) and (b) were conducted assuming a constant $n_e=n_T$ through the Cretaceous sediments and $n_e=0.01$ in the kimberlite. Simulations in (c) assumed a constant $ne=n_T$ in the Cretaceous sediments and kimberlite and a change of the upper boundary applied to the surficial sand from no mass flux to -135‰ at the onset of the 2nd Kansan (460 ka BP), the 3rd Kansan (370 ka BP), and the 4th Kansan (290 ka BP). The influx of Holocene water into the lower Mannville aquifer ranged from 10 ka BP in (a) and (b) to 20 ka BP in (c).

Simulations were also conducted to investigate if the use of a low n_e value (n_e=0.01) in the kimberlite at 140-10-087 was appropriate. This was done by assigning an $n_e=n_T$ (0.40) in the kimberlite (312-275 m asl). To achieve the fits to the measured profile presented in Figure 5.14c, the timing of deposition of the Saskatoon Group till was varied between the 2nd Kansan glacial

period (460 ka BP) and the 4th Kansan (290 ka BP), the upper boundary (δ^2H=-135‰) was applied at the onset of the Holocene (20 ka BP), and influx of Holocene-aged meteoric water was estimated to be 20 ka BP. Various permutations were considered (data not presented) but only the best fits to the measured data are presented here. In all simulations, it was not possible for the model to simulate the low δ^2H values in the measured profile below the Saskatoon Group intertill aquifer with the use of an n_e=0.40 in the kimberlite, so this was not explored further.

In the simulations described above, a constant boundary was assigned as a region to the lower Mannville aquifer during the Holocene (10 to 20 ka BP). Additional simulations were warranted to investigate if the measured data could be reproduced by assigning a no mass flux boundary condition to the lower Mannville during the Holocene to estimate the length of time required for the δ^2H values to increase to modern values by diffusion from the upper Mannville only (Figure 5.15). In these simulations, the no mass flux lower boundary for the lower Mannville was applied for the duration of the Holocene (20 ka BP; Figure 5.15a), the duration of the Wisconsin glaciation and Holocene Interglacial (105 ka BP; Figure 5.15a), and the duration of the Illinois glacial, Sangamon Interglacial, Wisconsin glacial, and Holocene Interglacial (205 ka BP (Figure 5.15a). In all simulations, no good fit to the measured data was observed. Another simulation was conducted where 50 m of the underlying Souris River Dolomite was added below the lower Mannville aquifer (Figure 5.15b). The dolomite was assigned a D_e=1.2×10^{-10} m^2 s^{-1}, an n_e=0.1, and an initial concentration of 0‰ based on data collected and simulations conducted by Hendry et al. (2013). Three simulations were conducted; in the first simulation, a no mass flux boundary was applied to the lower Mannville during the Holocene (20 ka BP); in the second, a no flux boundary was applied to the lower Mannville during the Wisconsin glaciation and the Holocene (105 ka BP); and in the third, a no flux boundary was applied during the Illinois, Sangamon, Wisconsin, and Holocene (205 ka BP). Results show that diffusion of δ^2H into the lower Mannville aquifer during interglacial periods cannot accurately describe the shape of the measured profile and that only an influx of isotopically enriched water during the Holocene (10-20 ka BP) is able to accurately describe the measured data. The poor fit may also be due to the δ^2H being flushed out of the 50 m of dolomite during glacial periods creating too low of a concentration gradient to have an effect on the shape of the profile at the end of the simulation. Because no data exist at this site for the Souris River Dolomite or sediments deposited below the dolomite, no further assumptions were made for these simulations. Hendry and Harrington

(2014) make a similar observation at their K2 site near Esterhazy, SK, where there was a sharp increase in Cl concentration at the base of the Lower Colorado shale. They attribute the increase in Cl concentration in the Mannville to influx of meteoric water during the Holocene (10 ka BP) and use these data to estimate timing since the last influx of glaciogenic water into the Mannville aquifer at the K2 site. Because the simulations were not able to accurately reproduce the measured data, this boundary condition was not considered further for δ^2H with depth.

The influence of the glacial history prior to the Nebraska Glaciation in the area or a more well constrained timing of deposition of the Saskatoon Group glacial till may provide an improved fit between the simulated profile and the measured data; however, the profile as shown in Figure 5.12a-b was believed to be a reasonable fit to both the measured data and the paleo-hydrogeologic conditions at the study area. The addition of more glacial and interglacial periods to the simulation would also increase the complexity and make it more difficult to justify in the model.

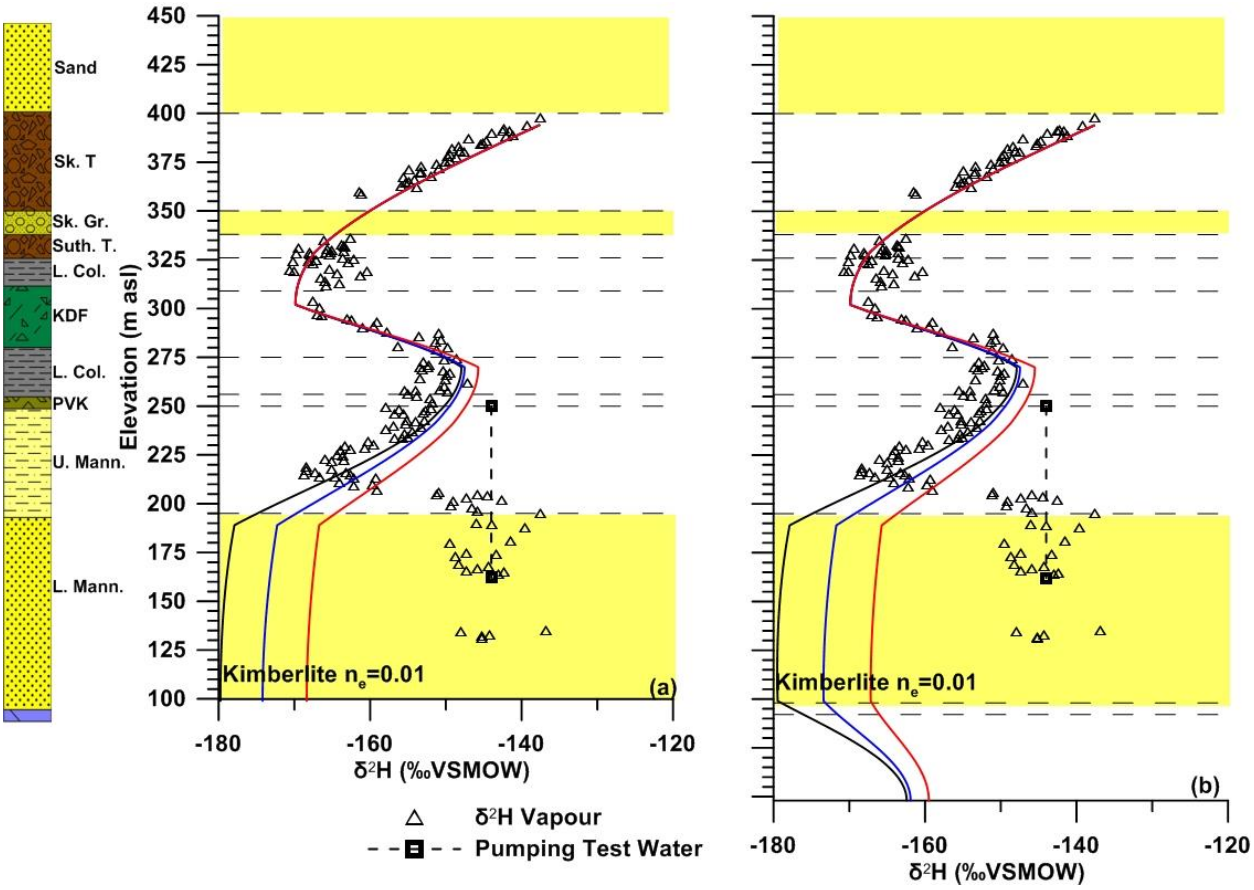

Figure 5.15. Measured and simulated δ^2H profiles versus elevation from the surficial sand to the base of the Cretaceous sediments (a) and from the surficial sand to 50 m below the Souris River Dolomite and lower Mannville aquifer contact (b). Simulations in (a) were conducted assuming $n_e=n_T$ in the Cretaceous sediments and $n_e=0.01$ in the kimberlite, constant δ^2H in the Mannville aquifer during glaciation, and no mass flux during interglacial periods, influx of glaciogenic water into the intertill aquifer from the onset of the Nebraska (800 ka BP) to the end of the Aftonian II interglacial (460 ka BP), and infiltration of modern water in the surifical sand at the onset of the Mindel Riss (240 ka BP). Simulations in (b) were conducted with the same evolution timing as presented in (a) but with 50 m of Souris River Dolomite added with an initial concentration of 177,000 mg L^{-1}. A no mass flux boundary was applied to the lower Mannville during the Holocene in simulations in (a) and (b) for 10 (black line), 15 (blue line), and 20 ka BP (red line).

5.8.4. Characterizing the Evolution of Cl in the Cretaceous Sediments at 140-10-087 using the Complex Glacial History of the Study Area

The modeling of Cl transport used the same assumptions with respect to n_e as discussed in Sections 5.4 and 5.8.1 (i.e., $n_e=0.4n_T$ or $n_e=0.6n_T$ for Cl in the Cretaceous sediments and $n_e=n_T$ for glacial till). The kimberlite at 140-10-087 (312-275 m asl) was again assigned an n_e of 0.01 based on studies by Katsube and Kjarsgaard (1996) and Stripp et al. (2006) and because of the simulated best fit to the measured data in Figure 5.12a. Because the pore spaces are filled with secondary calcite and serpentine that are not negatively charged, the $n_e=0.01$ that was estimated to be the best fit for the δ^2H profile at 140-10-087 was also used for the Cl profile. A D_e value of 1.5×10^{-10} m^2 s^{-1} were assigned for Cl in the glacial till and Cretaceous shale. A D_e value of 1.7×10^{-10} m^2 s^{-1} was assumed for the Mannville sands, silts, and clays and a D_e of 7×10^{-11} m^2s^{-1} was applied to the KDF unit (Figures 5.15a-b and Figures 5.10c-d) similar to what was described in Section 5.8.1. These values were consistent with the D_e for Cl in till and Cretaceous shale reported by Hendry et al. (2000) and Hendry et al. (2013). The upper boundary applied to the top of the glacial till, as well as the initial concentration in the glacial till, was 40 mg L^{-1}, based on the lowest measured value of meteoric water in squeezed pore water samples collected near the water table. A series of simulations were conducted using values of 100, 500, and 1000 mg L^{-1} applied as a region to the lower Mannville during glacial periods to address the variability of Cl concentration measured in the lower Mannville (Figure 5.10a,b). This lower boundary (Cl concentrations of 100, 500, and 1,000 mg L^{-1}) was applied during glacial periods and a no mass flux boundary was applied to the lower Mannville interglacial periods to allow Cl to increase in the Mannville aquifer by diffusion from the overlying upper Mannville sediments during interglacial periods. As was the case for the simulation of δ^2H at 140-10-087, a boundary of 40 mg L^{-1} was applied during the Holocene (20 ka BP) to simulate an influx of meteoric water into the Mannville aquifer in the last 10 to 20 ka BP. The pore water Cl concentration profiles with depth were simulated using an initial concentration of 20,000 mg L^{-1} in the Cretaceous-aged Lower Colorado shales and upper Mannville silt and sand (Hendry and Harrington, 2014), consistent with the shales being deposited in a marine environment and initial Cl concentrations used by Mazurek et al. (2011). The pore water Cl concentration profile was simulated using the same simulation timing as that of the δ^2H profile outlined in Table 5.6 and Section 5.8.3.

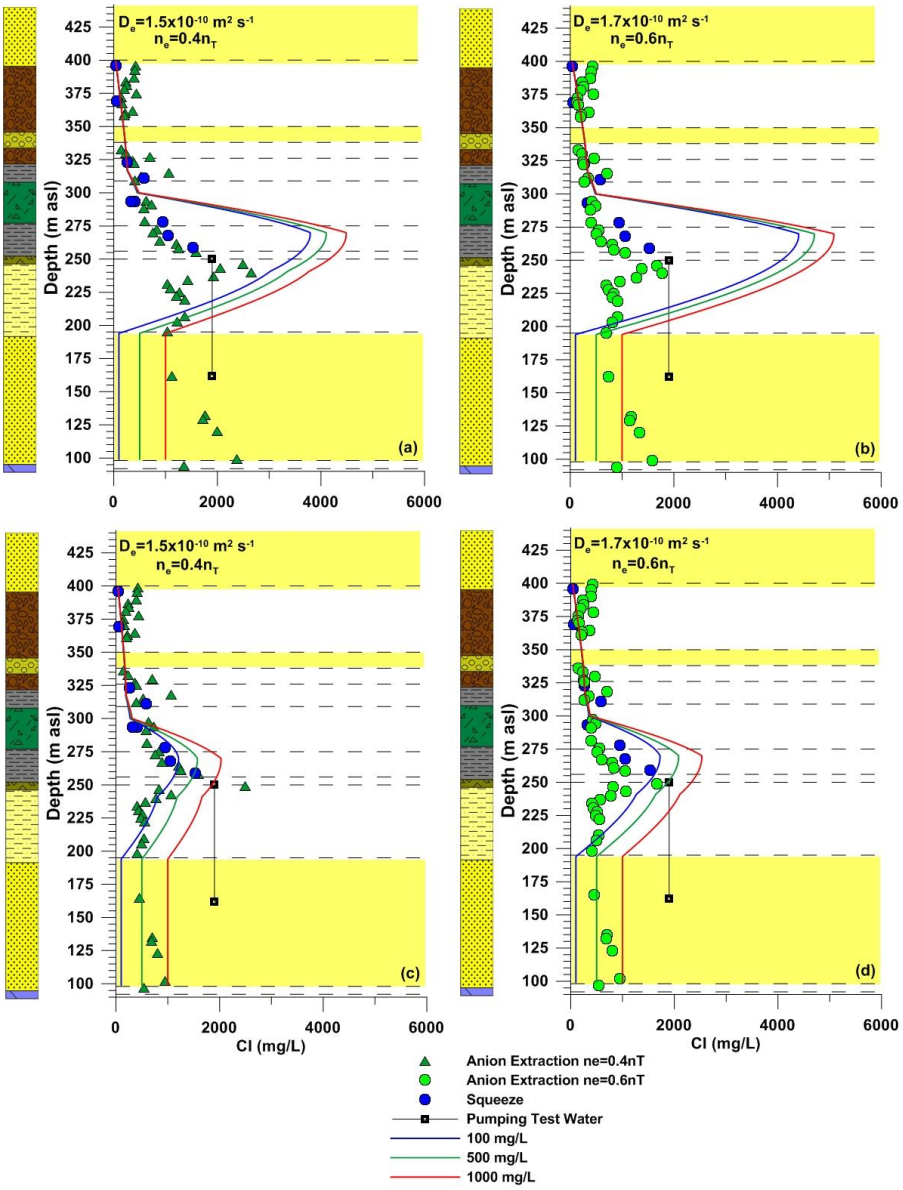

Figure 5.16. Measured and simulated pore water Cl concentration versus elevation (m asl) at 140-10-087 through the glacial till and Cretaceous sediments. Timing of evolution was consistent with that presented for δ^2H versus elevation in Figure 5.14. Simulations were conducted assuming $n_e=0.4n_T$ in the Cretaceous sediments and $n_e=0.01$ in the kimberlite in (a) and $n_e=0.6n_T$ in the Cretaceous sediments and $n_e=0.01$ in the kimberlite in (b). Simulations in (c) were conducted assuming $n_e=0.4n_T$ in the Cretaceous shale, $n_e=n_T$ in the upper Mannville, and $n_e=0.01$ in the kimberlite. Simulations in (d) were conducted assuming $n_e=0.6n_T$ in the Cretaceous shale, $n_e=n_T$ in the upper Mannville, and $n_e=0.01$ in the kimberlite. All simulations were conducted by applying a constant boundary on the lower Mannville of 100 to 1,000 mg L^{-1} during glacial periods, no mass flux during interglacial periods, and a constant boundary of 100 to 1,000 mg L^{-1} during the Holocene (20 ka BP).

Results of simulations using $n_e=0.4n_T$ and $n_e=0.6n_T$ in the Lower Colorado and Mannville Cretaceous-aged sediments are presented in Figure 5.16a and b. The evolution time was the same as that used in simulation 3 of the δ^2H model at 140-10-087 (Table 5.6), with the upper boundary applied at the onset of the Sangamon Interglacial, Saskatoon Group till deposited at the onset of the 2nd Kansan glaciation, and a constant boundary applied at the top of the Sutherland group till to simulate a constant source of glaciogenic water in the Saskatoon Group aquifer between the end of the Nebraska glaciation (625 ka BP) and the onset of the 4nd Kansan glaciation (460 ka BP). A change in timing of the upper boundary made little difference to the shape of the simulated profile because the pore water Cl concentration during glacial and interglacial periods was the same (40 mg L^{-1}). Based on these results, no additional evolution times were presented. Using D_e values of 1.5×10^{-10} and 1.7×10^{-10} m^2s^{-1} in the Cretaceous shale for $n_e=0.4n_T$ and $n_e=0.6n_T$ through the whole Lower Colorado shale (281.6 to 257.1 m asl) and upper Mannville (250.6 to 199.6 m asl), simulated profiles poorly approximated the measured data (Figure 5.10a and b).

Simulations were also conducted to explore the possibility that the upper Mannville sands, silts, and clays had n_e values equal to the measured n_T (Figures 5.16 c and d). Best fits (determined visually) to the measured data were observed when simulated with $n_e=0.4n_T$ in the Cretaceous shale (312 to 251 m asl), $n_e=0.01$ in the KDF (312 to 281 m asl), and $n_e=n_T$ in the upper Mannville (and corresponding D_e values of 1.5×10^{-10}, 7.0×10^{-11}, and 2.3×10^{-10} m^2s^{-1}, respectively).

Another simulation was conducted to illustrate the effect of applying a no mass flux boundary to the lower Mannville aquifer during the Holocene (20 ka BP; Figure 17a). This simulation was conducted using the best fit to the measured data in Figure 5.15c, using a D_e of 1.5×10^{-10} m^2 s^{-1}, an $n_e=0.4n_T$ in the Cretaceous shale, and an $n_e=n_T$ in the upper Mannville. The poor fit to the measured Cl concentration in the lower Mannville aquifer was attributed to the lack of data in the underlying Devonian Dolomite (Souris River Formation). Because the Souris River formation is known to have greater concentrations of Cl than the overlying Cretaceous shales, diffusion upward from this formation would increase the Cl concentration in the Mannville aquifer during interglacial periods (Hendry and Harrington, 2014). To test this hypothesis, 50 m of Devonian Dolomite was added to the base of the lower Mannville aquifer in

the simulation and given a D_e of 1.2×10^{-10} m^2s^{-1}, an n_e of 0.1, and an initial Cl concentration of 177,000 mg L^{-1} based on data collected and simulations conducted by Hendry and Harrington (2014) for the same geologic formation. This initial concentration was likely an overestimation of the Cl concentration in the dolomite because no Prairie Evaporate Formation exists at depth at the study site. Only the best fit to the measured data was considered for these simulations ($D_e=1.5\times10^{-10}$ m^2s^{-1} and $n_e=0.4n_T$ in the Cretaceous shale, $D_e=2.3\times10^{-10}$ m^2s^{-1} and $n_e=n_T$ in the upper Mannville, and the lower boundary applied as a region to the lower Mannville during glacial periods of 100 to 1,000 mg L^{-1}). The results of the simulations (Figure 5.17b) suggest that a no flux boundary condition applied to the lower Mannville during the Holocene has little effect on the simulated Cl concentration with depth, similar to what was observed for δ^2H at 140-10-087. Therefore, this boundary condition was not considered for the modeling of δ^2H and Cl with depth at OVB-10-207.

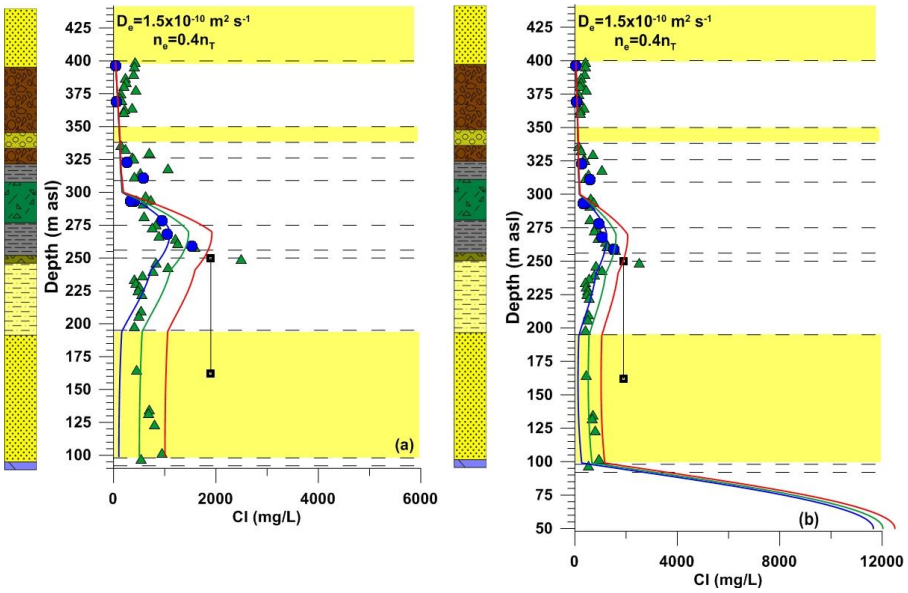

Figure 5.17. Measured and simulated Cl concentration versus elevaton (m asl) at 140-10-087. Simulations in (a) were conducted using the same evolution timing presented for Cl concentration in Figure 5.15, n_e=0.4n_T in the Cretaceous shale, n_e=n_T in the upper Mannville sediments, n_e=0.01 in the KDF, a constant Cl concentration of 100 to 1,000 mg L^{-1}, and no mass flux boundary applied to the lower Mannville aquifer during glaciations and interglacial periods. Simulations in (b) were conducted by adding 50 m of Souris River dolomite below the lower Mannville aquifer with an initial concentration of 177,000 mg L^{-1}. A no mass flux boundary was applied to the lower Mannville during the Holocene in (a) and (b) for 10 ka (black line), 15 ka BP (blue line), and 20 ka BP (red line).

5.8.5. Characterizing the Evolution of δ^2H in the Cretaceous Sediments at OVB-10-207 using the Complex Glacial History of the Study Area

The same D_e values that were used for the δ^2H profile at 140-10-087 were applied to the δ^2H in the glacial till, Cretaceous shale, and Mannville sands, silts, and clays at OVB-10-207 (2.3×10^{-10} m^2s^{-1}). The average δ^2H value in the surficial sand (-130‰) was assigned as the upper boundary and -180‰ was assigned as the initial value in the glacial sediments. As was the case at 140-10-087, the lower boundary condition alternated between δ^2H values of -180‰ (Hendry and Wassenaar, 1999) during glacial periods and no boundary condition during interglacial periods. Initial conditions in the Cretaceous sediments were also assumed to be that of present-day seawater (0‰) because the shales were deposited in a marine environment (Mazurek et al., 2011; Hendry et al., 2013). The n_T values for each geologic unit were estimated based on results of laboratory experiments (Figure 5.3) and, as such, the n_e values for Saskatoon and Sutherland glacial till, shale, and Mannville sediments were assigned the mean measured values of 0.24, 0.34, 0.45, and 0.37, respectively.

The evolution timing used to simulate the δ^2H profile at 140-10-087 was also used to simulate the δ^2H profile at this site (Figure 5.9a; Table 5.6; Section 5.8.3). The upper boundary applied to the top of the Saskatoon Group glacial till was applied during the Illinois interglacial (195 ka BP) in simulation 1, the Sangamon glacial period (135 ka BP) in simulation 2, and the Wisconsin glacial (95 ka BP) in simulation 3 (Figure 5.11a). Because the corehole was drilled to the base of the Cretaceous shale at this site, there were no data available to identify the thickness of the low K upper Mannville sand, silt, and clay. Thus, the same thickness as that observed at 140-10-087 (250-195 m asl) was assigned to this profile. The influx of meteoric water during the Holocene was estimated to be between 10 and 20 ka BP at 140-10-087; thus, an evolution timing of 15 ka BP was assigned to the simulation at OVB-10-207. While these simulations approximated the general shape of the measured δ^2H profile with depth, none provided a reasonable fit to the measured data (Figure 5.18a).

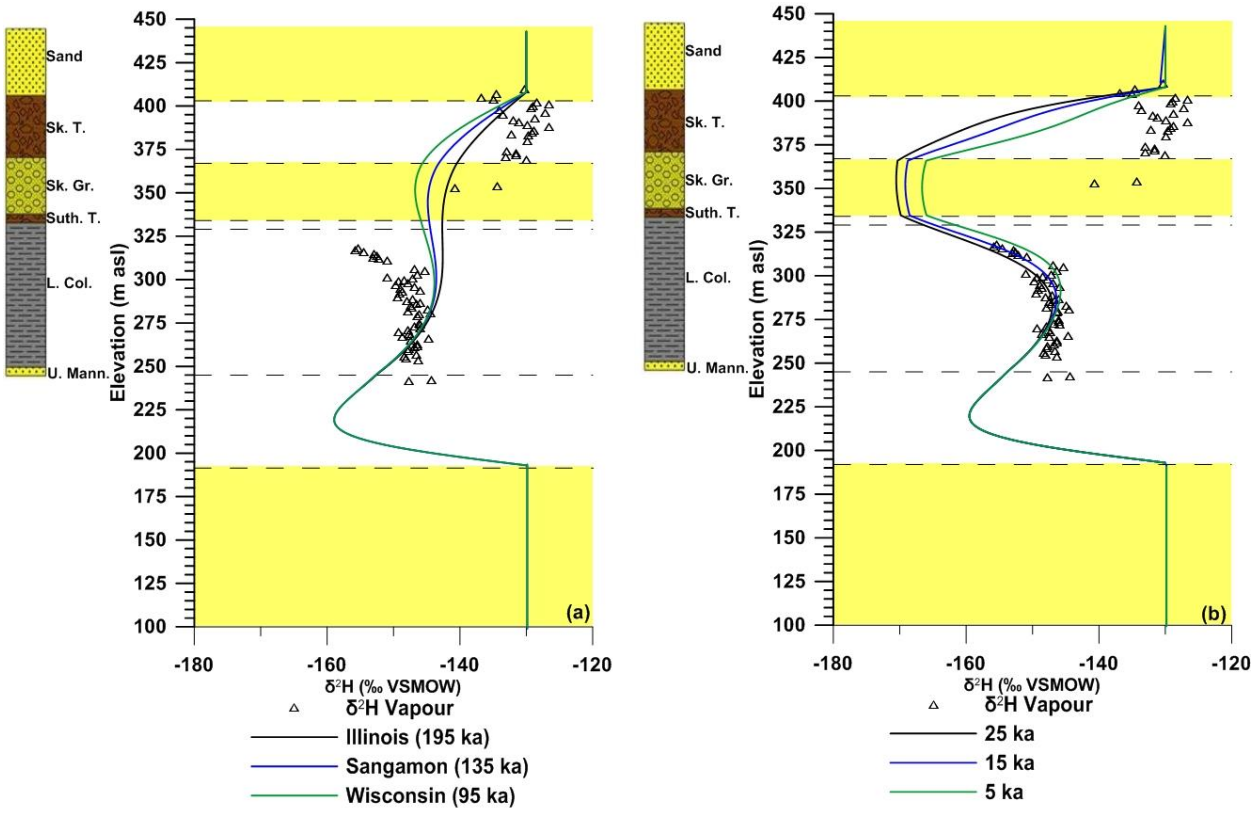

Figure 5.18. Measured and simulated pore water δ^2H versus elevation (m asl) through the glacial till and Cretaceous sediments at OVB-10-207. Simulations were conducted by applying a constant glaciogenic value to the lower Mannville aquifer during glacial periods, a no mass flux boundary during interglacial periods, and a constant δ^2H value representative of modern water (-130‰) during the Holocene (15 ka BP). An influx of glaciogenic water was applied to the intertill aquifer between the onset of the Nebraska glaciation (800 ka BP) and the end of the Aftonian II interglacial (460 ka BP). The upper boundary applied to the surficial sand was changed from no mass flux to modern water (-120‰) at the onset of the Illinois (195 ka BP), the onset of the Sangamon (135 ka BP), and the onset of the Wisconsin (95 ka BP) in (a). An additional analysis was added in (b) to simulate recharge of glaciogenic water (-165‰) at the end of the Wisconsin glaciation for a period of 5 to 15 ka before the onset of the Holocene (15 ka BP). All simulations were conducted assuming $n_e=n_T$ through the Cretaceous sediments.

In subsequent simulations (Figure 5.18b), it was hypothesized that the Saskatoon Group aquifer at this site was recharged with glaciogenic water (δ^2H=-165‰) when the Fort à la Corne delta was forming in the study area and glacial melt-water was draining into glacial Lake Saskatchewan during the Wisconsin glaciation (Christiansen et al., 1995) until the onset of the Holocene warming period (10-20 ka BP). A D_e one order of magnitude greater than that of the

glacial till and Cretaceous shale (2.3×10^{-9} m^2 s^{-1}) was applied to the Saskatoon Group gravel aquifer to simulate the effect of dispersive mixing from lateral groundwater flow within the aquifer when it was opened during the formation of the Fort à la Corne delta (Hendry et al., 2013). The flushing of the aquifer was simulated to last between 5 and 25 ka BP, prior to the onset of the Holocene; however, the best fit to the measured profile was observed between 5 and 15 ka BP, consistent with the timing of deposition of the Fort à la Corne delta in the study area (Christiansen et al., 1995). Because the Saskatoon Group aquifer was not observed at all drillholes at the study area, it was assumed that the recharge area for the Saskatoon Group aquifer at OVB-10-207 could have been open during formation of the delta while the recharge area for the Saskatoon Group aquifer at 140-10-087 was not. Alternatively, the Saskatoon Group aquifer observed at 140-10-087 was thinner and consisted of sand and silt as opposed to the thicker gravel aquifer observed at OVB-10-207, which may have resulted in diffusion dominated transport at 140-10-087 and advection dominated transport at OVB-10-207 (Hendry and Schmeling, in submission). Further analysis of the Saskatoon Group aquifer at both sites would be required to investigate transport mechanisms within the aquifer; however, core loss during drilling and sample collection by Clifton Associates resulted in no recovery in the aquifer at OVB-10-207. The poor fit to the measured data in the Saskatoon Group glacial sediments above the aquifer (403.9 to 367.9 m asl) may be a result of contamination by D_2O spiked drill mud while trying to recover the core that slipped out of the core barrel downhole during drilling.

5.8.6. Characterizing the Evolution of Cl in the Cretaceous Sediments at OVB-10-207 using the Complex Glacial History of the Study Area

In keeping with the n_e values estimated at 140-10-087, an $n_e=0.4n_T$ (Figure 5.10a,c) and an $n_e=0.6n_T$ (Figure 5.10b,d) were used to calculate pore water Cl concentrations in the Cretaceous sediments. Values of $n_e=n_T$ were used for Cl in the glacial till. The upper boundary and initial concentration in the till applied to the simulation was 40 mg L^{-1}, consistent with the simulation of Cl concentration with depth at 140-10-087. Because the Cl concentration in the Mannville could not be quantified at this site, the same lower boundary conditions applied to the δ^2H model at 140-10-087 were used for these simulations (100, 500, and 1,000 mg L^{-1}). A lower boundary applied as a region to the lower Mannville aquifer of 100, 500, and 1,000 mg L^{-1} was applied to the base of the upper Mannville (assumed to be at 195 m asl at this site). The initial Cl concentration of the Cretaceous shale was assumed to be 20,000 mg L^{-1} (Hendry and Harrington,

2014). The pore water Cl concentration profile was simulated using the same simulation timing as that of the δ^2H profile at this site. It was also assumed that the Saskatoon Group intertill aquifer was flushed for 10 ka at the end of the Wisconsin glaciation, as per the best fit to the measured δ^2H profile at this site (Figure 5.18a,b).

A reasonable fit (determined visually) to the measured data was obtained when the profile was simulated with an $n_e=0.4n_T$ in the Cretaceous shale (323 to 250 m asl) and Mannville sediments (250 to 195 m asl). The best fit to the measured data (Figure 5.19d) was observed when the Cl profile was simulated with an $n_e=n_T$ in the Mannville sediments and an $n_e=0.6n_T$ in the Cretaceous shale, the same evolution time as that described for the δ^2H profile at this corehole, an initial Cl concentration in the Cretaceous shale and Mannville sediments of 20,000 mg L^{-1}, and lower boundary conditions between 100 and 1000 mg L^{-1} applied to the top of the lower Mannville aquifer (195 m asl).

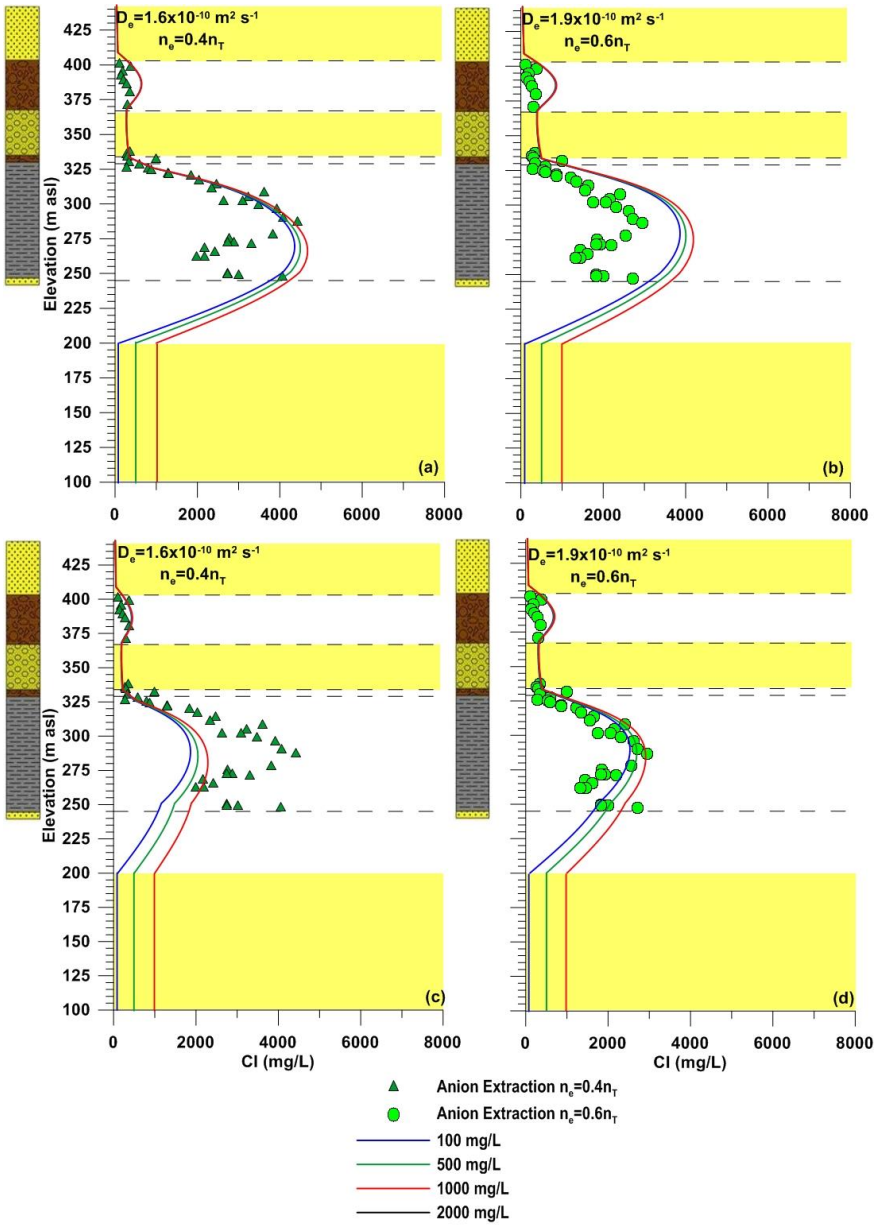

Figure 5.19. Measured and simulated pore water Cl concentration versus elevation (m asl) through the glacial till and Cretaceous sediments at OVB-10-207. Simulations were conducted using the same evolution time presented in Figure 5.17b for δ^2H and n_e=0.4n_T in the Cretaceous sediments in (a), n_e=0.6n_T in the Cretaceous sediments in (b), n_e=0.4n_T in the Cretaceous shale and n_e=n_T in the upper Mannville sediments in (c), and n_e=0.6n_T in the Cretaceous shale and n_e=n_T in the upper Mannville sediments in (d). The lower boundary assigned to the Mannville aquifer was 100 to 1,000 mg L^{-1} during glacial periods, no mass flux during interglacial periods, and 100 to 1,000 mg L-1 during the Holocene (15 ka BP). The upper boundary applied to the surficial sand was changed from no mass flux to 40 mg L^{-1} at the onset of the Illinois (195 ka BP).

5.8.7. Effects of Velocity on the Evolution of the δ^2H at 140-10-087 and OVB-10-207

All prior analyses were conducted as diffusion only for δ^2H and Cl at both sites. A final set of simulations was conducted to explore the effect of a vertical component of flow across the shale (advective transport) based on calculations of the Peclet number (Pe) at the study site. Using measured data, Pe values ranged from 0.5 to 5, suggesting vertical advection should be the dominant transport mechanism. The initial conditions, transport parameters (D_e, n_e), and boundaries assigned to the top of the glacial sediments and the lower Mannville aquifer were the same as those described for the best fits to the measured profiles in Sections 5.8.3 and 5.8.5 for 140-10-087 (Figure 5.12a) and OVB-10-207 (Figure 5.18b), respectively. Two sets of simulations were conducted, the first with an upward component of groundwater flow and the second with a downward component of groundwater flow across the shale. The upward component of groundwater flow was consistent with present-day measured head data in the aquitard, based on hydraulic head data from 140-10-087 as well as regionally located piezometers installed by SRK (Ugorets and Pereira, 2011). The downward component of groundwater flow could be expected during periods of glaciation when the site could have been under 2000 m of hydraulic head (Hendry et al., 2013). Based on Darcy calculations conducted using the measured K (2×10^{-10} to 1×10^{-11} m s^{-1}), n_T (0.36), and vertical gradients (0.03), groundwater velocities at the study site could range from 1.7×10^{-11} to 8.3×10^{-12} m s^{-1} (2.6 to 5.4 m 10 ka^{-1}) through the Cretaceous Shale. In the simulations, the range of groundwater velocities were assigned as 0.01, 0.1, and 1 m 10 ka^{-1} upward (Figure 5.20a,c) and 0.01, 0.1, and 1 m 10 ka^{-1} downward (Figure 5.20b,d).

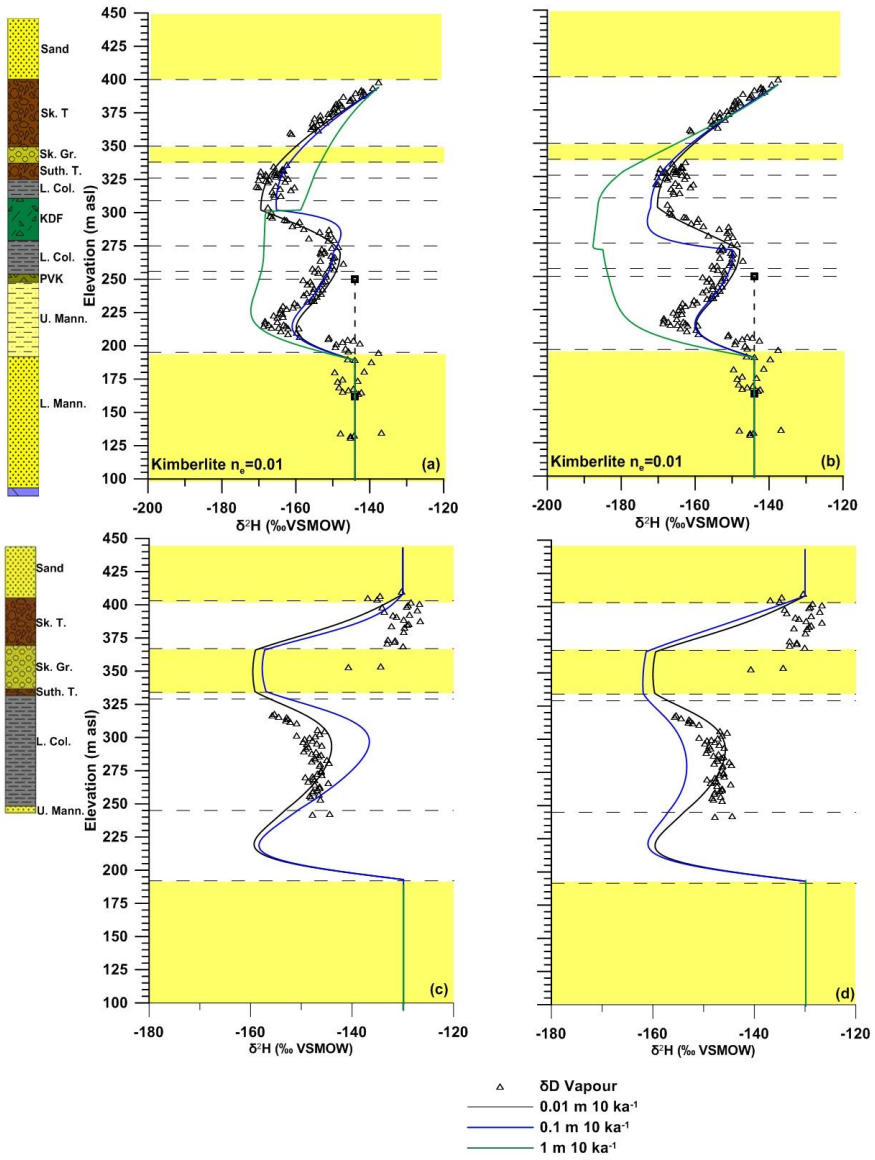

Figure 5.20. Measured and simulated pore water δ^2H versus elevation at 140-10-087 and OVB-10-207. Evolution times, boundary conditions, and transport parameters in (a) and (b) are consistent with the best fits to the measured data presented in Figure 9a for 140-10-087 and in (c) and (d) are consistent with Figure 5.17b for OVB-10-207, except advective velocities of 0.01, 0.1, and 1 m 10 ka^{-1} were applied to the sedimentary sequence both upward (a) and (c) and downward (b) and (d).

Results of the simulations suggest that groundwater velocities at 140-10-087 and OVB-10-207 are less than 0.1 m 10 ka^{-1}. Using the simulated groundwater velocity, the bulk K through the shale at 140-10-087 and OVB-10-207 was calculated to be 4×10^{-12} m s^{-1}, which was at least one to two orders of magnitude lower than that measured with triaxial testing. This K was consistent with values measured in shales throughout the Williston Basin (Smith et al., 2013;

Hendry et al., 2013; Shaw and Hendry, 1998), suggesting that potential gradients imposed on the shale during glaciation resulted in very little advection (Hendry et al., 2013).

5.9. Summary of Transport Modeling

A comparison of fits between the measured data and the complex simulations of the δ^2H and Cl profiles suggest that the timing of evolution and paleo-hydrogeologic history are consistent for both naturally occurring tracers at both the geologically simple and complex sites in the study area. The shape of the δ^2H and Cl profiles in the glacial sediments and 1-D transport simulations of the data collected at OVB-10-207 suggest that the Saskatoon Group aquifer was flushed with glaiciogenic water (δ^2H=-165‰) during the end of the Wisconsin glaciation, when the Fort à la Corne delta was being deposited in the study area (Christiansen et al., 1995). In contrast, the Saskatoon Group aquifer at 140-10-087 was not. In these simulations, the upper and lower boundaries, as well as initial conditions in the glacial till, Cretaceous Shale, and upper and lower Mannville sediments, were consistent at both study sites and diffusion was assumed to be the only transport mechanism (V=0). The δ^2H depth profiles were simulated by flushing the lower Mannville with glaciogenic water (δ^2H=-180‰) during glaciation and assigning a no mass flux boundary during interglacial cycles to simulate diffusion of δ^2H into the aquifer from the overlying sediments. The best fits to the measured δ^2H data were observed when the Mannville was flushed during every glacial event during the Late Pleistocene at both study sites. Similarly, the best fits to the measured Cl concentration profiles at both sites were simulated by flushing the lower Mannville with glaciogenic water (i.e., water with a Cl concentration of 100, 500, and 1,000 mg L^{-1}) during glacial periods and a no mass flux boundary interglacial periods. Increased evolution timing and more knowledge of the glacial history of the study area between 1,800 and 800 ka BP may have provided more reasonable fits to the measured Cl data. The lack of information on Early Pleistocene depositional history of the study area made it difficult to justify an increase the evolution timing in the simulations.

Poor fits to the measured δ^2H profile at 140-10-087 were obtained when D_e and n_e values equal to those of the overlying and underlying Cretaceous shale were applied to the kimberlite unit. A reasonable fit to the measured profile was obtained when an n_e=0.01 was applied to the kimberlite ($D_e=7.0\times10^{-11}$ m^2 s^{-1}). This low n_e for the kimberlite could be attributed to the effects of hydrothermal alteration after deposition and the associated infilling of the pore spaces with

secondary calcite, serpentine, and magnetite (Katsube and Kjarsgaard, 1996; Stripp et al., 2006). The good fit to the measured data also suggests that fractures observed during core logging have little to no effect on solute transport in the kimberlite or the overlying and underlying shale. Calculation of the dimensionless Fs number less than 1 at 140-10-087 (0.008) supported the results of the simulations (van der Kamp, 1992). The lack of effect of fracturing on the profile may be due to the fractures being infilled with calcite and serpentine shortly after kimberlite volcanism (and subsequent hydrothermal alteration) and/or to the fractures not being interconnected. The latter explanation was considered less likely because of the small fracture spacing (0.3 to 1.0 m in the kimberlite).

Values of n_e assigned to the Cretaceous shale and upper Mannville silt, sand, and clay in the model and used to calculate Cl concentration with depth ranged from $n_e=0.4n_T$ to $n_e=0.6n_T$, based on n_e values from the literature. Simulations of the Cl concentration with depth at both sites suggest that either a longer evolution timing is necessary to simulate the measured data or the n_e in the upper Mannville is the same as the n_T. Simulations conducted with an assigned n_e value equal to n_T in the upper Mannville produced good fits to the measured data at both sites. The best fit to the measured Cl concentration profiles with depth were observed when an $n_e=0.4n_T$ was applied to the Cretaceous Shale at 140-10-087 and $n_e=n_T$ in the upper Mannville. Conversely, the best fit to the measured Cl data at OVB-10-207 was observed when an $n_e=0.6n_T$ was applied to the Cretaceous Shale and $n_e=n_T$ was applied to the upper Mannville. Results of these simulations suggest that the n_e and D_e of each hydrogeological unit be measured before Cl is used to establish solute transport mechanisms at a complex study site. In contrast, simpler laboratory testing to estimate total porosity, coupled with the use of a well-documented D_e values (2.3×10^{-10} m^2 s^{-1}; Hendry et al., 2013) for Cretaceous shales, can be used to effectively simulate δ^2H with depth at both drillholes. This suggests that for study sites with a complex paleo-hydrogeologic evolution and geology, δ^2H is a more practical natural tracer that can more effectively define solute transport mechanisms.

Knowledge of the paleo-hydrogeologic history of the study area was essential to simulate the measured δ^2H and Cl data at both 140-10-087 and OVB-10-207. Good fits to the measured data for all four tracer profiles could be reasonably estimated by simulating the Late Pleistocene glacial history of the study area (800 ka BP to present). Better fits to the measured data could be

resolved by considering diffusion of δ^2H and Cl out of the Cretaceous shale into the overlying 850-1000 m of Late Cretaceous and Tertiary sediments that were eroded during Eocene to Pliocene time (~58-2 Ma; Taylor et al., 1961; Hendry et al., 2000). Also, knowledge of the earliest glacial advances across the study area between 1.8 Ma and 800 ka BP and the deposition of glacial sediments that have since been eroded during later glaciations, as well as a better understanding of the thickness of the Sutherland Group glacial sediments prior to deposition of the Saskatoon Group glacial sediments, could provide better evolution times for the simulations. However, the glacial history described by Christiansen (1968) and Christiansen (1992) and used in the simulations resulted in good fits to the measured data and was considered reasonable.

A comparison between simplified and complex simulations of the measured δ^2H and Cl with depth revealed that, although these simulations provided good overall fits to the measured natural tracer profiles, the paleo-hydrogeologic history associated with the simplified simulations was unrealistic. In the simplified models, it was assumed that all of the glacial sediments were deposited at the onset of the Late Pleistocene glaciations and that there was no effect of infiltration of meteoric water at the water table during interglacial periods. It was also assumed that the Mannville group aquifer was perpetually flushed for 765-775 ka BP. The complex models were constructed based on the glacial history of the study area (Christiansen 1968, 1992) and, as such, were considered a more reasonable estimate of the solute transport mechanisms and evolution timing of the measured δ^2H and Cl with depth.

Modeling of the measured pore water δ^2H and Cl versus elevation at 140-10-087 and OVB-10-207 showed that the profiles can be simulated by diffusive transport only. Modeling suggests that the vertical groundwater velocity (either upward or downward) averaged <0.01 m 10 ka^{-1} over the past 800 ka in the shale aquitard. Results are similar to findings by Hendry et al. (2013) and suggest that the hydraulic gradients imposed during glaciation resulted in little advection. Simulations also suggest that the measured K_v from triaxial testing in the Lower Colorado shale was one to two orders of magnitude greater than estimated from solute transport simulations. Conversely, triaxial K_v values in the shale were one to two orders of magnitude lower than K_v values estimated from 2-D axisymmetric pumping test simulations. Triaxial K_v values were likely overestimated by as much as two orders of magnitude as a result of the low effective stress applied to the samples during testing. Similar results were obtained in the Pierre

Shale at the K2 site near Esterhazy, Saskatchewan (Smith et al., 2013). The K_v values estimated from the pumping tests were greater than estimated from solute transport modeling and triaxial testing likely due to scale effects and heterogeneities in the aquitard and aquifer units (Neuzil, 1994).

SUMMARY, CONCLUSIONS, AND RECOMMENDATIONS FOR FUTURE WORK

6.1. Summary and Conclusions

This study was conducted as part of a long-term study of the hydrogeology and solute transport mechanisms of thick glacial till and Cretaceous bedrock shales within the Williston Basin. The goal of this research was to test the applicability of high-resolution, natural tracer profiles to estimate groundwater flow and solute transport through Cretaceous bedrock shales at a geologically complex study area. Two study sites were chosen for the study, the first in a geologically simple shale, not impacted by kimberlite volcanism, and the second a geologically complex, fractured shale, interbedded with hydrothermally altered kimberlite and kimberlite debris flows.

Triaxial K testing through the Cretaceous shale at both sites yielded values of 2×10^{-11} to 5×10^{-10} m s^{-1} in the shale and 2×10^{-11} to 3×10^{-10} m s^{-1} in the kimberlite and kimberlite debris flow, consistent with diffusion dominated aquitards in the Williston Basin (Hendry and Wassenaar, 1999; Hendry et al., 2000, 2011, 2013). An analysis of δ^2H values and Cl concentrations was used to identify hydrogeologic zones through the glacial till and Cretaceous aquitard at both sites and to verify *in situ* K_v values at larger scales and distance. The results of this analysis suggest that, despite the degree of complexity at these coreholes, the shape of the tracer profiles can be described by diffusion and that linear groundwater velocities were <0.1 m 10 ka^{-1} throughout the Late Pleistocene; this suggests a bulk K_v of the aquitard of 4×10^{-12} m s^{-1}. The presence of kimberlite and subsequent hydrothermal alteration at the complex study site (140-10-087) resulted in very low n_e values within the kimberlite media (n_e=0.01). This allowed water and solutes to travel through the kimberlite at this site more quickly than in the intact Cretaceous shale overlying and underlying the kimberlite in this corehole and through the whole profile at the geologically simpler site (OVB-10-207). The presence of fractures within the kimberlite material and the overlying and underlying Lower Colorado shale showed little to no effect on solute transport mechanisms, suggesting the fractures had either been sealed by calcite

and serpentine infilling or were not connected. Results also suggest that deposition of the kimberlite into the Cretaceous shale had no measureable impact on hydrogeologic properties or solute transport mechanisms of the surrounding shale. As such, these sediments would act as an aquitard, minimizing water flow and solute transport.

One-dimensional natural tracer profiles are useful in defining solute transport mechanisms in simple, thick aquitard systems; however, to do so at this complex study site requires a rigorous understanding of the paleo-hydrogeologic history. Numerical simulations of δ^2H and Cl were used to define the timing and duration of activation of the Mannville Formation aquifer at the study site, placing the onset of glaciation at the study area 800 ka BP, deposition of the lower Saskatoon Group glacial till and Riddell member intertill aquifer between 625 and 460 ka BP, deposition of the upper Saskatoon Group glacial sediments between 460 and 260 ka BP, deposition of the Fort à la Corne delta in the area at 10 to 15 ka BP, and onset of the Holocene warming period at about 10 ka BP. Results of numerical simulations also suggest that the Saskatoon Group intertill aquifer was either not connected across the study area or that recharge of glaciogenic water during the Wisconsin period may have occurred at the simple study site (OVB-10-207) but did not influence the shape of the 1-D profiles of δ^2H and Cl at the complex study site (140-20-087). However, the smaller particle size in the Saskatoon Group aquifer at 140-20-087, when compared to the aquifer at OVB-10-207, may have resulted in diffusion-dominated transport within the former and advective transport within the latter. Simple simulations of the δ^2H and Cl depth profiles suggest that good fits to the measured data could be reasonably approximated with a simplified understanding of the paleo-hydrogeologic history but the results can be unrealistic. The simplified models may also over- or underestimate the evolution timing of the measured natural tracer profiles.

The use of multiple independent tracers, such as Cl and δ^2H, in aquitard studies can be used to improve confidence when trying to establish solute transport mechanisms at complex study sites. However, the use of the natural conservative tracer Cl can result in a great deal of uncertainty when trying to establish the paleo-hydrogeologic history of the study area as well as initial and boundary conditions. The initial pore water Cl concentration in Cretaceous sediments is extremely variable across the basin, ranging from 10,000 to 60,000 mg L^{-1} (Connelly et al., 1990). This makes it extremely difficult to discern the initial conditions at a study site without

knowledge of the pore water Cl concentrations below the Mannville Group Aquifer. Because the Prairie Evaporite Formation did not exist at the study area, the initial Cl concentration in the Cretaceous shales was assumed to be a result of diffusive mixing between seawater and glaciogenic water, with no influence from Cl diffusing out of halite or potash from underlying formations. Further, the fact that Cl concentrations remained similar (40-500 mg L^{-1}) during glacial and interglacial periods was useful for predicting the timing of evolution of pore water Cl concentration with depth at a study site using the traditional modeling approach. Using the traditional approach, the bounding aquifers have constant concentrations applied and the solute is allowed to diffuse in or out of the aquitard. This can lead to a considerable underestimation of the timing of evolution of the concentration profile and provides no evidence as to the paleo-hydrogeologic history of the study area. Results of this study also suggest that, because n_e and D_e values for Cl transport are so variable, the n_e and D_e of each hydrogeologic unit should be measured before Cl can be used to establish solute transport mechanisms at a complex study site. This, in turn, suggests that δ^2H is a more practical natural tracer that can more effectively define solute transport mechanisms at study areas with a complex history and geology.

Transport modeling of 1-D tracer profiles in complex aquitards can be considered non-unique. The shape of the profiles can be interpreted in a number of ways. In the current study, the complexity of the aquitard system as well as the presence of two separate aquifer systems increased the difficulty of defining initial and boundary conditions, especially when simulating the Cl concentration profiles. At complex study sites, traditional studies (i.e., pumping tests, slug testing) and 3-D modeling may better provide concrete hydrogeologic data than the application of 1-D tracer profiles.

6.2. Recommendations for Future Research

1. Additional pumping tests could be designed at 140-10-089 and near OVB-10-207 to sufficiently stress the Lower Colorado shale (enough to be recorded by transducers installed within the shale aquitard). An equivalent pump test is necessary near the unimpacted corehole to determine whether the resulting bulk K_v can be attributed to kimberlite volcanism.

2. A 3-D model of pumping tests 1 and 2 could more accurately simulate vertical and horizontal groundwater flow within the Lower Colorado aquitard and Mannville aquifer. A 2-D model, such as the one presented in this thesis (Appendix A), cannot accurately incorporate the

potential impact of the emplacement of more than 70 kimberlite bodies on water flow through the Lower Colorado aquitard during pumping of the Mannville aquifer.

3. While this study investigated the dominant solute transport mechanisms of minimally impacted shale and a complex shale at the Shore Gold study site, more information is required within the kimberlite bodies to describe both the hydrogeological properties and solute transport mechanisms of the kimberlite media itself. Natural tracer profiles of δ^2H and Cl within and surrounding a kimberlite body could provide a 3-D study of the kimberlite pipes.

4. A study of 1-D δ^2H and Cl profiles, as well as high resolution pore water noble gases (^4He and ^{40}Ar) and ^{14}C-DIC, could provide quantitative dating of groundwater in the range of 1,000 a up to many Ma (Rübel et al., 2002; Stute et al., 1992). Groundwater age-dating of porewater with depth within the kimberlite pipes could provide insight into the role of the kimberlite pipes as conduits for groundwater infiltration into the underlying Mannville aquifer at the study area. Additional high-resolution profiles could be constructed at sites that do not intersect the Saskatoon Group intertill aquifer to estimate its connectivity within the study area and its impact on the hydrogeology and solute transport mechanisms.

5. Laboratory testing of D_e and n_e within the kimberlite materials is warranted to better constrain these variables for transport modeling.

REFERENCES

American Society for Testing and Materials (ASTM) (2009) D7263-09: Standard Test Methods for Laboratory Determination of Density (Unit Weight) of Soil Specimens. In: Annual Book of ASTM Standards, West Conshohocken, PA.

American Society for Testing and Materials (ASTM) (2010a) D2216-10: Standard Test Methods for Laboratory Determination of Water (Moisture) Content of Soil and Rock by Mass. In: Annual Book of ASTM Standards, West Conshohocken, PA.

American Society for Testing and Materials (ASTM) (2010b) D5084-10: Standard Test Methods for Measurement of Hydraulic Conductivity of Saturated Porous Materials Using a Flexible Wall Permeameter. In: Annual Book of ASTM Standards, West Conshohocken, PA.

Bachu S (1985) Influence of lithology and fluid flow on the temperature distribution in a sedimentary basin: a case study from the Cold Lake area, Alberta, Canada. Tectonophys 120(3-4): 257-284.

Bangsund AL, Hendry MJ, Fernández AM (2012) Geochemical effects of incremental high-pressure squeezing on pore waters from argillaceous aquitards. Presented at the 5th International Meeting on Clays in Natural and Engineered Barriers for Radioactive Waste Confinement, Montpellier, FR.

Barbour SL, Hendry MJ and Wassenaar LI (2012) In situ experiment to determine advective-diffusive controls on solute transport in a clay-rich aquitard. J. of Cont. Hydrol. 131(1-4): 79-88.

Barone FS, Rowe RK, Quigley RM (1990) Laboratory determination of chloride diffusion coefficient in an intact shale. Can Geotech J 27: 177-184.

Barone FS, Rowe RK, Quigley RM (1992) A laboratory estimation of diffusion and adsorption coefficients for several volatile organics in a natural clayey soil. J Contam Hydrol 10: 225-250.

Benson SM, Cole DR (2008) CO2 sequestration in deep sedimentary formations. Elements 4: 325-331.

Berryman AK, Scott Smith BH, Jellicoe BC et al (2004) Geology and diamond distribution of the 140/141 kimberlite, Fort á la Corne, central Saskatchewan, Canada. Lithos 76(1): 99-144.

Booth CJ, Spande ED (1992) Potentiometric and Aquifer Property Changes Above Subsiding Longwall Mine Panels, Illinois Basin Coalfield. Ground Water 30(3): 362-368.

Boudreau BP (1996) The diffusive tortuosity of fine-grained unlithified sediments. Geochim. Cosmochim. Acta, 60(16): 3139-3142.

Boudreau BP, Meysman PJR (2006) Predicted tortuosity of muds. Geology 34(8): 693-696.

Bowker KA (2006) Barnett Shale gas production, Fort Worth Basin: Issues and discussion. AAPG Bull 91(4): 523-533.

Capuano RM (1993) Evidence of fluid flow in microfractures in geopressured shales. AAPG Bull 77: 1303-1314.

Christiansen EA (1968) Pleistocene stratigraphy of the Saskatoon area, Saskatchewan, Canada. Can J Earth Sci 5: 1167-1173.

Christiansen EA (1992) Pleistocene stratigraphy of the Saskatoon area, Saskatchewan, Canada: an update. Can J Earth Sci 29: 1767-1778.

Christiansen EA, Sauer EK (1993) Red Deer Hill: a drumlinized glaciotectonic feature near Prince Albert, Saskatchewan, Canada. Can J Earth Sci 30: 1224-1235.

Christiansen EA, Sauer EK, Schreiner BT (1995) Glacial Lake Saskatchewan and Lake Agassiz deltas in east-central Saskatchewan with special emphasisi on the Nipawin delta. Can J Earth Sci 32: 334-348.

Clark ID, Fritz P (1997) Environmental isotopes in hydrogeology. CRC Press.

Clifton Associates Ltd. (2011) Orion South Geotechnical Program Summary Waste Stockpile Area Fort à la Corne, Saskatchewan. Clifton Associates Ltd., Saskatoon, SK.

Connolly CA, Walter LM, Baadsgaard et al (1990) Origin and evolution of formation waters, Alberta basin, western Canada sedimentary basin. I. chemistry. Appl Geochem 5(4) 375-395.

Cook P (2003) A Guide to Regional Groundwater Flow in Fractured Rock Aquifers. Adelaide, South Australia: CSIRO.

Croisé J, Schlickenrieder L, Marschall P et al (2004) Hydrogeological investigations in a low permeability claystone formation: the Mont Terri Rock Laboratory. Phys Chem Earth 29: 3-15.

Curtis JB (2002) Fractured shale-gas systems. AAPG Bull 86(11): 1921-1938.

Dawson FM, Evans CG, Marsh R et al (1994) Chapter 24: Uppermost Tertiary and Cretaceous Stratigraphy of the Western Canada Sedimentary Basin. In: Geological Atlas of the Western Canada Sedimentary Basin. Alberta Geological Survey Edmonton, AB.

Desaulniers DE, Cherry JA, Fritz P (1981) Origin, age and movement of pore water in argillaceous Quaternary deposits at four sites in southwestern Ontario. J Hydrol 50: 231-257.

Desaulniers DE, Kaufmann RS, Cherry JA, Bentley HW (1986) 37Cl-35Cl variations in a diffusion-controlled groundwater system. Geochim Cosmochim Acta 50: 1757-1764.

Domenico PA and Schwartz FW (1990) Physical and Chemical Hydrogeology. John Wiley & Sons, New York.

Eaton TT, Bradbury KR (2003) Hydraulic transience and the role of bedding fractures in a bedrock aquitard, southeastern Wisconsin, USA. Geophys Res Lett 30(18): HLS4-1–HLS4-5

Eaton TT, Anderson MP, Bradbury KR (2007) Fracture control on ground water flow and water chemistry in a rock aquitard. Groundwater 45(5): 601-615.

Edmunds WM, Bath AH (1976) Centrifuge extraction and chemical analysis of interstitial waters. Environ Sci Technol 10: 467-472.

Eichinger L (1983) A contribution to the interpretation of 14C groundwater ages considering the example of a partially confined sandstone aquifer. Radiocarbon 25: 347-356.

El-Kadi AI, Plummer N, Aggarwal P (2011a) NETPATH-WIN: An interactive user version of the mass-balance model, NETPATH. Groundwater 49(4): 593-599.

El-Kadi AI, Plummer N, Aggarwal P (2011b) Supporting information to: NETPATH-WIN: An interactive user version of the mass-balance model, NETPATH. http://www-naweb.iaea.org/napc/ih/documents/other/NETHPATH%20Supporting%20Info.pdf

Ewert WD, Brown FH, Puritch EJ (2009) Technical report and resource estimate update on the Star Diamond Project, Fort á la Corne area, Saskatchewan, Canada. P&E Mining Consultants Inc. Brampton, ON.

Feth JH (1981) Chloride in natural continental water: A review U.S. Geol Surv Water Supply Pap 2176: 30 pp.

Fetter CW (1999) Contaminant Hydrogeology. New Jersey: Prentice Hall.

Fetter CW (2001) Applied Hydrogeology. New Jersey: Prentice Hall.

Freeze RA, Cherry JA (1979) Groundwater. New Jersey: Prentice Hall.

Fontes JC, Garnier JM (1979) Determination of the initial 14C activity of the total dissolved carbon: A review of the existing models and a new approach. Water Resour Res 15: 399-413.

Gautschi A (2001) Hydrogeology of a fractured shale (Opalinus Clay): Implications for deep geological disposal of radioactive wastes. Hydrogeol J 9: 97-107.

GEO-SLOPE International Ltd (2007) Seepage Modeling with SEEP/W 2007. An Engineering Methodology 2nd Edition. Calgary, AB.

Gillham RW, Cherry JA (1982) Contaminant migration in saturated unconsolidated geologic deposits. Geological Society of America Special Papers 189: 31-62.

Gimmi T, Waber HN, Gautschi A et al (2007) Stable water isotopes in pore water of Jurassic argillaceous rocks as tracers for solute transport over large spatial and temporal scales. Water Resour Res 43: W04410.

GNS Science (2010) Sample Collection for Water Dating Analysis [online]. http://bullywug.gns.cri.nz/services/waterdating/cfc.html

Grasby SE, Betcher R (2000) Pleistocene recharge and flow reversal in the Williston basin, central North America. J Geochem Explor 69-70: 403-407.

Grasby S, Osadetz K, Betcher R et al (2000) Reversal of the regional-scale flow system of the Williston Basin in response to Pleistocene glaciation. Geol 28(7): 635-638.

Hantush, MS (1967) Flow of Grounwater in Relatively Thick Leaky Aquifers. Water Resour Res 3(2): 583-590.

Hart DJ, Bradbury KR, Feinstein DT (2006) The vertical hydraulic conductivity of an aquitard at two spatial scales. Groundwater 44(2): 201-211.

Hendry MJ, Harrington G (2014) Comparing vertical profiles of natural tracers in the Williston Basin to estimate the onset of deep aquifer activation. Water Resour Res 50: 6496-6506.

Hendry MJ, Schmeling E (in submission) Estimating dominant solute transport mechanisms in saturated unconsolidated sediments. Water Resour Res.

Hendry MJ, Wassenaar LI (1999) Implications of the distribution of δD in pore waters for groundwater flow and the timing of geologic events in a thick aquitard system. Water Resour Res 35(6): 1751-1760.

Hendry MJ, Wassenaar LI (2004) Characterizing the hydrogeology of a complex clay-rich aquitard system using detailed vertical profiles of the stable isotopes of water. J. of Hydrol. 293(1): 47-56.

Hendry, MJ, Wassenaar LI (2011) Millennial-scale diffusive migration of solutes in thick clay-rich aquitards: Evidence from multiple environmental tracers. Hydrogeol J 19: 259-270.

Hendry MJ, Wassenaar LI, Kotzer T et al (2000) Chloride and chlorine isotopes (36Cl and δ37Cl) as tracers of solute migration in a thick, clay-rich aquitard system. Water Resour Res 36(1): 285-296.

Hendry MJ, Kelln CJ, Wassenaar LI (2004) Characterizing the hydrogeology of a complex clay-rich aquitard system using detailed vertical profiles of the stable isotopes of water. J Hydrol 293: 47-56.

Hendry MJ, Barbour SL, Zettl J et al (2011) Controls on the long-term downward transport of δ2H of water in a regionally extensive, two-layered aquitard system. Water Resour Res 47(W06505): 1-13.

Hendry MJ, Barbour SL, Novakowski K et al (2013) Palaeo-hydrogeology of the Cretaceous sediments of the Williston Basin using stable isotopes of water. Water Resour Res 49: 4580-4592.

Huysmans M, Dassargues A (2005) Review of the use of Péclet numbers to determine the relative importance of advection and diffusion in low permeability environments. Hydrogeol J 13: 895-904.

Ingerson E, Pearson FJ Jr (1964) Estimation of age and rate of motion of groundwater by the 14C-method, In: Recent Researches in the Fields of Atmosphere, Hydrosphere, and Nuclear Geochemistry. Sugawara Festival Volume. Ed. Y. Miyake and T. Koyama, 263-283, Maruzen Co., Tokyo.

Jessop AM, Vigrass LW (1989) Geothermal measurements in a deep well at Regina, Saskatchewan. J Volcanol Geotherm Res 37(2): 151-166.

Johnson SL, Wright AH (2003) Mine void water resource issues in Western Australia. Western Australia, Water and Rivers Comm. Hydrogeol. Record Series, Report HG 9: 93 pp.

Katsube TJ and Kjarsgaard BA (1996) Physical property characteristics of Canadian kimberlites In: Searching for diamond in Canada, AN LeCheminant, RNW DiLabio, and KA Richardson (eds.); Geological Survey of Canada, Open File 3228, p. 241-242.

Keller CK, van der Kamp G, Cherry JA (1986) Fracture permeability and groundwater flow in clayey till near Saskatoon, Saskatchewan. Can Geotech J 23: 229-240.

Kelln CJ, Wassenaar LI, Hendry MJ (2001) Stable isotopes (δ18O, δ2H) of pore waters in clay-rich aquitards: a comparison and evaluation of measurement techniques. Groundw Monit Remed 21(2): 108-116.

Koehler G, Wassenaar LI, Hendry MJ (2000) An automated technique for measuring δD and δ18O values of porewater by direct CO2 and H2 equilibration. Anal Chem 72: 5659-5664.

Koroleva M, Alt-Epping P, Mazurek M (2011) Large-scale tracer profiles in a deep claystone formation (Opalinus Clay at Mont Russelin, Switzerland): Implications for solute transport processes and transport properties of the rock. Chem Geol 280: 284-296.

Lavastre V, Jendrzejewski N, Agrinier P et al (2005) Chlorine transfer out of a very low permeability clay sequence (Paris Basin, France): 35Cl and 37Cl evidence. Geochim Cosmochim Acta 69(21): 4949-4961.

Leckie DA, Kjarsgaard BA, Bloch J et al (1997) Emplacement and reworking of Cretaceous, diamond-bearing, crater facies kimberlite of central Saskatchewan, Canada. GSA Bull 109(8): 1000-1020.

Lefebvre N, Kurszlaukis S (2008) Contrasting eruption styles of the 147 Kimberlite, Fort á la Corne, Saskatchewan, Canada. J Volcanol Geotherm Res 174: 171-185.

Leo CJ and Booker JR (1996) A time-stepping finite element method for analysis of contaminant transport in fractured porous media. International journal for numerical and analytical methods in geomechanics, 20(12): 847-864.

Lis G, Wassenaar LI, Hendry MJ (2008) High-precision laser spectroscopy D/H and 18O/16O measurements of microliter natural water samples. Anal Chem 80(1): 287-293.

Mazurek M, Lanyon WG, Vomvoris S et al (1998) Derivation and application of a geologic dataset for flow modeling by discrete fracture networks in low-permeability argillaceous rocks. J Contam Hydrol 35: 1-17.

Mazurek M, Alt-Epping P, Bath A et al (2011) Natural tracer profiles across argillaceous formations. Appl Geochem 26(7): 1035-1064.

McNeil DH, Gilboy CF (2000) Cretaceous stratigraphy in four cores from the vicinity of the Fort á la Corne Kimberlite Field, east-central Saskatchewan-preliminary results. Saskatchewan Energy and Mines Miscellaneous Report 2000-4.1, Summary of Investigations 2000(1): 98-105.

Mitchell JK (1993) Fundamentals of soil behavior. John Wiley and Sons, Inc., New York.

Mook WG (1972) On the reconstruction of the initial 14C content of groundwater from the chemical and isotopic composition. In: Proceedings of Eighth International Conference on Radiocarbon Dating, v. 1, Royal Society of New Zealand, Wellington, New Zealand: 342-352.

Neuman, SP and Witherspoon PA (1972) Field Determination of the Hydraulic Properties of Leaky Multiple Aquifer Systems. Water Resour Res 8(5):1284-1298.

Neuzil CE (1986) Groundwater Flow in Low-Permeability Environments. Water Resour Res 22(8): 1163-1195.

Neuzil CE (1993) Low Fluid Pressure Within the Pierre Shale: A Transient Response to Erosion. Water Resour Res 29(7): 2007-2020.

Neuzil CE (1994) How permeable are clays and shales? Water Resour Res 30(2): 145-150.

Neuzil CE, Belitz K (1996) Fracture control of the hydrogeology of the North American midcontinental Cretaceous shales. In: Fluid Flow Through Faults and Fractures in Argillaceous Formations, Proceedings of a Joint NEA/EC Workshop Berne, Switzerland 10-12 June 1996: 157-162.

Nichols TC Jr, Collins DS, Davidson RR (1986) In situ laboratory geotechnical tests of the Pierre Shale near Hayes, South Dakota-A characterization of engineering behaviour. Can Geotech J 23: 181-194.

Palombi DD (2008) Regional Characterization of the Northeastern Margin in the Williston Basin. MSc Thesis. Department of Earth and Atmospheric Sciences, University of Alberta, Edmonton, AB.

Patriarche D, Ledoux E, Simon-Coinçon R et al (2004) Characterization and modeling of diffusion process for mass transport through the Tournemire argillites (Aveyron, France). Appl Clay Sci 26: 109-122.

Patterson RJ, Frape SK, Dykes LS et al (1978) A coring and squeezing technique for the detailed study of subsurface water chemistry. Can J Earth Sci 15: 162-169.

Pearson FJ (1999) What is the porosity of a mudrock? Geological Society London Special Publications 158(1): 9-21.

Person M, McIntosh J, Bense J et al (2007) Pleistocene hydrology of North America: the role of ice sheets in reorganizing groundwater flow systems. Reviews of Geophysics, 45(3).

Pittari A, Cas RAF, Lefebvre N et al (2006) Facies characteristics and architecture of body 219 Fort á la Corne, Saskatchewan, Canada: implications for kimberlitic mass flow processes in a marine setting. In: Kimberlite Emplacement Workshop, Saskatoon, Saskatchewan, 7-12 September 2006.

Plummer LN, Prestemon EC, Parkhurst DL (1994) An Interactive Code (NETPATH) For Modeling NET Geochemical Reactions Along a Flow PATH Version 2.0. U.S. Geological Survey Water-Resources Investigations Report 94: 4169.

Remenda VH, Cherry JA, Edwards TWD (1994) Isotopic composition of old ground water from Lake Agassiz: Implications for late Pleistocene climate. Science 266(5193): 1975-1978.

Remenda VH, van der Kamp G, Cherry JA (1996) Use of vertical profiles of $\delta^{18}O$ to constrain estimates of hydraulic conductivity in a thick, unfractured aquitard. Water Resour Res 32(10): 2979-2987.

Rowe RK, Badv K (1996) Chloride migration through clayey silt underlain by fine sand or silt. J. Geotech. Eng. 122(1): 60-68.

Rübel AP, Sonntag C, Lippmann J et al (2002) Solute transport in formations of very low permeability: Profiles of stable isotope and dissolved noble gas contents of pore water in the Opalinus Clay, Mont Terri, Switzerland. Geochim Cosmochim Acta 66(8): 1311-1321.

Rubio RF, Lorea DF (1993) Mine water drainage. Mine Water Environ 12: 107-130.

Sacci E, Michelot JL, Pitsch H et al (2001) Extraction of water and solutes from argillaceous rocks for geochemical consideration: methods, processes and current understanding. Hydrogeol J 9(1): 17-33.

Scott Smith BH, Orr RG, Robertshaw P et al (1998) Geology of the Fort á la Corne Kimberlites, Saskatchewan. In: Seventh International Kimberlite Conference, Cape Town, South Africa. Abstracts volume: 772-774.

Shackelford CD, Daniel DE (1991) Diffusion in saturated soil. 1: Background. J Geotech Eng 117(3): 467-484.

Shaw JR, Hendry MJ (1998) Hydrogeology of a thick clay till and Cretaceous clay sequence, Saskatchewan, Canada. Can Geotech J 35: 1041-1052.

Skempton AW (1954) The pore-pressure coefficients *A* and *B.* Geotechnique 4: 146-147.

Smith LA, Van der Kamp G, Hendry MJ (2013) A new technique for obtaining high-resolution pore pressure records in thick claystone aquitards and its use to determine in situ compressibility. Water Resour Res 49: 1-12, doi:10.1002/wrcr.20084.

Stripp GR, Field M, Schumacher JC, Sparks RSJ and Cressey G (2006) Post-emplacement serpentinization and related hydrothermal metamorphism in a kimberlite from Venetia, South Africa. J Metamorph Geol. 24: 515-534.

Stute M, Sonntag DJ, Schlosser P (1992) Helium in deep circulating groundwater in the Great Hungarian PlainFlow dynamics and crustal mantle fluxes. Geochim Cosmochim Acta 56: 2051-2067.

Tamers MA (1975) Validity of radiocarbon dates on groundwater. Geophys Surv 2: 217-239.

Taylor RS, Mathews WH, Kupsch WO (1961) Tertiary. In: Geological History of Western Canada, Alberta Soc. Of Petrol. Geol, Calgary, Alberta, Canada, pp 190-194.

Teasdale PR, Batley GE, Apte SC et al (1995) Pore water sampling with sediment peepers. TrAC Trends Anal Chem 14(6): 250-256.

Terzaghi K (1923) Die Berechnung der Durchlässigkeitsziffer des Tones aus dem Verlauf der hydrodynamischen Spannungserscheinungen, Sitz. Akad. Wissen. Wien D. matem.-naturw. K1., part IIa, 132, 125-138. [English translation by Clayton CRI, Seinhagen HM, A method of calculating the coefficient of permeability of clay from the variation of hydrodynamic stress with time, As cited in Clayton CRI, Steinhagen HM, Prowrie W (1995) Terzaghi's theory of consolidation, and the discovery of effective stress. Geotech Eng 113(4): 191-205].

Ugorets V, Pereira C (2011) Groundwater Modeling of Feasibility Dewatering Requirements for Star and Orion South Pits and Possible Hydrogeological Impact. SRK Consulting Inc. Lakewood, CO.

Van der Kamp G (1992) Evaluating the effect of fractures on solute transport through fractured clayey aquitards. In: Modern Trends in Hydrogeology, Hamilton, ON, 11-13 May 1992, International Association of Hydrogeologists: 468-476.

Van der Kamp G (2001) Methods for determining the in situ hydraulic conductivity of shallow aquitards-an overview. Hydrogeol J 9(1): 5-16.

Van der Kamp G, Van Stempvoort DR, Wassenaar LI (1996) The radial diffusion method: 1. Using intact cores to determine isotopic composition, chemistry, and effective porosities for groundwater in aquitards. Water Resour Res 32(6): 1815-1822.

Van Loon LR, Soler JM, Bradbury MH (2003) Diffusion of HTO, 36Cl- and 125I- in Opalinus Clay samples from Mont Terri: Effect of confining pressure. J Contam Hydrol 61(1-4): 73-83.

Van Loon LR, Jakob A (2005) Evidence for a second transport porosity for the diffusion of tritiated water (HTO) in a sedimentary rock (Opalinus Clay – OPA): application of through- and out-diffusion techniques. Trans Porous Media 61: 193-214.

Van Loon LR, Glaus MA, Müller W (2007) Anion exclusion effects in compacted bentonites: towards a better understanding of anion diffusion. Appl Geochem 22: 2536-2552.

Vargas C, Ortega-Guerrero A (2004) Fracture hydraulic conductivity in the Mexico City clayey aquitard: Field piezometer rising-head tests. Hydrogeol J 12: 336-344.

Waber HN, Smellie JAT (2008) Characterization of pore water in crystalline rocks. Appl Geochem 23: 1834-1861.

Wang HF (2000) Theory of Linear Poroelasticity with Applications to Geomechanics and Hydrogeology. Princeton University Press, Princeton, NJ.

Wassenaar LI, Hendry MJ, Chostner VL et al (2008) High resolution pore water δ^2H and $\delta^{18}O$ measurements by H_2O(liquid)-H_2O(vapour) equilibration laser spectroscopy. Environ Sci Technol 42(24): 9262-9267.

Williams JH, Paillet FL (2002) Using flowmeter pulse tests to define hydraulic connections in the subsurface: a fractured shale example. J Hydrol 265(1-4): 100-117.

Wittrup MB, Kyser TK (1990) The petrogenesis of brines in Devonian potash deposits of western Canada. Chem Geol 82: 103-128.

Wolff, RG (1970) Field and Laboratory Determination of the Hydraulic Diffusivity of a Confining Bed. Water Resour Res 6(1):194-203.

Wu Q, Wang M (2006) Characterization of water bursting and discharge into underground mines with multilayered groundwater flow systems in the North China coal basin. Hydrogeol J 14(6): 882-893.

Zonneveld JP, Kjarsgaard BA, Harvey SE et al (2004) Sedimentologic and Stratigraphic constraints on emplacement of the Star Kimberlite, east-central Saskatchewan. Lithos 76(1): 115-138.

Zonneveld JP, Kjarsgaard BA, Harvey SE et al (2007) The influence of depositional setting and fluctuating accommodation space on kimberlite edifice preservation: implications for volcanological models of diamondiferous kimberlites at Fort à la Corne, Saskatchewan, Canada. Geological Society of America Abstracts with Programs 39(6): 1-20.

APPENDIX A. NUMERICAL SIMULATION OF PUMPING TESTS 1 AND 2

Pumping tests were initiated in a well completed in the Mannville at 140-10-089 (Figure 2.1) on October 22 and October 25, 2010. The pumping well was 69 m west and 75 m north of 140-10-087. The intake screen of the pumping well extended from 254.1 to 162.6 m asl and consisted of stainless steel water well Johnson screen with a 3 mm slot size and an outside diameter of 0.30 m. Pumping tests 1 and 2 were conducted for 3 hours and 22 days, respectively. Pumping test 1 was conducted at a constant rate of $Q=0.056\ m^3\ s^{-1}$ and pumping test 2 was conducted at a variable rate (Table A.1). Pressure head was recorded at 140-10-087 for the duration of the tests and for 118 d following the end of pumping. Two-dimensional, axisymmetric, transient groundwater flow modeling was performed to estimate K_h in the lower Mannville aquifer and one-dimensional steady state modeling of h_t in the aquitard sequence was performed to estimate K_v in the upper Mannville and Lower Colorado, given the lack of response in the Lower Colorado shale to the pumping test.

Table A.1. Measured input flux point boundary condition values versus time used in the axisymmetric finite element model to simulate hydraulic head in pumping test 2 conducted at 140-10-089 between October 25 and November 14, 2010.

Time (days)		Time (s)	Q ($m^3 s^{-1}$)
October 25, 2010	10:00 am	0	-0.056
October 26, 2010	12:00 pm	93600	0
October 26, 2010	3:00 pm	104400	-0.056
October 31, 2010	7:00 pm	550800	0
November 1, 2010	3:00 am	579600	-0.056
November 14, 2010	10:00 am	1731600	0

Numerical Modeling

Finite element modeling of transient flow within the aquifer/aquitard sequence was performed using the commercial finite element model SEEP/W (GEO-SLOPE International Ltd. 2007). Two transient analyses were conducted. The first analysis simulated the transient, axisymmetric flow within the aquifer/aquitard sequence during pumping test 1 (Figure A.1), which was run for 3 h and allowed to recover. This analysis was conducted to calibrate the model and estimate values of the K_v and K_h of the Upper and Lower Mannville, respectively, during a time period in which the drawdown cone did not extend far enough to be influenced by kimberlite pipes in the region (the kimberlite pipes within the Mannville aquifer are significantly smaller than the EM boundary in Figure 2.1). The second analysis evaluated the transient, axisymmetric flow during pumping test 2 (Figure A.1), which was run for 22 d. The K values obtained for the upper and lower Mannville from pumping test 1 were utilized during the simulation of pumping test 2 to evaluate whether the drawdown response changed as a result of leakage through the kimberlite pipes during the 22 day pumping test. Because no drawdown was observed at the transducers installed at 301.1 and 280.5 m asl at 140-10-087, a steady state one-dimensional model was constructed to determine the K_v through the Lower Colorado using the

K_v of the Upper Mannville in the pumping test 2 transient analysis and the steady state head distribution recorded by the transducers installed at 140-10-087 (Figure A.1). However, a one-dimensional steady state analysis is not capable of determining whether or not leakage through the kimberlite pipes occurred. The lack of response in the lower Colorado shale to the pumping test in the Mannville aquifer does not imply there was no vertical leakage during the pumping tests, only that there was an inability to sufficiently stress the system to induce such leakage.

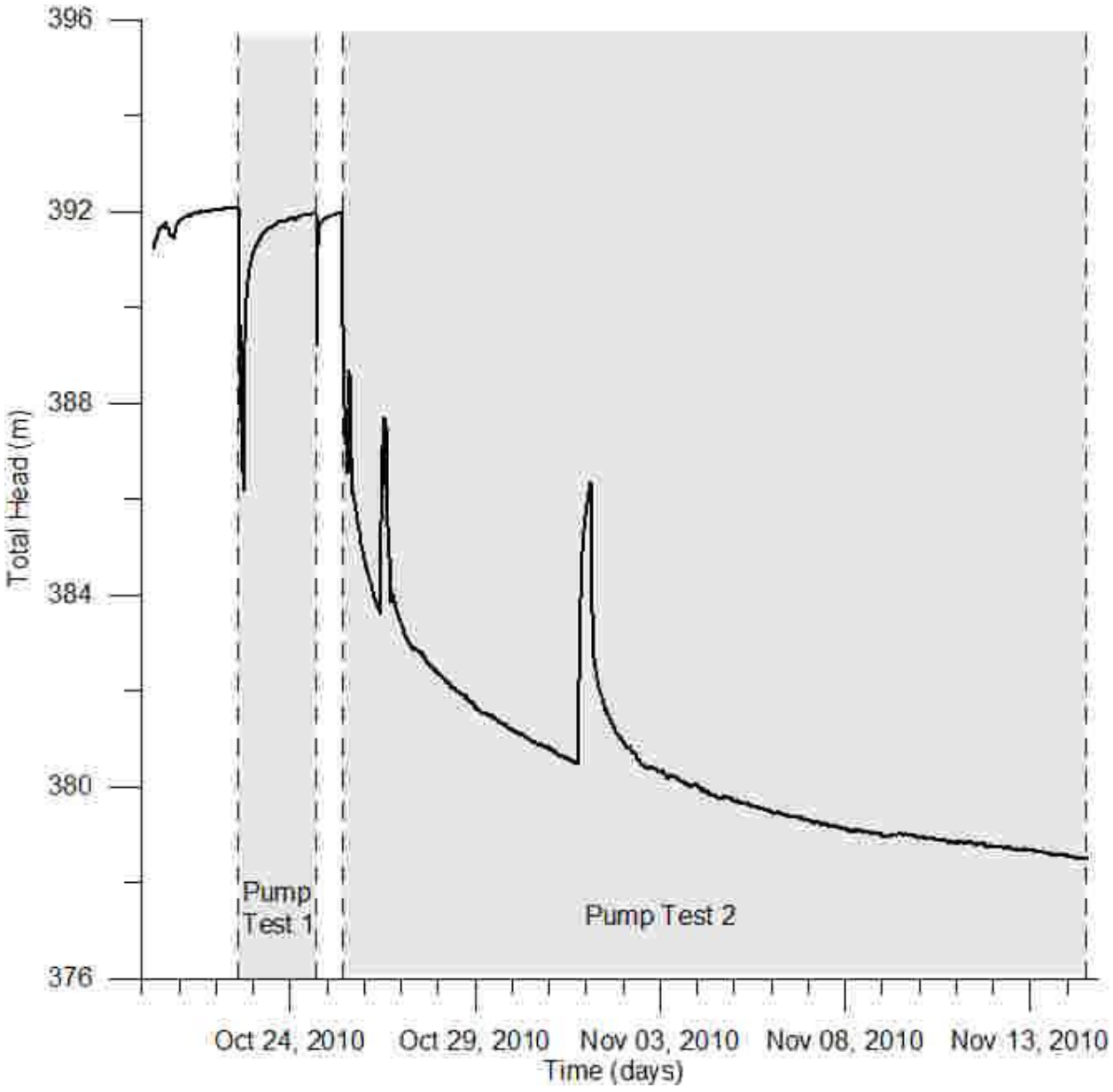

Figure A.1. Total head drawdown observed at transducer installed at 271.3 m BG at 140-10-087. Grey shading indicates pumping tests 1 and 2, the data from which were used for axi-symmetric finite element modeling.

The first two dimensional model of transient flow (pumping test 1) was developed in axi-symmetric mode (Figure A.2). The model was set up to have a 1.5 km radius. The model included 14 m of the Lower Colorado shale (326.6 to 312.6 m asl), 31 m of KDF (312.6 to 281.6 m asl), 23 m of Lower Colorado shale (281.6 to 258.6 m asl), 8 m of PVK (258.6 to 250.6 m asl), 60 m of Upper Mannville shale, silt, and sand (250.6 to 190.6 m asl), and 95 m of Lower Mannville sand (aquifer; 190.6 to 92.6 m asl). The mesh size within a 50 m radial distance of the well screen was 10 m. The well screen extended from 254.1 to 162.6 m asl, had a radius of 0.15 m, and was assigned a material type with a large K value so the pumping rate (Q) could be applied to a point within the well, rather than directly to the formation.

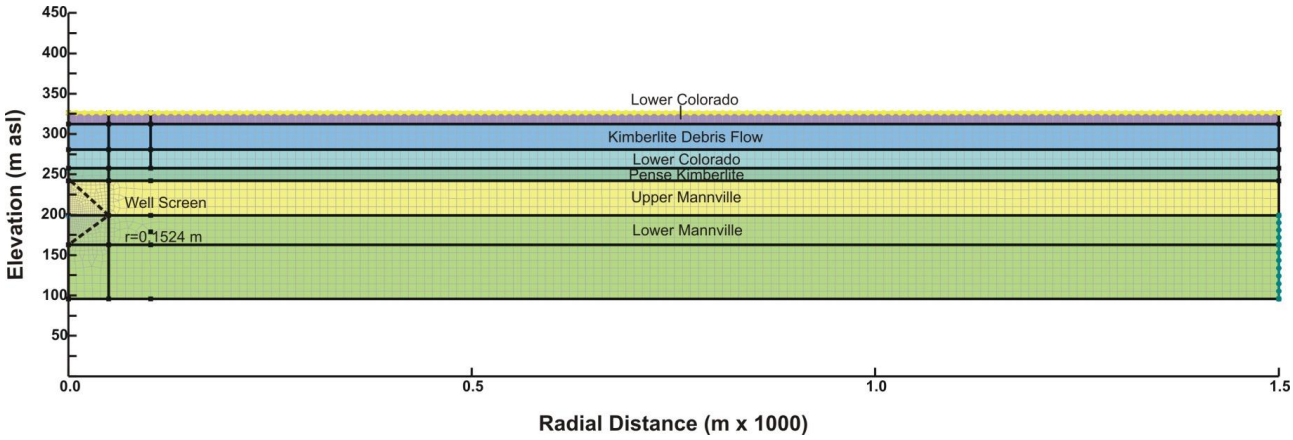

Figure A.2. Sketch of two-dimensional, finite element model in axi-symmetric mode constructed in SEEP/W (GEOSLOPE International Ltd., 2007).

The initial conditions were developed by simulating an initial steady state flow system in which an initial static total head value of 391.9 m was applied to the entire thickness of the Lower Mannville aquifer (190.6 to 92.6 m asl) and a total head value of 386.9 m was applied to the top of the Lower Colorado (326.6 m asl); these conditions aimed to simulate vertical flow through the aquitard system (326.6 to 250.6 m asl), based on long-term monitoring of the total head profile observed in VWP installed at 301.1, 280.5, 241.9, and 174.3 m asl in the monitoring well at 140-10-087. Values of S_s, determined from barometric response, and values of n_t, determined from geotechnical properties, were assigned to the material properties of each

geologic formation in the model (Lower Colorado, KDF, PVK, Upper and Lower Mannville). The model was also simulated with a no flux boundary condition at the top of the Lower Colorado. No difference was observed between the two models, suggesting little to no vertical discharge upward through the aquitard sequence (assuming only vertical flow). A transient analysis was used to simulate the drawdown during pumping test 1 (Figure A.1). A point in the well screen at the boundary between the upper and lower Mannville was assigned as a discharge boundary condition ($m^3\ s^{-1}$) to simulate water being withdrawn from inside the borehole annulus. A constant pumping rate was assigned at the node to represent the measured Q at the well head (-0.056 $m^3\ s^{-1}$). The values of K_v and K_h were varied in the upper and lower Mannville and the results visually optimized to the field-test results (Figure A.3). The resulting K_v and K_h values were considered representative of the Upper and Lower Mannville formation, because influence from the regionally located kimberlite pipes or from the Saskatchewan River was unlikely given the drawdown cone extended only 1 km from the pumping well (Figure 2.1).

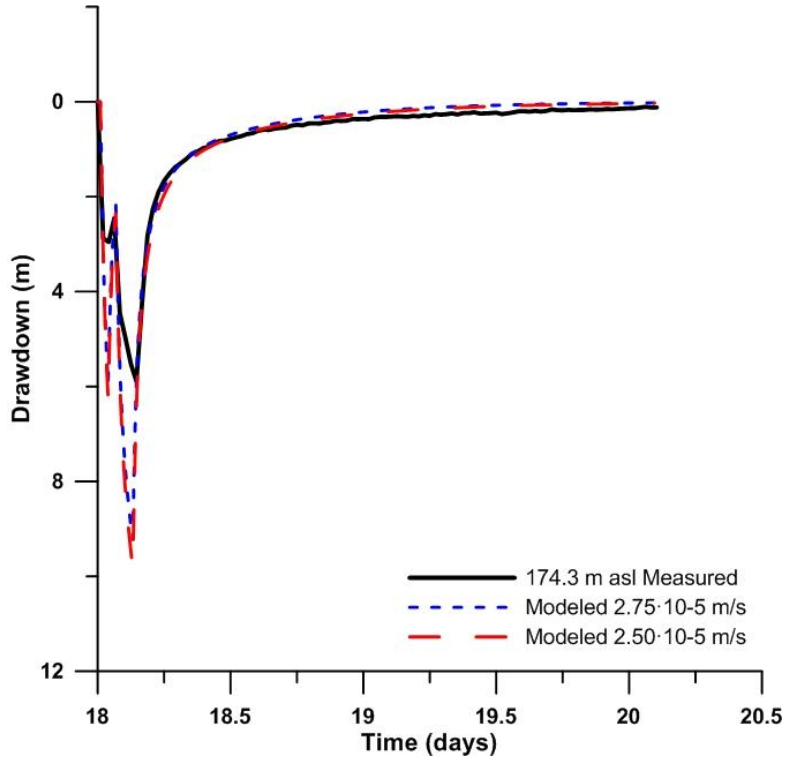

Figure A.3. Modeled drawdown of pumping test 1 conducted at 140-10-089 to determine K_h of the lower Mannville aquifer as well as calibrate the axisymmetric pumping test model. Drawdown was recorded in the VWP installed at 271.3 m BG at 140-10-087. Because transducer and barometer data were recorded in 30 min increments, the measured drawdown is

incomplete; this resulted in a smaller observed drawdown than modeled. Pumping test 1 was initiated at 140-10-087 (October 22, 2010 at 1:00 pm; Figure A.1).

Before the transient analysis of pumping test 2 (Figure A.1) could be simulated, the actual drawdown at the VWP installed at 241.9 m asl was estimated because it had not fully recovered from installation before pumping tests 1 and 2 were initiated (Figure A.4a). The measured recovery, recorded by the VWP at 241.9 m BG after pumping test 2 was completed (21.6 days; Nov. 14 to Dec. 6, 2010; Figure A.4a), was assumed equivalent to the recovery that would have been observed had pumping tests 1 and 2 not been initiated. This recovery was then added to the observed drawdown during pumping test 2 to estimate the actual drawdown during pumping (Figure A.4b).

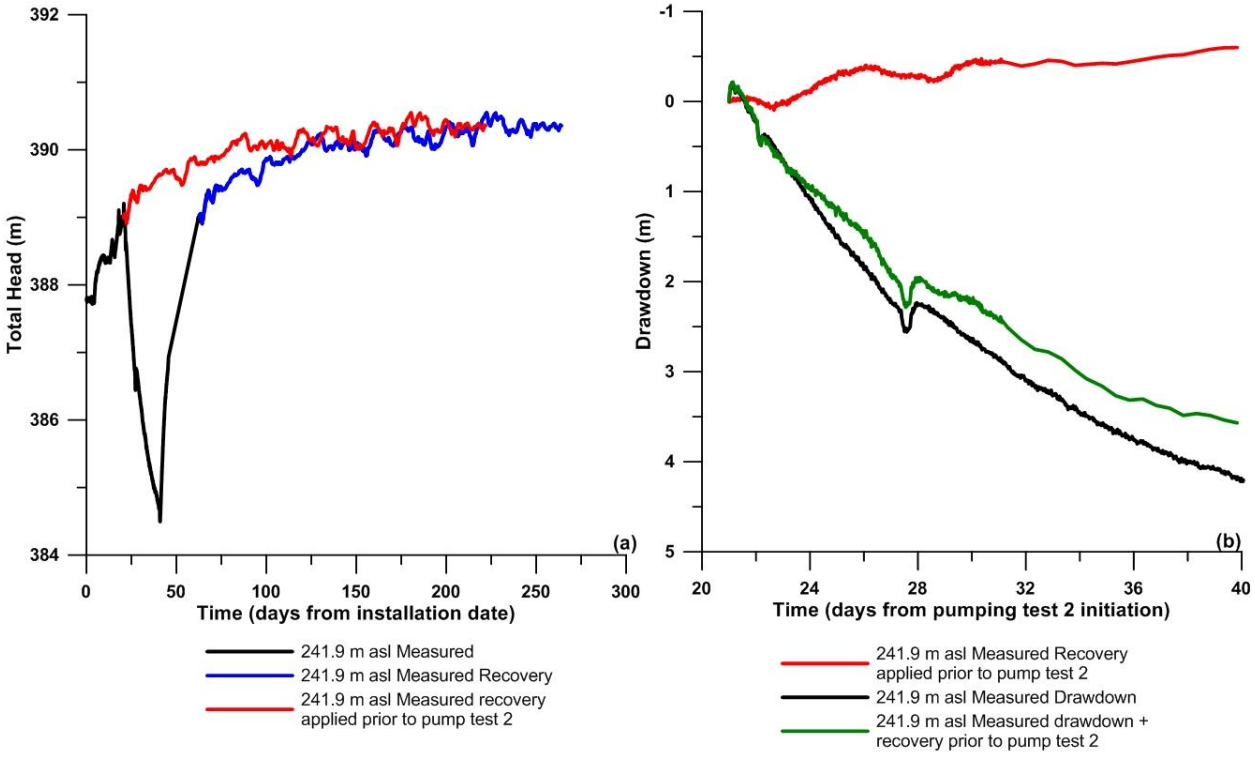

Figure A.4. To compensate for the non-steady-state conditions caused by incomplete recovery of the VWP installed at 203.7 m asl in the upper Mannville, the corrected drawdown was calculated by adding the recovery curve observed after installation of the VWP (day 0; a) to the recovery curve recorded after pumping test 2 was initiated (b).

A second version of the model was also simulated to represent pumping test 2 (Figure A.2) with a radius of 15 km. A 10 m mesh size was assigned to the 50 m radial distance from the well screen. The well screen had a radius of 0.15 m and extended from 254.1 to 162.6 m asl. The

well volume was assigned a material type with a large K, so the pumping rate could again be applied to a point within the well, rather than directly to the formation.

As for the simulation of pumping test 1, initial steady state conditions were developed by assigning a total head value of 391.9 m to the entire thickness of the Lower Mannville aquifer (190.6 to 92.6 m asl) and a total head boundary to the top of the Lower Colorado (326.6 m asl) of 386.9 m to simulate vertical flow through the aquitard system. Values of S_s, determined from barometric response, and values of n_t, determined from geotechnical properties, were assigned to the material properties of the Lower Colorado, KDF, PVK, and Upper and Lower Mannville formations in the model. The point in the well screen was assigned a time-dependant discharge boundary condition to simulate water being withdrawn from the borehole annulus, as well as periods when the pump was turned off (Table A.1). The values of K_v ($2\text{-}4\times10^{-9}$ m s^{-1}) and K_h ($2.5\text{-}2.75\times10^{-5}$ m s^{-1}) determined from the simulation of pumping test 1 were also assigned in pumping test 2. The simulated drawdown using the K_v and K_h values fully enveloped the drawdown measured by VWPs installed at 241.9 and 174.3 m asl in the Upper and Lower Mannville, respectively, suggesting that vertical leakage through the kimberlite pipes did not influence the drawdowns observed during pumping test 2.

Because no drawdown was observed at the transducers installed at 301.1 and 280.5 m asl at 140-10-087, a steady state analysis was developed to simulate the total head distribution through the Lower Colorado, KDF, PVK, and Upper Mannville (Figure A.5). The model was set up as a column of elements 1 m wide and vertically included 14 m of Lower Colorado shale (326.6 to 312.6 m asl), 31 m of KDF (312.6 to 281.6 m asl), 23 m of Lower Colorado shale (281.6 to 258.6 m asl), 8 m of PVK (258.6 to 250.6 m asl), and 60 m of Upper Mannville shale, silt, and sand (250.6 to 190.6 m asl). Total head values of 387.25 and 391.9 m were assigned to 301.1 and 190.6 m asl, respectively, based on long-term monitoring of VWPs installed at 140-10-087. Using the K_v estimated in the Upper Mannville ($2\text{-}4\times10^{-9}$ m s^{-1}), the measured steady state total head distribution was simulated through the Lower Colorado, KDF, and PVK (Figure A.6). The K_v estimated in the KDF (301.1 to 280.5 m asl) and Lower Colorado and PVK (280.5 to 250.6 m asl) were $3\text{-}5\times10^{-9}$ m s^{-1} and 9×10^{-10} to 2×10^{-9} m s^{-1}, respectively. These values were added to the two-dimensional transient flow model in pumping test 2 to simulate the drawdown of all four VWPs installed at 140-10-087 (Table A.2).

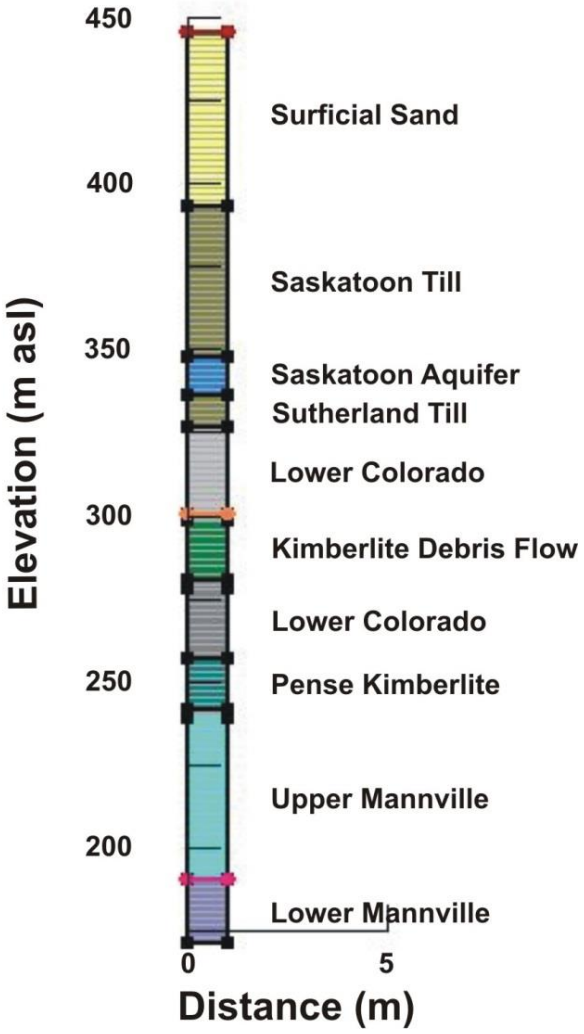

Figure A.5. Sketch of one-dimensional, finite element model constructed in SEEP/W to estimate K_v of Pense kimberlite, Lower Colorado, and KDF sediments (GEOSLOPE International Ltd., 2007).

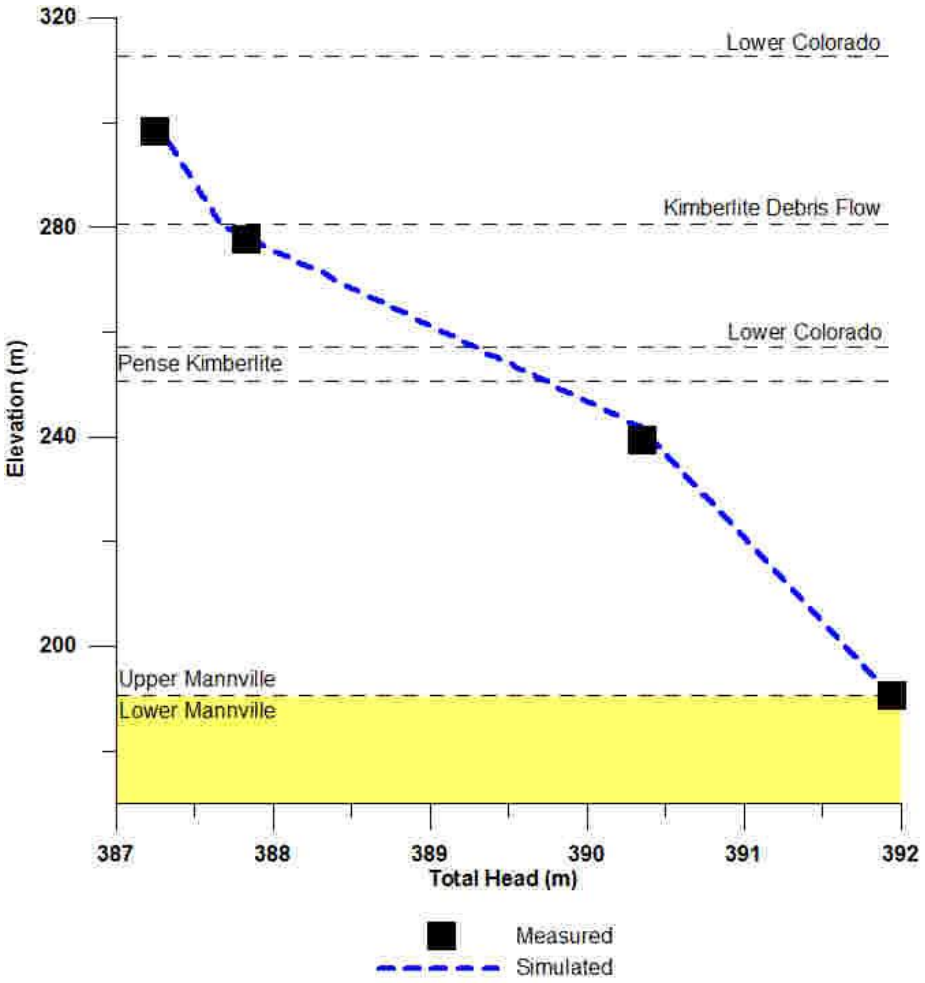

Figure A.6. One-dimensional finite element modeling of steady state head distribution at 140-10-087 to estimate K_v of Pense kimberlite, Lower Colorado, and KDF sediments from h_t data measured at transducers installed at 301.5, 280.5, and 241.9 m asl and using the best fit K_v applied to the axi-symmetric model in the Upper Mannville sediments.

K_h values were estimated from two-dimensional transient flow modeling and K_v values were estimated from one-dimensional steady state flow modeling (Table A.2; Figure A.7). K_v was estimated to be between 3×10^{-9} and 5×10^{-9} m s^{-1} in the KDF (301.1 to 280.5 m asl) and between 9×10^{-10} and 2×10^{-9} m s^{-1} in the Lower Colorado and PVK (280.5 to 250.6 m asl). The model assumed only vertical flow through the units.

Table A.2. Kv values in the Lower Colorado shale and upper and lower Mannville clay, silt, and sand at 140-10-087 estimated from axisymmetric modeling of pumping tests 1 and 2.

Interval	**K_v (m s^{-1})**
Colorado†	$3\text{-}5\times10^{-9}$
KDF†	$3\text{-}5\times10^{-9}$
Colorado	9×10^{-10} to 2×10^{-9}
PVK†	9×10^{-10} to 2×10^{-9}
Upper Mannville	$2\text{-}4\times10^{-10}$
Lower Mannville	$2.5\text{-}2.75\times10^{-5}$

† Formations impacted by kimberlite volcanism

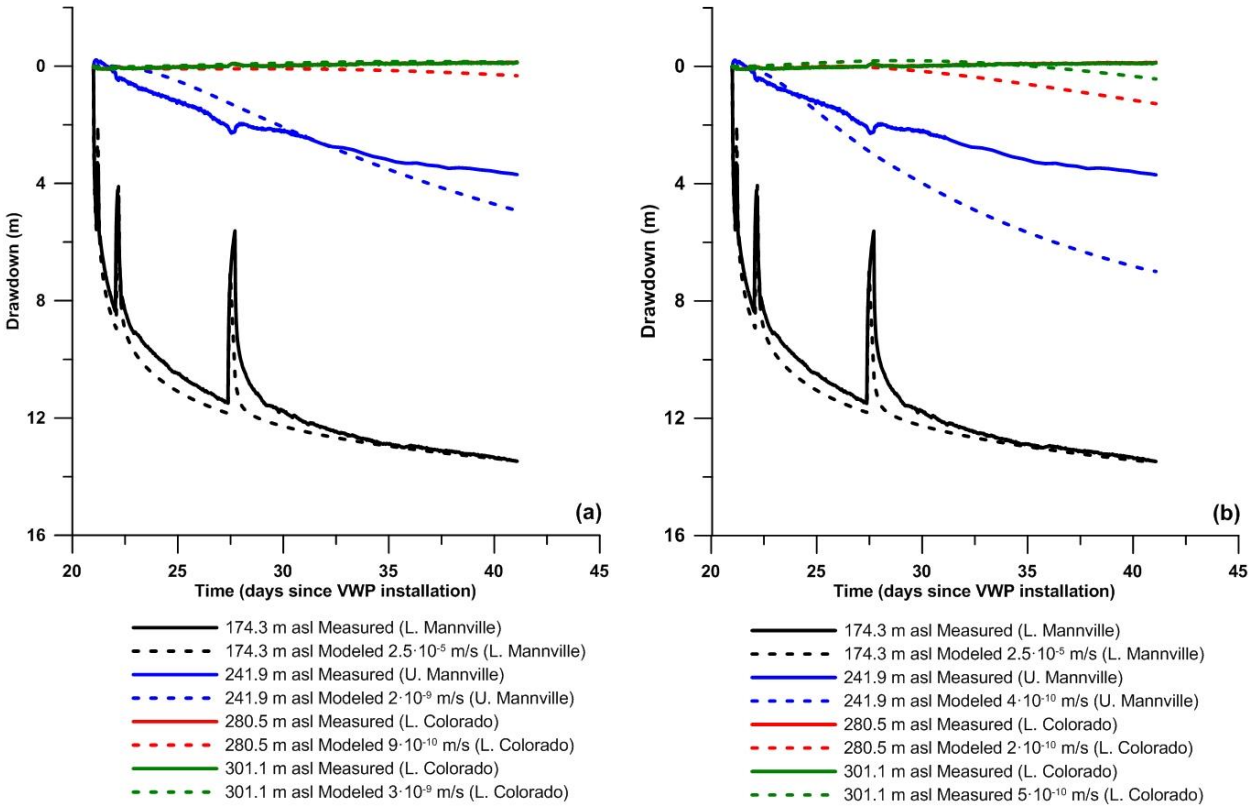
Drawdown (m)
Time (days since VWP installation)
(a)
174.3 m asl Measured (L. Mannville)
174.3 m asl Modeled 2.5·10-5 m/s (L. Mannville)
241.9 m asl Measured (U. Mannville)
241.9 m asl Modeled 2·10-9 m/s (U. Mannville)
280.5 m asl Measured (L. Colorado)
280.5 m asl Modeled 9·10-10 m/s (L. Colorado)
301.1 m asl Measured (L. Colorado)
301.1 m asl Modeled 3·10-9 m/s (L. Colorado)
(b)
174.3 m asl Measured (L. Mannville)
174.3 m asl Modeled 2.5·10-5 m/s (L. Mannville)
241.9 m asl Measured (U. Mannville)
241.9 m asl Modeled 4·10-10 m/s (U. Mannville)
280.5 m asl Measured (L. Colorado)
280.5 m asl Modeled 2·10-10 m/s (L. Colorado)
301.1 m asl Measured (L. Colorado)
301.1 m asl Measured 5·10-10 m/s (L. Colorado)
(c)
174.3 m asl Measured (L. Mannville)
174.3 m asl Modeled 2.75·10-5 m/s (L. Mannville)
241.9 m asl Measured (U. Mannville)
241.9 m asl Modeled 2·10-9 m/s (U. Mannville)
280.5 m asl Measured (L. Colorado)
280.5 m asl Modeled 9·10-10 m/s (L. Colorado)
301.1 m asl Measured (L. Colorado)
301.1 m asl Modeled 3·10-9 m/s (L. Colorado)
(d)
174.3 m asl Measured (L. Mannville)
174.3 m asl Modeled 2.75·10-5 m/s (L. Mannville)
241.9 m asl Measured (U. Mannville)
241.9 m asl Modeled 4·10-9 m/s (U. Mannville)
280.5 m asl Measured (L. Colorado)
280.5 m asl Modeled 2·10-9 m/s (L. Colorado)
301.1 m asl Measured (L. Colorado)
301.1 m asl Modeled 5·10-9 m/s (L. Colorado)

Figure A.7. Modeled drawdown of pumping test 2 conducted at 140-10-089 to estimate K_h of the Lower Mannville and K_v of the upper Mannville, lower Colorado, and KDF sediments as well as determine the affect of leakage from regionally located kimberlite pipes. Drawdown was simulated using K_v values of 2×10^{-9} m s^{-1} (A, C) and 4×10^{-9} m s^{-1} (B,D) in the Upper Mannville and K_h values of 2.5×10^{-5} (A, B) and 2.75×10^{-5} m s^{-1} (C,D). Values of S^s applied to the Upper and Lower Mannville (2.5×10^{-6} m^{-1}) as well as Lower Colorado and KDF ($3.7\text{-}3.8\times10^{-6}$ m^{-1}) were determined using barometric efficiencies. Pumping test 2 was initiated 21 days after VWPs began recording data at 140-10-087 (October 25, 2010 at 10:00 am; Figure A.1).

Two inherent problems with the design of the pumping test conducted at 140-10-089 were evident. First, the transducers installed in the Lower Colorado shale (301.1 and 280.5 m asl) and the upper Mannville (280.5 m asl) were not fully recovered from installation before the pumping test was initiated. Second, the pumping test was not performed for a sufficient amount of time for drawdown to be observed at the transducers installed in the Lower Colorado Formation, implying an inability to sufficiently stress the system to induce drawdown. Although the modeling exercise was implemented, the insufficient duration of the pumping test and limited recovery of h_t at three of the VWPs installed in the Lower Colorado and upper Mannville undermine the validity of using the pump test data to estimate a K_v of the Lower Colorado Formation. Furthermore, the lack of recovery at the VWP installed in the upper Mannville (241.9 m asl) cast doubt on the reliability of the calibrated parameters from pumping test 1 and their applicability to pumping test 2.

A one-dimensional model was used to estimate K_v because of the lack of drawdown in the Lower Colorado and upper Mannville; however, the pattern of head distribution observed and possible lateral connection via fractured zones in the Lower Colorado to the river undermine the usefulness of this model to estimate K_v in the aquitard sequence. Given the lack of data available for the numerical simulation and the fact that there was no equivalent pumping test or modeling conducted near the unimpacted site (OVB-10-207), equivalent bulk K_v properties could not be inferred. There is no way to determine, from the data set available (based solely on the pumping tests and one and two-dimensional modeling), whether the resulting bulk K_v was one to two orders of magnitude greater than lab-based K_v values due to kimberlite volcanism or not.

APPENDIX B. BATCH TESTING OF AQUEOUS EXTRACTIONS FROM CORE SAMPLES FOR Cl ANALYSES

1.0 EXPLANATION

To determine the optimum leaching time and water:rock ratio for aqueous extraction of Cl, batch testing was performed on three samples of the minimally impacted Lower Colorado shale from corehole OVB-10-207 at 305, 290, and 249 m asl. These samples were chosen because of their tendency to swell when added to de-ionized water (samples from 140-10-087 did not swell).

2.0 METHODS

Pore water Cl concentrations were determined for core samples using the aqueous extract data and a method similar to van Loon et al. (2007). The core samples were dried in an oven at 90 °C for 48 hours and powdered using a titanium carbide swing mill. Sub-samples of the dried, crushed core samples were added to de-ionized water in 50 mL centrifuge tubes at water:rock ratios of 2:1, 3:1, 4:1, and 5:1 and shaken with a Burrel Scientific Model 75 wrist action shaker for 1, 5, 10, and 100 hours. The samples were then centrifuged at 3000 rpm for 2 hours in an IEC Centra-4B centrifuge, and filtered through 0.45 μm nitrate membrane filter paper. Each combination of water to rock ratio and leaching time was run in triplicate. The resulting aqueous phases were collected in 20 mL scintillation vials and stored at room temperature until analyses could be performed. Porewater Cl concentrations were determined for all samples using the method presented in Section 4.5.2.

3.0 RESULTS AND DISCUSSION

Anion extraction batch test Cl concentration results are presented in Figure B.1 and can be found in Table D.6. Water:rock ratios of 2:1, 3:1, 4:1, and 5:1 and leaching times of 1, 5, 10, and 100 hours at 305 m asl (Figure B.1a) resulted in similar Cl concentrations (of each triplicate sample run at each water:rock ratio and leaching time), with the exception of data for water:rock ratios of 4:1 and 5:1 and a leaching time of 1 h that are not presented due to analytical errors. Samples run at a water:rock ratio of 3:1 resulted in Cl concentrations greater than samples run at 2:1, 4:1, and 5:1 at leaching times of 5 and 10 hours. Samples collected from 290 m asl (Figure B.1b) resulted in similar Cl concentrations for water:rock ratios of 3:1, 4:1, and 5:1; however,

Cl- concentrations for a water:rock ratio of 2:1 were not within one standard deviation at leaching times of 5 and 10 hours. Samples collected at 249 m asl ran within one standard deviation of the mean for all water:rock ratios and leaching times (Figure B.1c). Based on the results, an optimum water:rock ratio of 2:1 and leaching time of 1 hour was used for all other anion extractions at 140-10-087 and OVB-10-207.

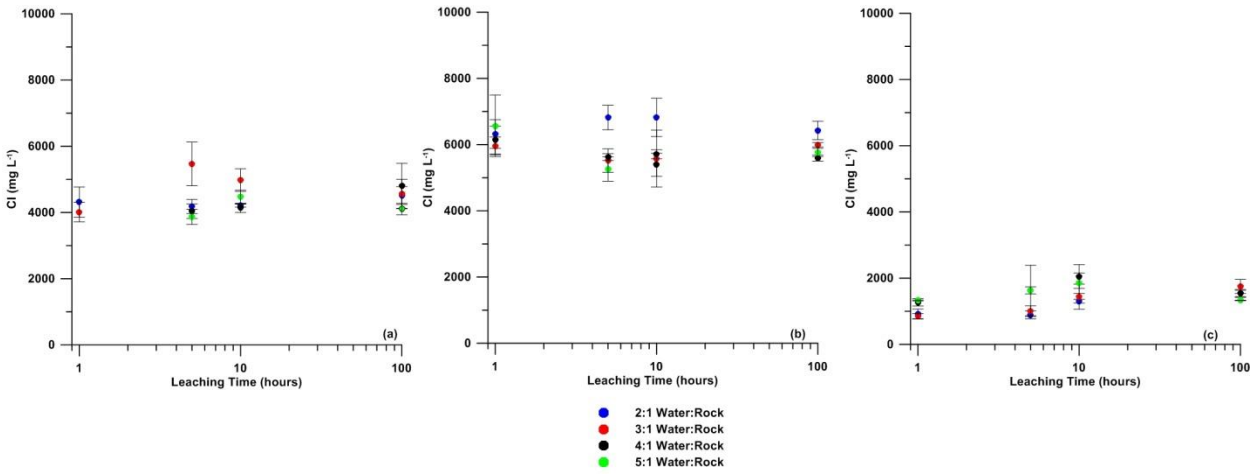

Figure B.1. Measured Cl concentrations plotted against leaching times of 1, 5, 10, and 100 hours and water:rock ratios of 2:1, 3:1, 4:1, and 5:1 for samples from 305 m asl (a), 290 m asl (b), and 249 m asl (c).

APPENDIX C. VAPOUR EQUILIBRATION TESTS TO DETERMINE EFFECTS OF STORAGE TIME ON δ^2H AND $\delta^{18}O$ ANALYSES

1.0 EXPLANATION

To determine the length of time samples can be stored for vapour equilibration analysis, core samples from OVB-10-207 were run 1 month, 5 months, and 1 year after collection. Similarly, core samples from 140-10-087 were run 5 months and 1 year after collection. Samples from 140-10-087 were not run 1 month after collection due to problems with the picarro vapour isotope analyzer. This is the reason these tests were undertaken.

2.0 METHODS

Core samples from OVB-10-207 were collected in April 2010, stored in Coleman 48 qt coolers, and initially run 1 month after collection. After this initial analysis, they were transferred to cardboard boxes where they were stored until they were run again 5 months and 1 year after collection. Samples collected from 140-10-087 were collected in May 2010 and stored in Coleman 48 qt coolers and initially run 5 months after collection. Core samples collected from 140-10-087 were stored in coleman 48 qt coolers until they were run again 1 year after collection. Core samples were analyzed on a Picarro L1120-i vapour isotope analyzer. For full details of the $H_2O_{(liquid)}$-$H_2O_{(vapour)}$ equilibration method, see Section 4.5.3.

3.0 RESULTS AND DISCUSSION

Values of δ^2H and $\delta^{18}O$ collected during the storage test were plotted against the Saskatoon Meteoric Water Line (SMWL; Figure C.1). At OVB-10-207, δ^2H and $\delta^{18}O$ values plotted on the SMWL within the 95% confidence interval (CI), whereas core samples analyzed after 5 months and 1 year show evaporative trends and plot on evaporation lines below the SMWL. Similarly, values of δ^2H and $\delta^{18}O$ analyzed 5 months and 1 year after collection at 140-10-087 show evaporative effects; however, such effects were less evident than those at OVB-10-207 because the 140-10-087 samples were stored in air-tight, Coleman 48 qt coolers for the entire year; those collected at OVB-10-207 were stored in cardboard boxes after their initial analyses (1 month after collection). The results of this long-term storage test suggest samples to be analyzed for isotope analyses must be stored in airtight coolers and should be measured as soon as possible before the effects of evaporation render the data unusable.

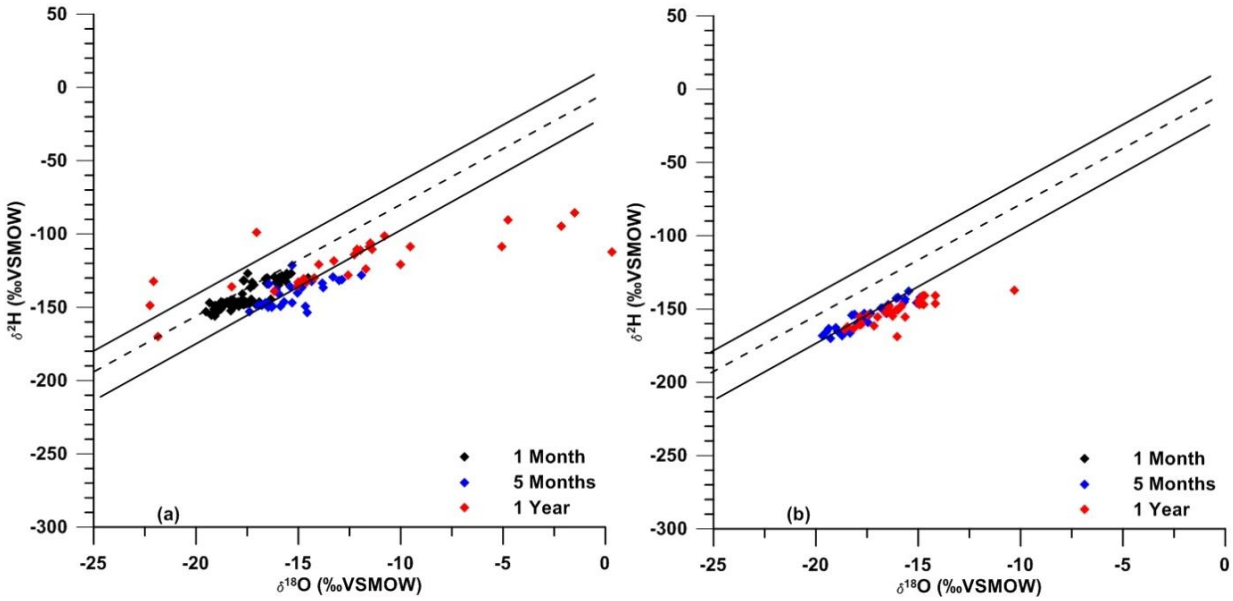

Figure C.1. Plot of δ^2H versus $\delta^{18}O$ of porewater collected from core samples at OVB-10-207 after 1 month, 5 months, and 1 year of storage (a) and plot of δ^2H versus $\delta^{18}O$ for porewater collected from core samples at 140-10-087 after 5 months and 1 year of storage. The solid line represents the Saskatoon local meteoric water line and the dashed lines represent the 95% confidence interval of precipitation data.

APPENDIX D. RAW GEOTECHNICAL AND GEOCHEMICAL DATA

Table D.1. Raw gravimetric water content (ω), bulk density (ρ), and total porosity (nt) values estimated from core samples collected at 140-10-087 and OVB-10-207.

140-10-087				**OVB-10-207**			
Elevation (m asl)	**ω**	**ρ_d**	**n_t**	**Elevation (m asl)**	**ω**	**ρ_d**	**n_t**
395.9	7	2.17	18	412.8	32	1.11	59
392.4	6	2.17	18	409.8	32	1.13	58
389.9	7	2.10	21	406.8	35	1.04	62
386.9	8	2.10	21	403.8	7	2.12	21
383.9	8	2.07	22	400.8	9	2.02	25
380.9	9	2.05	23	398.3	7	2.09	23
378.0	9	2.05	23	394.8	8	2.07	23
375.0	10	2.05	23	391.8	7	2.08	23
372.0	8	1.98	25	388.8	6	2.14	21
368.9	9	2.03	24	385.8	8	2.07	24
367.3	8	2.00	24	382.8	6	2.19	19
361.5	8	2.10	21	379.8	8	2.07	24
360.0	8	2.04	23	376.8	9	2.02	25
358.0	15	1.94	27	373.8	10	1.83	32
332.9	15	1.61	39	370.8	11	1.89	30
330.0	8	1.83	31	355.8	7	2.15	20
326.9	9	1.86	30	319.8	21	1.39	49
325.6	21	1.76	34	316.8	22	1.45	46
323.9	20	1.44	46	313.8	26	1.21	55
322.4	19	1.49	44	310.8	27	1.22	55
317.9	20	1.53	42	307.8	23	1.23	55
311.9	16	1.56	41	304.3	20	1.36	49
309.1	32	1.55	42	301.8	19	1.49	45
294.2	18	1.30	51	298.8	19	1.44	47
291.1	25	1.51	43	295.8	21	1.43	47
288.6	38	1.11	58	292.8	20	1.41	48
288.2	15	1.49	44	289.8	19	1.48	45
286.4	21	1.28	52	286.8	21	1.37	49
282.0	20	1.68	36	283.8	22	1.38	49
278.4	19	1.67	37	280.8	17	1.51	44
272.4	16	1.50	43	277.8	19	1.51	44
269.9	16	1.57	41	274.8	19	1.55	43
264.0	17	1.63	38	271.8	19	1.55	43

261.5	20	1.58	40	270.8	19	1.54	43
258.0	18	1.62	39	267.8	19	1.56	42
255.3	10	1.78	33	265.0	20	1.43	47
246.0	17	1.54	42	261.8	16	1.63	39
243.5	14	1.87	30	258.8	16	1.65	39
240.0	12	1.66	37	254.3	18	1.55	43
236.9	13	1.68	36	253.0	15	1.62	40
233.9	14	1.70	36	251.8	17	1.64	39
231.1	14	1.62	39	250.8	15	1.68	38
227.8	12	1.73	35	248.8	17	1.53	43
224.9	14	1.72	35	247.3	18	1.50	44
222.1	12	1.66	37	245.3	12	1.80	33
219.3	13	1.72	35	244.8	11	1.95	28
214.1	16	1.73	35				
210.9	13	1.75	34				
210.9	12	1.65	38				
207.0	18	1.67	37				
203.0	13	1.74	35				
195.2	22	1.65	38				
191.9	22	1.38	48				
177.9	25	1.35	49				
170.9	10	1.88	29				
164.9	23	1.38	48				
162.0	22	1.51	43				
131.9	11	1.86	30				
129.2	11	1.85	30				
125.9	11	1.81	32				
120.1	13	1.77	33				
98.9	9	1.90	28				
93.9	9	1.99	25				

Table D.2. Extract and squeezed Cl concentrations of core samples collected at 140-10-087 and OVB-10-207.

140-10-087 Elevation (m asl)	$n_e=0.4n_T$ mg/L extract	$n_e=0.6n_T$ mg/L extract	OVB-10-207 Elevation (m asl)	$n_e=0.4n_T$ mg/L extract	$n_e=0.6n_T$ mg/L extract	140-10-087 Elevation (m asl)	Squeezed mg/L
445.6	427	427	400.8	113	113	398.0	42
445.6	402	402	398.3	382	382	371.2	57
445.6	389	389	394.8	184	184	325.0	266
445.6	234	234	391.8	136	136	313.0	584
445.6	252	252	388.8	212	212	295.3	412
445.6	197	197	385.8	276	276	280.2	943
445.6	441	441	379.8	366	366	269.9	1056
445.6	147	147	370.8	301	301	260.9	1528
445.6	133	133	337.3	349	349	295.3	328
445.6	158	158	335.3	272	272	295.3	352
445.6	365	365	333.8	306	306		
445.6	213	213	331.8	993	993		
445.6	200	200	329.8	338	338		
445.6	152	152	327.8	592	592		
445.6	232	232	325.8	279	279		
445.6	696	464	325.0	795	530		
445.6	371	247	323.8	883	589		
445.6	388	259	321.8	1291	861		
445.6	1062	708	321.0	1302	868		
445.6	521	347	316.8	2034	1356		
445.6	401	267	313.8	2469	1646		
445.6	629	419	310.8	2349	1566		
445.6	730	487	307.8	3615	2410		
445.6	587	392	304.3	3237	2158		

445.6	599	399	301.8	3098	2065		
445.6	827	551	298.8	3479	2320		
445.6	762	508	295.8	3929	2620		
445.6	897	598	289.8	4076	2717		
445.6	1213	808	286.8	4432	2955		
445.6	1256	838	277.8	3829	2553		
445.6	1584	1056	274.8	2763	1842		
445.6	2500	1667	271.8	2889	1926		
445.6	2060	1373	270.8	3303	2202		
445.6	2651	1767	267.8	2177	1452		
445.6	1918	1279	265.0	2417	1611		
445.6	1432	955	261.8	2181	1454		
445.6	1033	689	258.8	1989	1326		
445.6	1098	732	253.0	1066	711		
445.6	1272	848	251.8	1376	918		
445.6	1209	806					
445.6	1371	914					
445.6	1364	910					
445.6	1227	818					
445.6	1036	691					
445.6	1117	745					
445.6	1765	1177					
445.6	1717	1144					
445.6	1999	1333					
445.6	2370	1580					
445.6	1355	903					

Table D.3. Chemical analyses of pumping test water collected during pumping test 2 at 140-10-089 (Figure 2.1).

	Sample 1	**Sample 2**	**Sample 3**
Analyte	**mgL^{-1}**	**mgL^{-1}**	**mgL^{-1}**
P^{5+}	0.07	0.06	0.06
As^{5+}	0.01	0.01	0.01
Se^{4+}	0.03	0.03	0.03
Rb^{+}	0.03	0.03	0.03
Ba^{2+}	0.02	0.01	0.01
Sr^{2+}	2.79	2.78	2.8
Zn^{2+}	0.22	0.13	0.07
Cr^{3+}	0.02	0.01	0.02
B^{3+}	2.13	2.15	2.26
Li^{+}	0.58	0.75	0.76
Na^{+}	1201.28	1182.39	1285.19
NH_4^{+}	1.97	2.04	1.90
K^{+}	39.84	40.03	42.16
Ca^{2+}	193.27	198.02	203.28
Mg^{2+}	61.27	64.87	64.38
Al^{3+}	0.37	0.23	0.17
Mn^{2+}	0.10	0.11	0.10
Fe^{2+}	0.00	0.00	0.00
Alkalinity HCO_3^{-}	283.04	302.56	317.2
Br^{-}	5.43	5.83	5.76
Cl^{-}	2013.69	1889.41	1921.69
F^{-}	2.85	2.95	2.94
NO_3^{-}	9.62	11.80	8.31
PO_4^{3-}	0.00	0.00	0.00
SO_4^{2-}	724.20	687.54	699.90
C-14 (Fmdn)		0.0621+/-0.0008	
$\delta^{13}C$(‰)		-12.20	
$\delta^{18}O$(‰)	-18.28	-18.59	-18.40
$\delta^{2}H$(‰)	-143.39	-144.92	-144.17
Ionic Strength	0.09	0.09	0.09
epm (%)	-5.93	-3.53	-1.08

Table D.4. δ^2H and $\delta^{18}O$ values of core samples collected at 140-10-087.

140-10-087				
Elevation (m asl)	**δ^2H**	**$\delta^{18}O$**	**δ^2H error**	**$\delta^{18}O$ error**
398.6	-137.6	-15.4	0.8	0.3
394.6	-139.2	-15.3	0.8	0.3
392.6	-142.3	-15.7	0.8	0.3
391.6	-142.5	-15.8	0.8	0.3
391.6	-141.6	-15.5	0.8	0.3
390.6	-143.9	-16.2	0.8	0.3
389.6	-141.2	-15.6	0.8	0.3
388.6	-142.0	-16.0	0.8	0.3
387.6	-147.1	-16.7	0.8	0.3
386.7	-144.7	-16.3	0.8	0.3
385.6	-145.1	-16.3	0.8	0.3
384.6	-145.4	-16.1	0.8	0.3
383.7	-148.3	-16.5	0.8	0.3
382.6	-149.1	-16.8	0.8	0.3
381.7	-148.1	-16.4	0.8	0.3
380.8	-147.6	-16.7	0.8	0.3
379.6	-149.5	-17.0	0.8	0.3
378.7	-149.8	-16.3	0.8	0.3
377.8	-148.6	-16.8	0.8	0.3
376.5	-149.5	-16.7	0.8	0.3
375.7	-150.1	-17.6	0.8	0.3
374.8	-151.3	-16.7	0.8	0.3
373.6	-153.3	-17.2	0.8	0.3
372.6	-150.9	-17.0	0.8	0.3
371.6	-154.9	-17.6	0.8	0.3
370.6	-153.3	-17.3	0.8	0.3
369.9	-153.5	-17.7	0.8	0.3
368.6	-151.9	-17.2	0.8	0.3
367.6	-155.6	-17.7	0.8	0.3
366.6	-154.2	-17.6	0.8	0.3
365.7	-154.8	-18.1	0.8	0.3
365.0	-155.3	-17.5	0.8	0.3
363.6	-155.9	-18.3	0.8	0.3
362.6	-153.9	-17.9	0.8	0.3
336.6	-161.5	-18.6	0.8	0.3
335.6	-161.2	-18.5	0.8	0.3
333.5	-162.5	-18.6	0.8	0.3

332.6	-166.1	-18.6	0.8	0.3
332.1	-163.8	-18.8	0.8	0.3
331.6	-163.5	-18.5	0.8	0.3
331.1	-163.3	-18.7	0.8	0.3
330.7	-169.4	-19.4	0.8	0.3
329.7	-165.6	-19.4	0.8	0.3
329.6	-165.1	-18.9	0.8	0.3
329.1	-163.5	-18.8	0.8	0.3
328.6	-168.1	-19.3	0.8	0.3
328.2	-165.9	-18.8	0.8	0.3
328.1	-165.2	-18.8	0.8	0.3
326.8	-169.7	-18.7	0.8	0.3
326.1	-167.9	-18.7	0.8	0.3
325.6	-165.3	-18.7	0.8	0.3
325.1	-163.6	-18.4	0.8	0.3
324.6	-162.2	-18.6	0.8	0.3
324.1	-167.1	-18.8	0.8	0.3
323.6	-170.1	-18.0	0.8	0.3
320.6	-168.1	-18.7	0.8	0.3
320.1	-162.9	-18.5	0.8	0.3
319.6	-167.5	-18.2	0.8	0.3
318.6	-165.4	-18.8	0.8	0.3
317.6	-170.6	-19.2	0.8	0.3
316.6	-170.1	-19.3	0.8	0.3
314.5	-160.4	-18.8	0.8	0.3
313.5	-164.3	-17.3	0.8	0.3
312.6	-161.3	-19.6	0.8	0.3
304.6	-166.5	-19.2	0.8	0.3
301.1	-165.9	-19.6	0.8	0.3
297.9	-164.1	-19.5	0.8	0.3
296.8	-165.8	-19.5	0.8	0.3
295.6	-167.5	-19.5	0.8	0.3
294.7	-166.6	-19.4	0.8	0.3
293.7	-167.0	-19.6	0.8	0.3
291.6	-166.3	-18.7	0.8	0.3
290.8	-163.1	-19.4	0.8	0.3
288.6	-162.5	-19.0	0.8	0.3
288.1	-159.1	-18.7	0.8	0.3
286.1	-159.5	-19.1	0.8	0.3
284.6	-161.0	-18.9	0.8	0.3
283.6	-157.9	-18.8	0.8	0.3

281.2	-151.0	-17.7	0.8	0.3
279.5	-153.6	-18.1	0.8	0.3
274.9	-150.7	-17.4	0.8	0.3
274.4	-151.3	-17.5	0.8	0.3
273.5	-156.4	-17.6	0.8	0.3
271.6	-149.7	-16.8	0.8	0.3
270.6	-151.2	-17.7	0.8	0.3
270.4	-148.6	-16.5	0.8	0.3
269.6	-150.3	-17.4	0.8	0.3
268.6	-152.9	-17.1	0.8	0.3
267.6	-152.2	-16.8	0.8	0.3
266.6	-153.4	-17.2	0.8	0.3
264.6	-152.5	-17.1	0.8	0.3
264.1	-153.1	-16.5	0.8	0.3
262.6	-150.4	-17.5	0.8	0.3
260.7	-149.5	-16.7	0.8	0.3
259.4	-149.9	-17.5	0.8	0.3
258.8	-153.3	-17.4	0.8	0.3
258.5	-150.1	-16.5	0.8	0.3
257.9	-147.1	-16.5	0.8	0.3
256.6	-150.2	-17.2	0.8	0.3
255.7	-150.8	-17.5	0.8	0.3
254.6	-154.0	-17.0	0.8	0.3
252.5	-155.5	-17.8	0.8	0.3
250.1	-149.7	-16.2	0.8	0.3
249.6	-155.0	-17.6	0.8	0.3
249.1	-153.9	-17.7	0.8	0.3
248.6	-152.1	-16.5	0.8	0.3
247.2	-151.9	-16.8	0.8	0.3
247.0	-158.0	-17.6	0.8	0.3
246.6	-151.9	-16.8	0.8	0.3
243.5	-156.1	-17.7	0.8	0.3
243.2	-152.7	-17.1	0.8	0.3
242.8	-153.0	-17.5	0.8	0.3
241.6	-156.8	-16.8	0.8	0.3
240.5	-155.6	-18.4	0.8	0.3
239.9	-155.2	-17.9	0.8	0.3
238.6	-152.8	-17.6	0.8	0.3
237.5	-153.9	-18.0	0.8	0.3
236.7	-155.3	-17.5	0.8	0.3
234.6	-157.0	-18.2	0.8	0.3

234.0	-153.3	-18.0	0.8	0.3
232.6	-157.9	-17.8	0.8	0.3
231.1	-154.4	-18.3	0.8	0.3
230.4	-155.4	-18.3	0.8	0.3
229.3	-155.0	-18.3	0.8	0.3
228.4	-155.7	-18.0	0.8	0.3
227.8	-156.8	-17.8	0.8	0.3
225.7	-160.3	-17.9	0.8	0.3
224.9	-159.6	-18.0	0.8	0.3
223.5	-163.4	-17.7	0.8	0.3
222.7	-160.7	-17.9	0.8	0.3
222.1	-162.6	-18.7	0.8	0.3
219.3	-164.0	-19.6	0.8	0.3
218.5	-164.3	-18.9	0.8	0.3
217.6	-163.6	-19.4	0.8	0.3
216.5	-166.0	-19.4	0.8	0.3
215.5	-163.5	-18.9	0.8	0.3
214.6	-165.0	-19.3	0.8	0.3
213.7	-168.4	-19.7	0.8	0.3
214.6	-165.0	-19.3	0.8	0.3
213.7	-168.4	-19.7	0.8	0.3
211.5	-163.2	-18.9	0.8	0.3
209.6	-167.3	-19.5	0.8	0.3
207.6	-162.6	-18.9	0.8	0.3
206.6	-168.7	-18.5	0.8	0.3
205.6	-164.7	-18.5	0.8	0.3
205.2	-166.7	-18.3	0.8	0.3
204.6	-162.1	-19.7	0.8	0.3
203.6	-159.3	-18.7	0.8	0.3
202.6	-164.1	-19.5	0.8	0.3
201.8	-159.7	-18.3	0.8	0.3
199.6	-162.2	-18.3	0.8	0.3
198.6	-159.1	-17.5	0.8	0.3
196.6	-151.0	-16.9	0.8	0.3
195.6	-151.2	-17.0	0.8	0.3
181.6	-145.9	-16.6	0.8	0.3
180.6	-144.5	-16.7	0.8	0.3
179.6	-147.3	-16.9	0.8	0.3
175.6	-142.6	-16.1	0.8	0.3
173.7	-149.1	-16.2	0.8	0.3
169.5	-149.3	-17.0	0.8	0.3

168.6	-146.6	-16.3	0.8	0.3
167.6	-145.8	-15.9	0.8	0.3
166.3	-137.6	-15.5	0.8	0.3
165.5	-146.0	-15.1	0.8	0.3
164.8	-144.0	-15.4	0.8	0.3
135.5	-139.6	-15.8	0.8	0.3
135.0	-141.5	-15.7	0.8	0.3
133.6	-149.5	-15.4	0.8	0.3
132.6	-147.3	-15.3	0.8	0.3
131.8	-143.3	-15.6	0.8	0.3
129.6	-148.7	-16.4	0.8	0.3
128.7	-148.3	-14.6	0.8	0.3
125.0	-144.3	-16.0	0.8	0.3
123.6	-145.8	-15.9	0.8	0.3
122.9	-147.3	-16.4	0.8	0.3
102.6	-142.4	-14.9	0.8	0.3
102.5	-143.0	-14.8	0.8	0.3
101.6	-136.8	-14.8	0.8	0.3
96.6	-148.0	-15.8	0.8	0.3
96.1	-144.2	-14.1	0.8	0.3
94.3	-145.2	-15.7	0.8	0.3
93.1	-145.2	-15.7	0.8	0.3

Table D.5. δ^2H and $\delta^{18}O$ values of core samples collected at OVB-10-207.

OVB-10-207				
Elevation (m asl)	**δ^2H**	**$\delta^{18}O$**	**δ^2H error**	**$\delta^{18}O$ error**
412.6	-130.3	-16.6	0.8	0.3
409.6	-134.5	-17.2	0.8	0.3
407.6	-136.8	-17.3	0.8	0.3
406.6	-135.0	-15.9	0.8	0.3
404.6	-128.5	-15.8	0.8	0.3
403.6	-126.6	-17.5	0.8	0.3
402.6	-128.9	-15.8	0.8	0.3
401.6	-129.2	-15.6	0.8	0.3
400.6	-134.1	-16.5	0.8	0.3
398.6	-127.2	-15.5	0.8	0.3
397.6	-133.6	-16.5	0.8	0.3
395.6	-128.7	-15.5	0.8	0.3
394.6	-131.9	-16.0	0.8	0.3
393.6	-131.2	-15.8	0.8	0.3
391.6	-129.8	-15.9	0.8	0.3
390.6	-126.6	-15.4	0.8	0.3
388.6	-128.8	-15.8	0.8	0.3
387.6	-129.2	-16.2	0.8	0.3
386.6	-132.2	-15.6	0.8	0.3
385.6	-129.7	-14.5	0.8	0.3
382.6	-129.9	-15.9	0.8	0.3
376.6	-133.0	-16.1	0.8	0.3
375.6	-131.6	-17.7	0.8	0.3
374.6	-131.6	-17.7	0.8	0.3
373.6	-133.1	-17.2	0.8	0.3
371.6	-130.0	-16.5	0.8	0.3
356.6	-134.3	-16.0	0.8	0.3
355.6	-140.7	-17.7	0.8	0.3
320.6	-155.4	-19.3	0.8	0.3
319.6	-155.8	-19.1	0.8	0.3
318.6	-154.5	-19.0	0.8	0.3
317.6	-152.9	-19.5	0.8	0.3
316.6	-152.6	-19.1	0.8	0.3
315.6	-153.0	-18.9	0.8	0.3
314.6	-152.2	-18.3	0.8	0.3
313.6	-150.9	-18.8	0.8	0.3
308.6	-146.8	-18.7	0.8	0.3

307.6	-145.3	-18.3	0.8	0.3
305.6	-146.4	-18.5	0.8	0.3
304.1	-151.0	-19.1	0.8	0.3
303.6	-147.2	-18.7	0.8	0.3
302.6	-148.4	-18.2	0.8	0.3
301.6	-149.3	-17.9	0.8	0.3
300.6	-147.8	-18.5	0.8	0.3
299.6	-149.7	-18.1	0.8	0.3
298.6	-146.9	-18.1	0.8	0.3
297.6	-149.0	-19.1	0.8	0.3
296.6	-146.0	-18.1	0.8	0.3
295.6	-148.6	-18.6	0.8	0.3
294.6	-149.1	-18.2	0.8	0.3
292.6	-149.4	-19.0	0.8	0.3
291.6	-147.1	-19.3	0.8	0.3
290.6	-148.0	-17.9	0.8	0.3
289.6	-146.0	-17.7	0.8	0.3
288.6	-146.6	-17.5	0.8	0.3
287.6	-147.4	-17.5	0.8	0.3
286.6	-147.2	-18.1	0.8	0.3
285.6	-144.9	-18.2	0.8	0.3
284.6	-147.9	-18.1	0.8	0.3
283.6	-144.5	-17.7	0.8	0.3
282.6	-146.2	-17.3	0.8	0.3
281.6	-146.4	-18.4	0.8	0.3
277.6	-146.1	-18.5	0.8	0.3
276.6	-146.0	-18.8	0.8	0.3
275.6	-146.8	-18.6	0.8	0.3
274.6	-146.0	-18.2	0.8	0.3
273.6	-147.8	-18.4	0.8	0.3
272.6	-149.3	-19.1	0.8	0.3
271.6	-147.6	-17.9	0.8	0.3
270.6	-147.4	-18.2	0.8	0.3
269.6	-148.6	-18.4	0.8	0.3
268.6	-144.7	-17.3	0.8	0.3
267.6	-147.4	-17.4	0.8	0.3
265.6	-146.4	-17.8	0.8	0.3
264.6	-146.4	-17.2	0.8	0.3
263.6	-146.8	-17.4	0.8	0.3
262.6	-147.7	-17.6	0.8	0.3
261.6	-147.8	-17.1	0.8	0.3

259.6	-146.6	-16.9	0.8	0.3
258.6	-148.3	-17.7	0.8	0.3
257.6	-148.0	-17.7	0.8	0.3
256.3	-146.3	-18.0	0.8	0.3
245.1	-144.3	-16.3	0.8	0.3
244.6	-147.7	-16.8	0.8	0.3

Table D.6. Anion extraction batch test results of samples leached at 305, 290, and 249 m asl at OVB-10-207.

Sample	Dry Sample (g)	Water added (g)	Cl (mg/L)	Dry Bulk Density (g/cm^3)	n_T	n_e	Pore water Cl (mg/L)	Time (h)
138A	10.01	20.00	151.62	1.54	0.35	0.30	4451.84	1
138B	10.02	20.00	159.66	1.54	0.35	0.30	4683.01	1
138C	10.02	20.00	129.43	1.54	0.35	0.30	3796.53	1
138D	10.00	30.01	86.28	1.54	0.35	0.30	3805.01	1
138E	10.02	30.03	95.79	1.54	0.35	0.30	4218.64	1
138M	10.03	20.01	151.00	1.54	0.35	0.30	4427.01	5
138N	10.01	20.03	136.85	1.54	0.35	0.30	4023.99	5
138O	10.01	20.09	138.76	1.54	0.35	0.30	4092.53	5
138P	10.01	30.09	137.92	1.54	0.35	0.30	6092.50	5
138Q	10.00	30.20	124.58	1.54	0.35	0.30	5528.99	5
138R	9.99	30.01	108.25	1.54	0.35	0.30	4778.64	5
138S	10.01	40.01	73.20	1.54	0.35	0.30	4299.43	5
138T	10.00	40.01	64.05	1.54	0.35	0.30	3765.82	5
138TR	10.00	40.01	68.81	1.54	0.35	0.30	4045.71	5
138U	10.01	40.02	68.67	1.54	0.35	0.30	4034.18	5
138V	5.00	24.99	52.46	1.54	0.35	0.30	3852.65	5
138W	5.00	25.01	49.60	1.54	0.35	0.30	3646.09	5
138X	5.03	24.99	56.19	1.54	0.35	0.30	4102.28	5
138Y	10.00	20.02	141.49	1.54	0.35	0.30	4162.61	10
138Z	10.00	19.99	143.18	1.54	0.35	0.30	4206.16	10
138AA	10.02	20.02	144.89	1.54	0.35	0.30	4254.22	10
138AB	10.01	30.03	108.42	1.54	0.35	0.30	4779.56	10
138AC	10.02	30.00	119.58	1.54	0.35	0.30	5261.05	10
138AD	10.01	29.99	104.56	1.54	0.35	0.30	4603.65	10
138ADR	10.01	29.99	119.73	1.54	0.35	0.30	5271.53	10
138AE	10.00	40.00	73.12	1.54	0.35	0.30	4297.79	10
138AF	10.00	39.99	69.06	1.54	0.35	0.30	4058.27	10

138AG	10.03	40.03	69.24	1.54	0.35	0.30	4061.08	10
138AH	10.01	25.00	115.68	1.54	0.35	0.30	4245.48	10
138AI	9.99	25.00	123.47	1.54	0.35	0.30	4540.77	10
138AJ	10.02	24.99	126.24	1.54	0.35	0.30	4626.86	10
138AK	10.05	20.01	162.41	1.54	0.35	0.30	4751.99	100
138AL	10.05	20.05	144.00	1.54	0.35	0.30	4221.83	100
138AM	10.01	20.03	155.21	1.54	0.35	0.30	4563.86	100
138AN	10.00	30.24	106.01	1.54	0.35	0.30	4710.95	100
138ANR	10.00	30.24	112.26	1.54	0.35	0.30	4988.62	100
138AO	10.02	30.01	104.24	1.54	0.35	0.30	4587.64	100
138AP	10.02	30.05	89.37	1.54	0.35	0.30	3938.64	100
138AR	10.05	40.02	95.37	1.54	0.35	0.30	5580.67	100
138AQ	10.03	40.00	76.89	1.54	0.35	0.30	4506.08	100
138AS	10.01	40.03	73.56	1.54	0.35	0.30	4323.09	100
138AT	5.00	25.17	52.94	1.54	0.35	0.30	3916.49	100
138AU	5.00	25.00	56.40	1.54	0.35	0.30	4144.42	100
138AV	5.01	25.10	57.81	1.54	0.35	0.30	4256.37	100
153A	10.01	20.00	250.69	1.54	0.37	0.30	6962.77	1
153B	10.01	20.78	209.45	1.54	0.37	0.30	6044.16	1
153BR	10.01	20.78	211.01	1.54	0.37	0.30	6089.16	1
153C	10.00	19.99	222.58	1.54	0.37	0.30	6184.97	1
153D	10.00	30.00	150.38	1.54	0.37	0.30	6271.07	1
153E	10.00	30.02	139.63	1.54	0.37	0.30	5826.92	1
153F	10.01	30.00	138.87	1.54	0.37	0.30	5785.46	1
153G	10.00	40.00	104.98	1.54	0.37	0.30	5837.10	1
153H	10.01	40.02	107.15	1.54	0.37	0.30	5954.82	1
153I	10.02	40.03	119.17	1.54	0.37	0.30	6617.95	1
153J	5.01	25.00	78.51	1.54	0.37	0.30	5445.91	1
153K	4.99	25.00	101.65	1.54	0.37	0.30	7078.98	1
153L	5.01	24.99	108.72	1.54	0.37	0.30	7538.48	1
153LR	5.01	24.99	89.60	1.54	0.37	0.30	6212.95	1
153M	10.00	20.01	260.37	1.54	0.37	0.30	7242.24	5

153N	10.00	20.02	236.04	1.54	0.37	0.30	6568.94	5
153O	10.00	19.99	239.24	1.54	0.37	0.30	6648.05	5
153P	10.01	30.06	136.36	1.54	0.37	0.30	5692.36	5
153Q	10.01	30.00	138.04	1.54	0.37	0.30	5750.83	5
153R	10.01	29.99	122.69	1.54	0.37	0.30	5109.52	5
153S	10.05	39.99	102.60	1.54	0.37	0.30	5675.15	5
153T	10.04	40.01	99.26	1.54	0.37	0.30	5498.70	5
153U	10.01	40.02	102.30	1.54	0.37	0.30	5685.30	5
153V	5.03	25.00	71.72	1.54	0.37	0.30	4954.88	5
153VR	5.03	25.00	71.65	1.54	0.37	0.30	4950.14	5
153W	5.01	25.83	76.31	1.54	0.37	0.30	5469.17	5
153X	5.02	25.02	81.88	1.54	0.37	0.30	5673.08	5
153Y	10.03	20.00	238.80	1.54	0.37	0.30	6619.29	10
153Z	10.00	19.99	268.97	1.54	0.37	0.30	7474.18	10
153AA	10.05	19.99	230.33	1.54	0.37	0.30	6368.63	10
153AB	10.00	30.01	125.45	1.54	0.37	0.30	5233.23	10
153AC	10.02	30.02	157.41	1.54	0.37	0.30	6555.67	10
153AD	10.03	30.01	118.84	1.54	0.37	0.30	4942.74	10
153AE	10.00	40.01	101.48	1.54	0.37	0.30	5644.10	10
153AF	10.03	40.01	91.01	1.54	0.37	0.30	5046.72	10
153AFR	10.03	40.01	92.72	1.54	0.37	0.30	5141.18	10
153AG	10.01	40.00	103.22	1.54	0.37	0.30	5733.78	10
153AH	5.02	25.01	83.10	1.54	0.37	0.30	5755.17	10
153AI	4.99	25.18	79.13	1.54	0.37	0.30	5550.63	10
153AJ	5.01	25.02	83.81	1.54	0.37	0.30	5817.86	10
153AK	10.00	20.07	237.83	1.54	0.37	0.30	6635.38	100
153AL	10.02	20.01	235.59	1.54	0.37	0.30	6540.05	100
153AM	9.99	20.01	219.51	1.54	0.37	0.30	6111.91	100
153AN	9.99	29.99	145.22	1.54	0.37	0.30	6060.03	100
153AO	9.99	30.05	144.68	1.54	0.37	0.30	6049.64	100
153AP	10.05	30.11	142.96	1.54	0.37	0.30	5953.92	100
153APR	10.05	30.11	142.21	1.54	0.37	0.30	5922.58	100

153AQ	10.04	40.10	99.18	1.54	0.37	0.30	5506.67	100
153AR	10.01	40.00	100.66	1.54	0.37	0.30	5591.48	100
153AS	10.02	40.01	102.41	1.54	0.37	0.30	5684.27	100
153AT	5.02	25.09	84.99	1.54	0.37	0.30	5905.03	100
153AU	5.01	24.99	81.95	1.54	0.37	0.30	5682.09	100
153AV	5.01	25.73	79.79	1.54	0.37	0.30	5696.55	100
194A	9.99	20.00	27.19	1.54	0.34	0.30	823.49	1
194B	10.01	20.74	26.74	1.54	0.34	0.30	838.18	1
194C	10.01	19.99	35.99	1.54	0.34	0.30	1087.39	1
194D	10.00	29.99	17.41	1.54	0.34	0.30	790.01	1
194DR	10.00	29.99	17.51	1.54	0.34	0.30	794.39	1
194E	10.03	30.03	21.15	1.54	0.34	0.30	957.89	1
194F	9.99	30.08	19.02	1.54	0.34	0.30	866.14	1
194G	10.02	40.07	18.91	1.54	0.34	0.30	1143.66	1
194H	10.00	40.03	21.56	1.54	0.34	0.30	1305.36	1
194I	10.01	40.01	22.56	1.54	0.34	0.30	1363.95	1
194J	5.00	24.99	17.36	1.54	0.34	0.30	1312.41	1
194JR	5.00	24.99	17.38	1.54	0.34	0.30	1313.98	1
194K	5.03	25.01	17.66	1.54	0.34	0.30	1328.48	1
194L	5.00	25.00	17.81	1.54	0.34	0.30	1347.41	1
194M	9.99	20.06	35.03	1.54	0.34	0.30	1064.02	5
194N	10.02	20.02	27.40	1.54	0.34	0.30	828.10	5
194NR	10.02	20.02	27.20	1.54	0.34	0.30	822.26	5
194O	10.00	20.05	27.81	1.54	0.34	0.30	843.36	5
194P	10.03	30.02	25.99	1.54	0.34	0.30	1176.73	5
194Q	10.00	20.10	31.82	1.54	0.34	0.30	967.45	5
194R	10.00	30.05	18.93	1.54	0.34	0.30	860.64	5
194S	10.02	40.00	40.59	1.54	0.34	0.30	2451.00	5
194T	10.00	40.00	24.59	1.54	0.34	0.30	1487.81	5
194U	10.01	40.02	15.57	1.54	0.34	0.30	941.66	5
194V	5.01	25.30	22.39	1.54	0.34	0.30	1710.58	5
194W	5.02	25.07	20.89	1.54	0.34	0.30	1577.93	5

194X	4.99	24.99	19.84	1.54	0.34	0.30	1502.84	5
194XR	4.99	24.99	22.83	1.54	0.34	0.30	1729.87	5
194Y	10.01	19.99	0.00	1.54	0.34	0.30	0.00	10
194Z	10.02	20.02	44.45	1.54	0.34	0.30	1343.54	10
194AA	10.02	19.99	41.80	1.54	0.34	0.30	1261.43	10
194AB	10.02	30.01	28.01	1.54	0.34	0.30	1269.21	10
194AC	10.00	30.00	41.23	1.54	0.34	0.30	1871.19	10
194AD	9.99	30.02	25.73	1.54	0.34	0.30	1169.85	10
194AE	3.02	12.37	27.18	1.54	0.34	0.30	1683.87	10
194AF	4.98	20.02	33.95	1.54	0.34	0.30	2064.85	10
194AG	5.01	19.99	39.79	1.54	0.34	0.30	2401.73	10
194AH	5.03	25.00	22.35	1.54	0.34	0.30	1680.64	10
194AHR	5.03	25.00	30.17	1.54	0.34	0.30	2268.19	10
194AI	5.02	25.04	20.74	1.54	0.34	0.30	1565.20	10
194AJ	4.98	25.01	24.66	1.54	0.34	0.30	1873.56	10
194AK	10.00	20.00	55.40	1.54	0.34	0.30	1676.06	100
194AL	10.02	20.00	48.65	1.54	0.34	0.30	1468.94	100
194AM	10.01	20.05	48.17	1.54	0.34	0.30	1459.61	100
194AN	10.00	30.00	42.22	1.54	0.34	0.30	1916.23	100
194AO	10.04	30.01	33.45	1.54	0.34	0.30	1512.34	100
194AP	10.00	30.00	40.13	1.54	0.34	0.30	1821.15	100
194AQ	10.04	40.01	26.98	1.54	0.34	0.30	1626.28	100
194AQR	10.04	40.01	26.74	1.54	0.34	0.30	1612.10	100
194AR	10.04	40.02	24.92	1.54	0.34	0.30	1502.57	100
194AS	10.00	39.99	23.54	1.54	0.34	0.30	1424.29	100
194AT	5.00	25.05	17.37	1.54	0.34	0.30	1316.35	100
194AU	5.02	25.01	17.62	1.54	0.34	0.30	1327.85	100
194AV	5.00	25.02	17.63	1.54	0.34	0.30	1334.25	100

APPENDIX E. X-RAY DIFFRACTION OF LOWER COLORADO SHALE SAMPLES TO DETERMINE CLAY CONTENT AND CLAY MINERALOGY

1.0 EXPLANATION

The samples from OVB-10-207 used for anion extraction analyses tended to swell, whereas samples from 140-10-087 did not exhibit the same behavior. To determine the reason for the swelling of clay samples, the clay content and clay mineralogy of 6 samples from 140-10-087 and 4 samples from OVB-10-207 were analyzed.

2.0 METHODS

Clay size fractionation and clay mineral analysis on the clay size fractions were performed on six oven dried core samples from 140-10-087 (320.6, 311.6, 296.6, 284.6, 281.1, and 260.6 m asl) and four from OVB-10-207 (319.6, 298.6, 280.6, and 258.6 m asl) by the Saskatchewan Research Council (SRC) on a Bruker D4-Endeavor X -ray diffractometer with Cu Kα radiation. The data were collected at room temperature between 2θ of 3 to 40° with a step size of 0.03° and a counting time of 0.5 s/step at an operating power of 40 kV/40 mA.

3.0 RESULTS

The clay size fraction (<2 μm; wt%) and clay mineralogy are presented in Table E.1. Samples from the Lower Colorado and KDF at 140-10-087 contained 9.9 to 60.1 wt% clay minerals. The Lower Colorado was divided into Lower Colorado shale above the kimberlite (326.6 to 312.6 m asl), KDF (312.6 to 280.6 m asl), and Lower Colorado shale below the kimberlite (280.6 to 256.6 m asl). The clay size fraction of the upper and lower shales (above and below the KDF) was 48.1 to 60.7 wt% while for the KDF was considerably less, at 9.9 to 47.3 wt%, due to the presence of kimberlite in this sequence. The Lower Colorado shale at OVB-10-207 contained 22.4 to 66.9 wt% clay size fraction. No kimberlite was observed in this sequence. The clay minerals in the Lower Colorado shale at both boreholes included smectite (30 to 65 wt%), illite (23 to 46 wt%), and lesser amounts of chlorite (0 to 9 wt%) and kaolinite (0-37 wt%; Table E.1). In general, kaolinite was more abundant in the lower part of the Lower Colorado shale. Samples in the KDF at 140-10-087 (312.6-280.6 m asl), which were mainly disturbed shale and lesser kimberlite (samples at 296.6 and 281.1 m asl), resembled the clay mineralogy of

the Lower Colorado shale but had a considerably lower clay fraction wt%. Samples in the KDF that were kimberlitic (samples at 311.6 and 284.6 m asl) contained 100% smectite (Table E.1).

Table E.1. Summary of clay fraction and XRD analysis of samples collected at 140-10-087 and OVB-10-207.

				Mineral Abundance (wt %)			
Borehole	**Elevation (m asl)**	**Geology**	**<2 µm wt%**	**Smectite**	**Illite**	**Chlorite**	**Kaolinite**
140-10-087	320.6	shale	48.1	53	46	1	0
	311.6	KDF	15.2	100	0	0	0
	296.6	KDF	9.9	65	32	0	3
	284.6	KDF	10.8	100	0	0	0
	281.1	KDF	47.3	49	41	9	0
	260.6	shale	60.7	54	23	7	16
OVB-10-207	319.6	shale	21.4	63	25	0	12
	298.6	shale	39.2	64	36	0	0
	280.6	shale	25.4	59	27	1	13
	258.6	shale	66.9	30	32	2	37

APPENDIX F. TRIAXIAL HYDRAULIC CONDUCTIVITY TEST REPORTS

TRIAXIAL HYDRAULIC CONDUCTIVITY TEST REPORT

Test reference: ASTM D 5084

MDH ENGINEERED SOLUTIONS

CLIENT:	U OF S
PROJECT:	-
MDH Job No:	L2290
DATE:	14-Jun-10

SAMPLE: SHORE 1 126m SGOB Shelby specimen

Testing Summary:		Initial Water Content =	22.1 %
Total back pressure =	215 kPa	Initial Dry Density =	1678 kg/m^3
Maximum effective stress =	24 kPa	Initial Deg of saturation =	100 %
Minimum effective stress =	17 kPa	Final Water Content =	38.8 %
Hydraulic gradient =	19	Final Dry Density =	1317 kg/m^3
Initial sample diameter =	59.29 mm	Final deg of saturation =	100 %
Initial sample height =	37.70 mm	**Final Hydraulic Conductivity:**	
Permeant:	de-aired tap-water	k = <3 E-09 cm/s @	51,765 minutes

Comments:

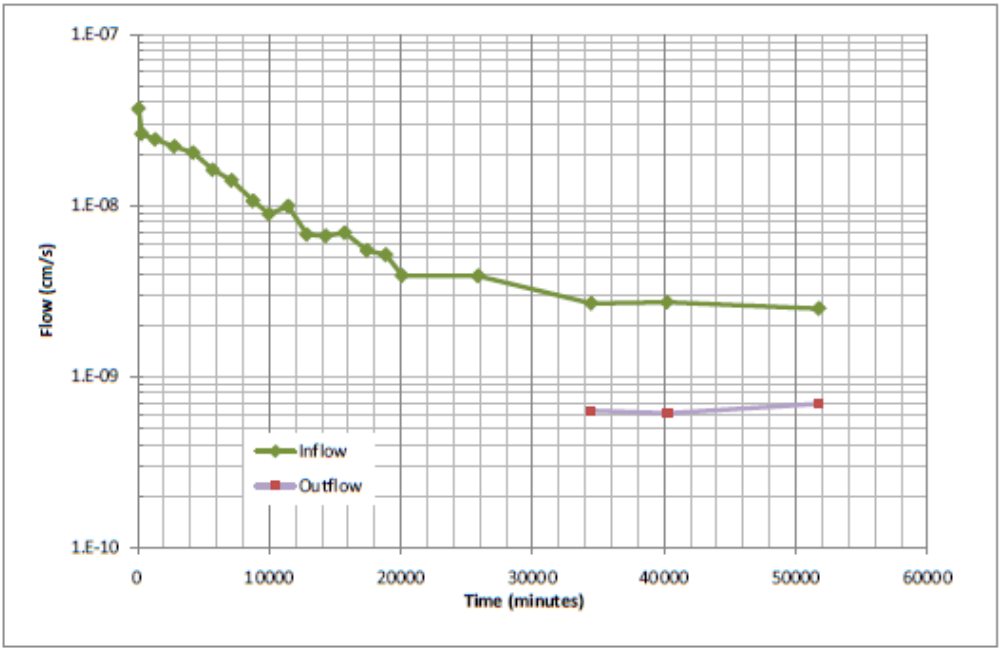

TRIAXIAL HYDRAULIC CONDUCTIVITY TEST REPORT

Test reference: ASTM D 5084

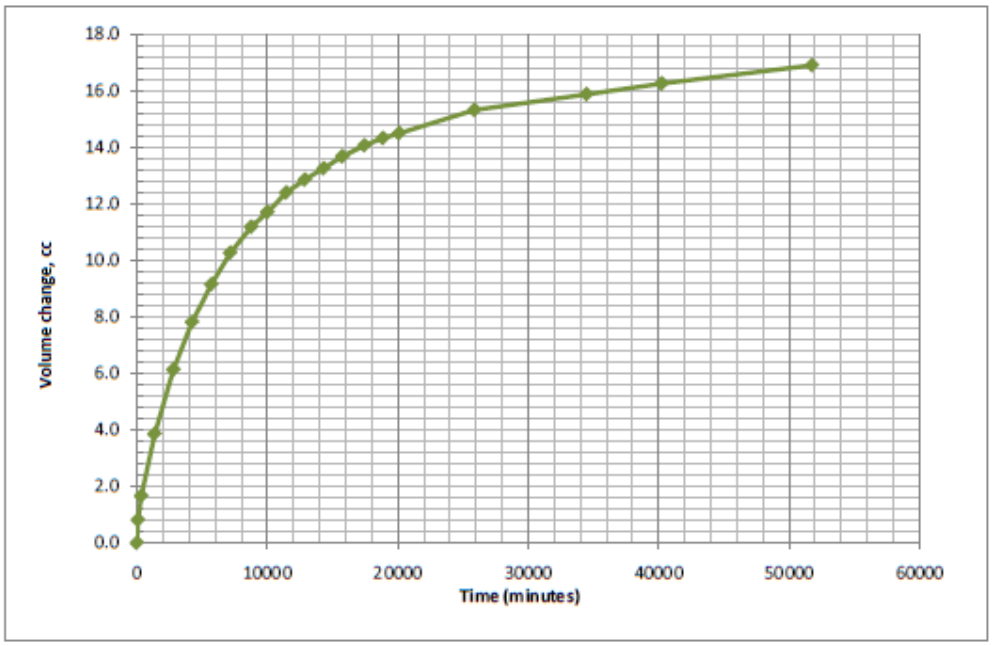

TRIAXIAL HYDRAULIC CONDUCTIVITY TEST REPORT

Test reference: ASTM D 5084

MDH ENGINEERED SOLUTIONS

CLIENT:	U OF S
PROJECT:	-
MDH Job No:	L2290
DATE:	14-Jun-10

SAMPLE: SHORE 1 137m SGOB Shelby specimen

Testing Summary:			
Total back pressure =	215 kPa	Initial Water Content =	20.7 %
Maximum effective stress =	24 kPa	Initial Dry Density =	1465 kg/m^3
Minimum effective stress =	17 kPa	Initial Deg of saturation =	66 %
Hydraulic gradient =	16	Final Water Content =	30.0 %
Initial sample diameter =	63.31 mm	Final Dry Density =	1524 kg/m^3
Initial sample height =	44.64 mm	Final deg of saturation =	100 %
Permeant:	de-aired tap-water	**Final Hydraulic Conductivity:**	
		k = 2.0 E-08 cm/s @ 9,998 minutes	

Comments:

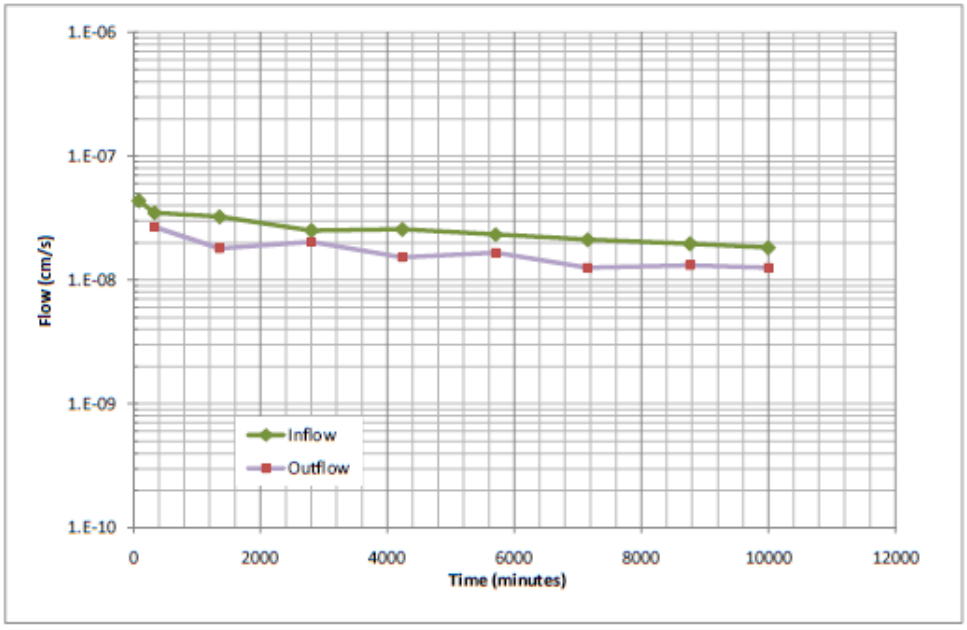

TRIAXIAL HYDRAULIC CONDUCTIVITY TEST REPORT

Test reference: ASTM D 5084

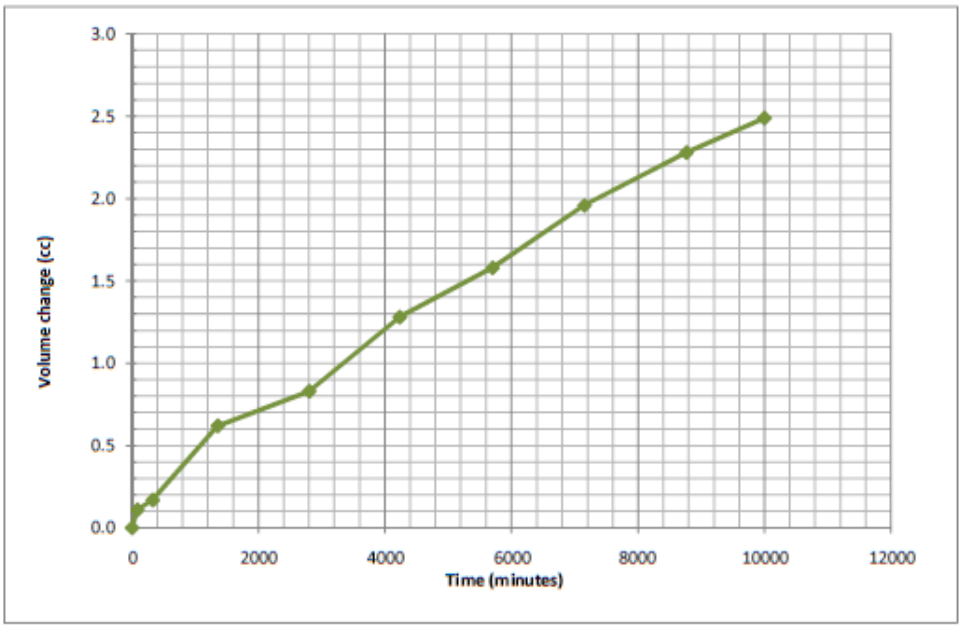

TRIAXIAL HYDRAULIC CONDUCTIVITY TEST REPORT

Test reference: ASTM D 5084

MDH ENGINEERED SOLUTIONS

CLIENT:	U OF S
PROJECT:	-
MDH Job No:	L2290
DATE:	14-Jun-10

SAMPLE: SHORE 1 158m SGOB Shelby specimen

Testing Summary:			Initial Water Content =	22.2 %
Total back pressure =	215 kPa		Initial Dry Density =	1628 kg/m^3
Maximum effective stress =	24 kPa		Initial Deg of saturation =	96 %
Minimum effective stress =	17 kPa		Final Water Content =	53.6 %
Hydraulic gradient =	19		Final Dry Density =	1082 kg/m^3
Initial sample diameter =	56.12	mm	Final deg of saturation =	99 %
Initial sample height =	38.30	mm	**Final Hydraulic Conductivity:**	
Permeant:	de-aired tap-water		k = <4 E-09 cm/s @ 51,761 minutes	

Comments:

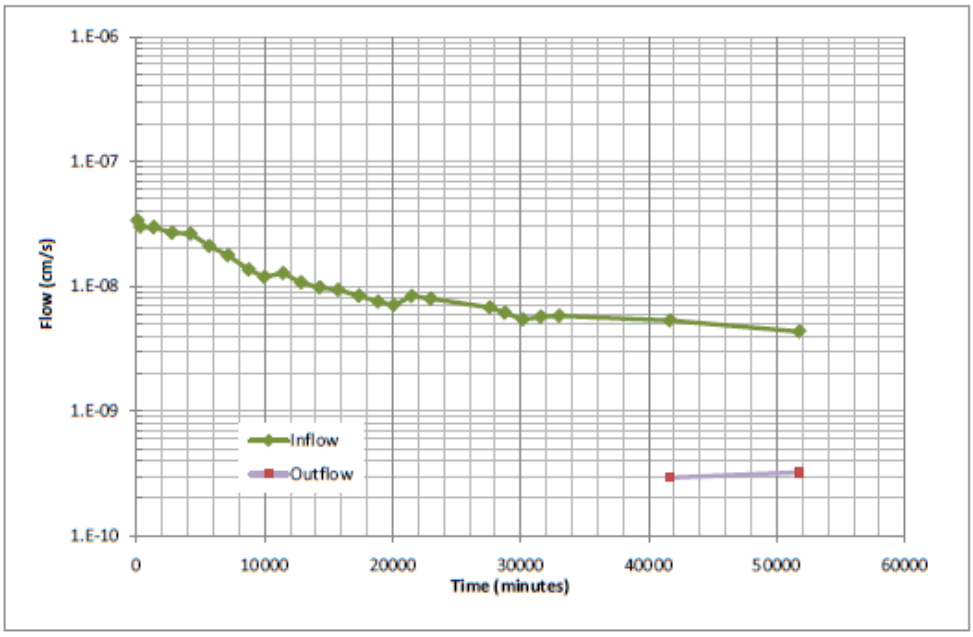

The testing services reported here have been performed in accordance with accepted local industry standards.

The results presented are for the sole use of the designated client only.

This report constitutes a testing service only. It does not represent any interpretation or opinion regarding specification compliance or material suitability.

Engineering interpretation will be provided by MDH Engineered Solutions Corp upon request.

TRIAXIAL HYDRAULIC CONDUCTIVITY TEST REPORT

Test reference: ASTM D 5084

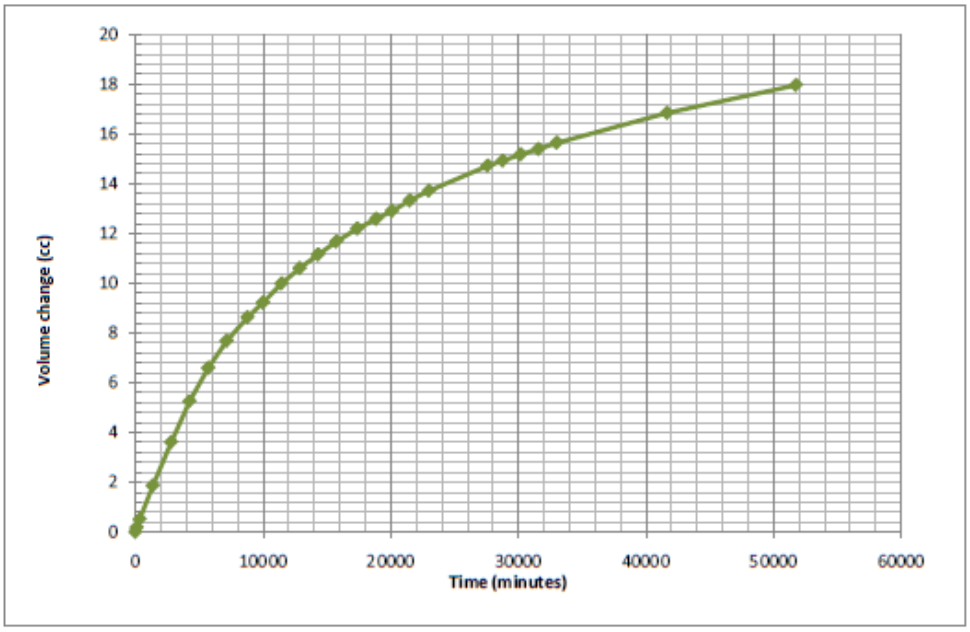

TRIAXIAL HYDRAULIC CONDUCTIVITY TEST REPORT

Test reference: ASTM D 5084

MDH ENGINEERED SOLUTIONS

CLIENT:	University of Saskatchewan
PROJECT:	-
MDH Job No:	L2290
DATE:	22-Jun-10

SAMPLE: SHORE 1 168m SGOB Shelby specimen

Testing Summary:			
Total back pressure =	215 kPa	Initial Water Content =	19.2 %
Maximum effective stress =	24 kPa	Inital Dry Density =	1686 kg/m^3
Minimum effective stress =	17 kPa	Initial Deg of saturation =	86 %
Hydraulic gradient =	18	Final Water Content =	39.0 %
Initial sample diameter =	54.47 mm	Final Dry Density =	1310 kg/m^3
Initial sample height =	40.60 mm	Final deg of saturation =	99 %
Permeant:	de-aired tap-water	**Final Hydraulic Conductivity:**	
		k = 2.0 E-09 cm/s @ 44,163 minutes	

Comments:

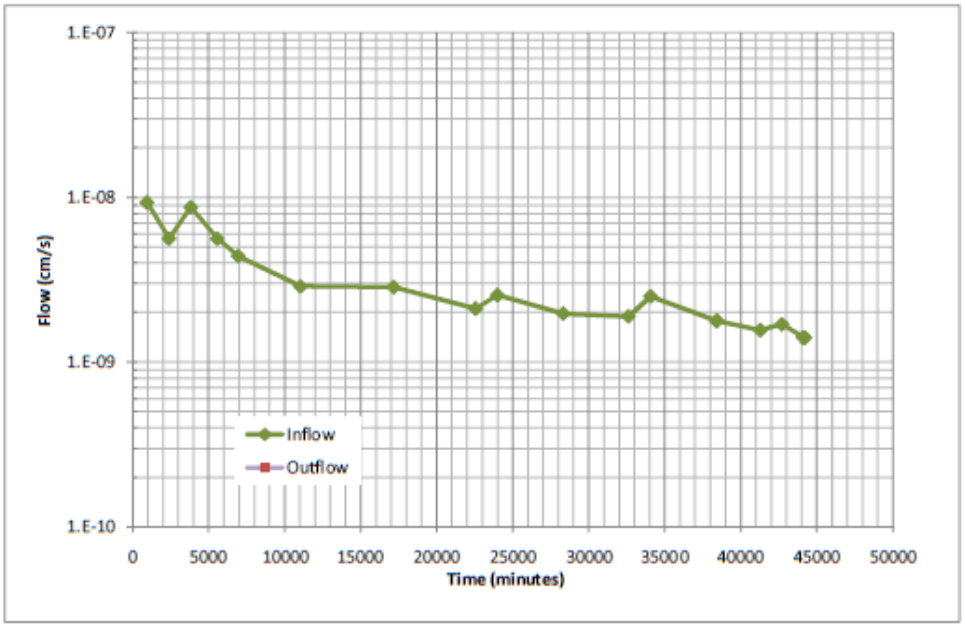

TRIAXIAL HYDRAULIC CONDUCTIVITY TEST REPORT

Test reference: ASTM D 5084

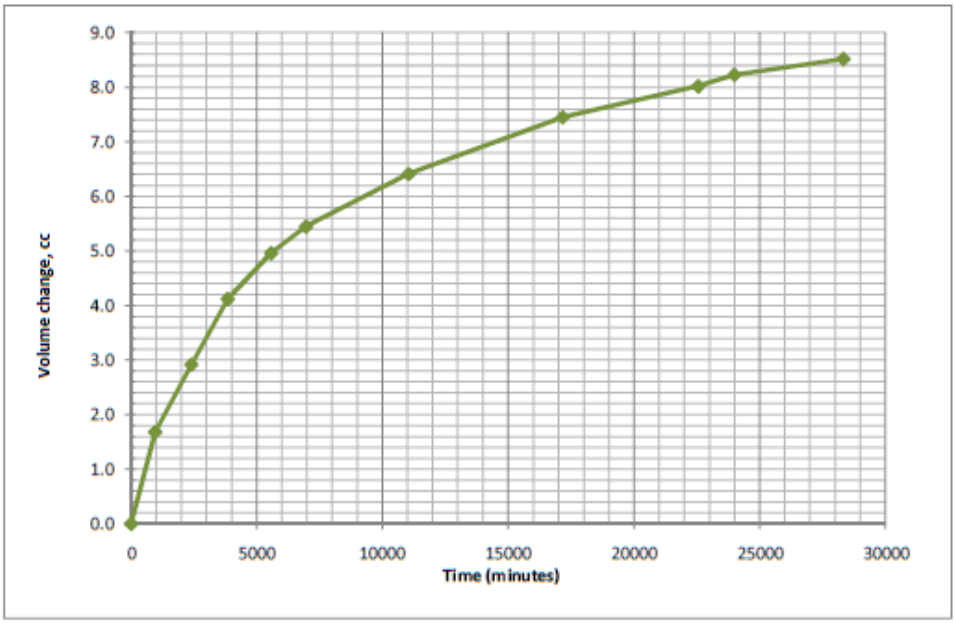

TRIAXIAL HYDRAULIC CONDUCTIVITY TEST REPORT

Test reference: ASTM D 5084

MDH ENGINEERED SOLUTIONS

CLIENT:	University of Saskatchewan
PROJECT:	-
MDH Job No:	L2290
DATE:	22-Jun-10

SAMPLE: SHORE 1 179.5m SGOB Shelby specimen

Testing Summary:			**Initial Water Content =**	18.1 %
Total back pressure =	215 kPa		Initial Dry Density =	1781 kg/m^3
Maximum effective stress =	24 kPa		Initial Deg of saturation =	85 %
Minimum effective stress =	17 kPa		Final Water Content =	52.3 %
Hydraulic gradient =	20		Final Dry Density =	1142 kg/m^3
Initial sample diameter =	55.08	mm	Final deg of saturation =	99 %
Initial sample height =	35.41	mm	**Final Hydraulic Conductivity:**	
Permeant:	de-aired tap-water		k = 4.0 E-09 cm/s @ 31,200 minutes	

Comments:

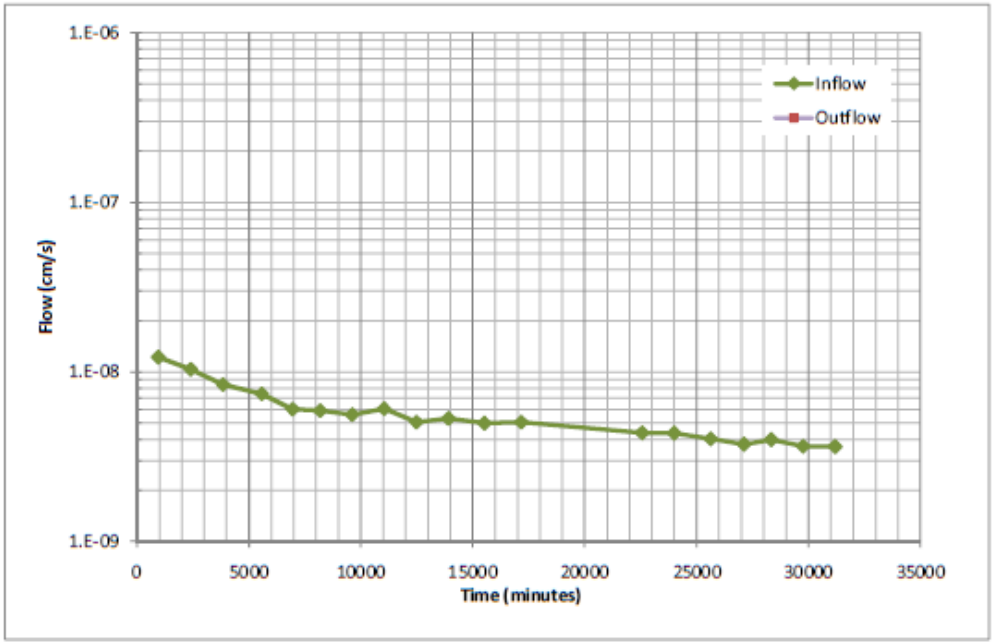

TRIAXIAL HYDRAULIC CONDUCTIVITY TEST REPORT

Test reference: ASTM D 5084

MDH ENGINEERED SOLUTIONS

CLIENT:	University of Saskatchewan
PROJECT:	-
MDH Job No:	L2290
DATE:	23-Aug-10

SAMPLE: Shore 2 @ 125m Shelby specimen

Testing Summary:

Total back pressure =	215 kPa	Initial Water Content =	18.5 %
Maximum effective stress =	24 kPa	Initial Dry Density =	1790 kg/m^3
Minimum effective stress =	17 kPa	Initial Deg of saturation =	100 %
Hydraulic gradient =	17	Final Water Content =	24.1 %
Initial sample diameter =	56.29 mm	Final Dry Density =	1601 kg/m^3
Initial sample height =	43.08 mm	Final deg of saturation =	100 %
Permeant:	de-aired tap-water	**Final Hydraulic Conductivity:**	
		k = 2.0 E-09 cm/s @ 76,297 minutes	

Comments:

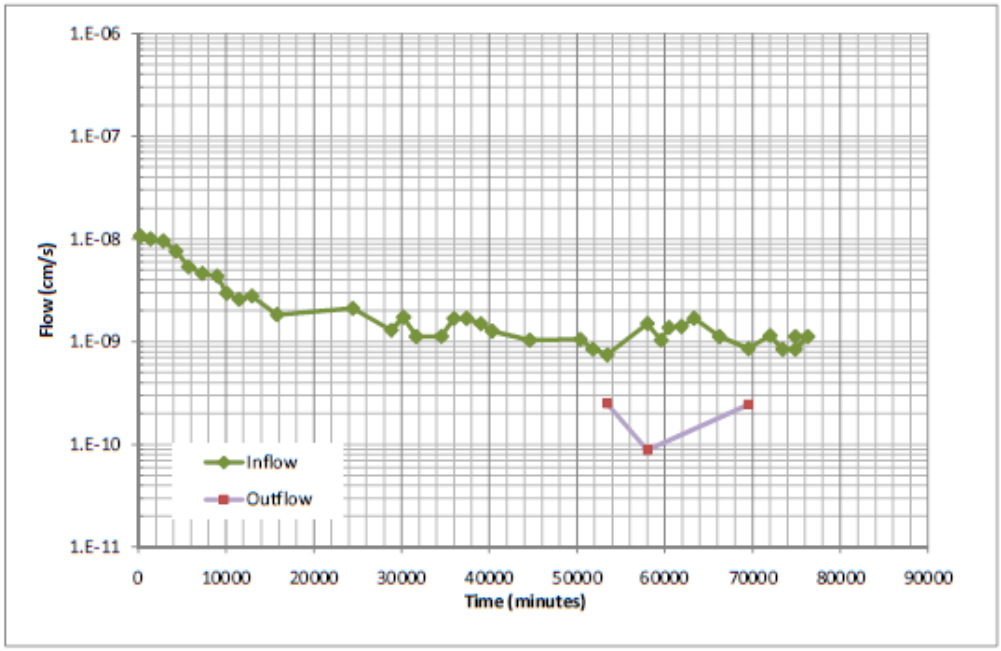

TRIAXIAL HYDRAULIC CONDUCTIVITY TEST REPORT

Test reference: ASTM D 5084

MDH ENGINEERED SOLUTIONS

CLIENT:	University of Saskatchewan
PROJECT:	-
MDH Job No:	L2290
DATE:	21-Jul-10

SAMPLE: SHORE 2 147.5m Shelby specimen

Testing Summary:			**Initial Water Content =**	15.1 %
Total back pressure =	215 kPa		Initial Dry Density =	1812 kg/m^3
Maximum effective stress =	24 kPa		Initial Deg of saturation =	80 %
Minimum effective stress =	17 kPa		Final Water Content =	27.7 %
Hydraulic gradient =	24		Final Dry Density =	1540 kg/m^3
Initial sample diameter =	56.60	mm	Final deg of saturation =	97 %
Initial sample height =	29.93	mm	**Final Hydraulic Conductivity:**	
Permeant:	de-aired tap-water		k = 2.0 E-09 cm/s @ 23,009 minutes	

Comments:

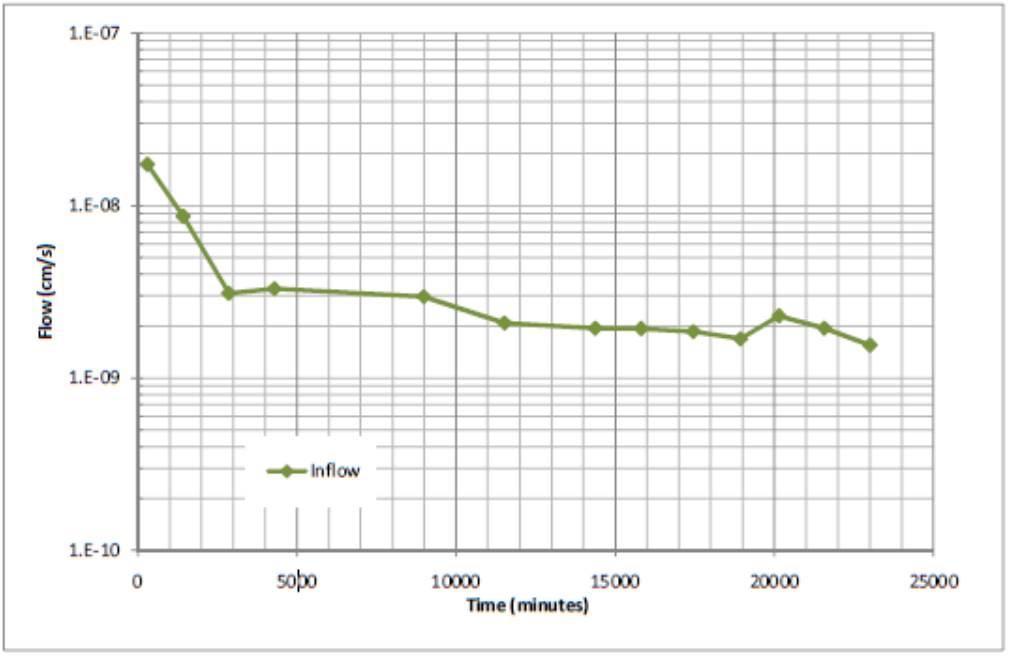

The testing services reported here have been performed in accordance with accepted local industry standards.

The results presented are for the sole use of the designated client only.

This report constitutes a testing service only. It does not represent any interpretation or opinion regarding specification compliance or material suitability.

Engineering interpretation will be provided by MDH Engineered Solutions Corp upon request.

TRIAXIAL HYDRAULIC CONDUCTIVITY TEST REPORT

Test reference: ASTM D 5084

MDH ENGINEERED SOLUTIONS

CLIENT:	University of Saskatchewan
PROJECT:	-
MDH Job No:	L2290
DATE:	21-Jul-10

SAMPLE: SHORE 2 165.6m Shelby specimen

Testing Summary:			Initial Water Content =	15.8 %
Total back pressure =	215 kPa		Initial Dry Density =	1782 kg/m^3
Maximum effective stress =	24 kPa		Initial Deg of saturation =	82 %
Minimum effective stress =	17 kPa		Final Water Content =	28.9 %
Hydraulic gradient =	22		Final Dry Density =	1533 kg/m^3
Initial sample diameter =	55.12	mm	Final deg of saturation =	100 %
Initial sample height =	32.50	mm	**Final Hydraulic Conductivity:**	
Permeant:	de-aired tap-water		k = 2.0 E-08 cm/s @ 4,299	minutes

Comments:

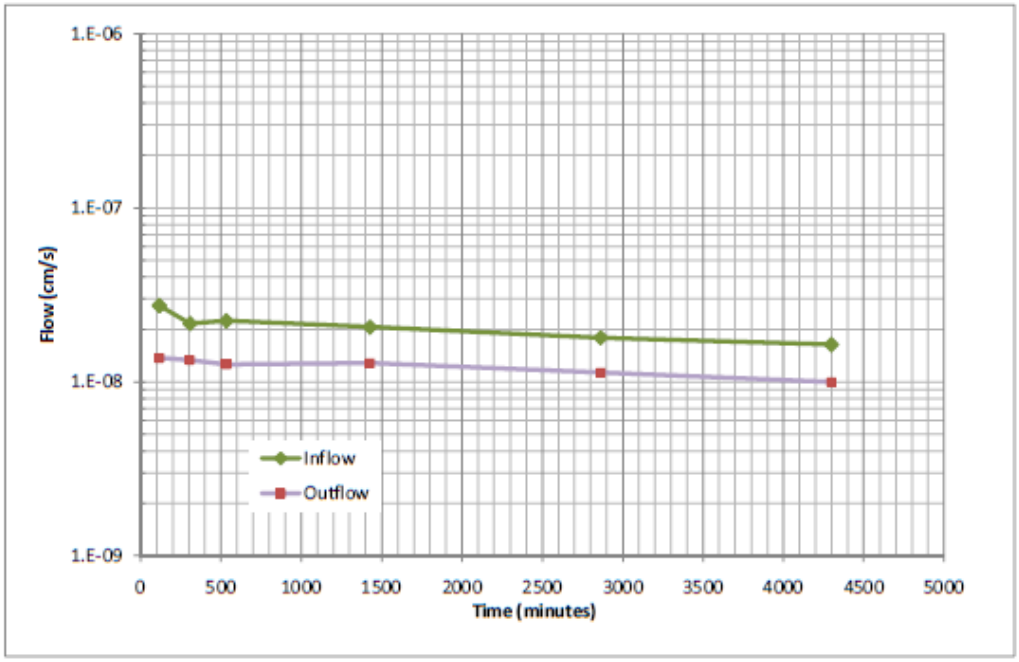

The testing services reported here have been performed in accordance with accepted local industry standards.

The results presented are for the sole use of the designated client only.

This report constitutes a testing service only. It does not represent any interpretation or opinion regarding specification compliance or material suitability.

Engineering interpretation will be provided by MDH Engineered Solutions Corp upon request.

TRIAXIAL HYDRAULIC CONDUCTIVITY TEST REPORT

Test reference: ASTM D 5084

MDH ENGINEERED SOLUTIONS

CLIENT:	University of Saskatchewan
PROJECT:	-
MDH Job No:	L2290
DATE:	16-Aug-10

SAMPLE: Shore 2 - 178.8m Shelby specimen

Testing Summary:		Initial Water Content =	13.1 %
Total back pressure =	215 kPa	Initial Dry Density =	1927 kg/m^3
Maximum effective stress =	24 kPa	Initial Deg of saturation =	98 %
Minimum effective stress =	17 kPa	Final Water Content =	27.4 %
Hydraulic gradient =	15	Final Dry Density =	1578 kg/m^3
Initial sample diameter =	57.74 mm	Final deg of saturation =	100 %
Initial sample height =	46.84 mm	**Final Hydraulic Conductivity:**	
Permeant:	de-aired tap-water	k = 1.0 E-08 cm/s @	5,741 minutes

Comments:

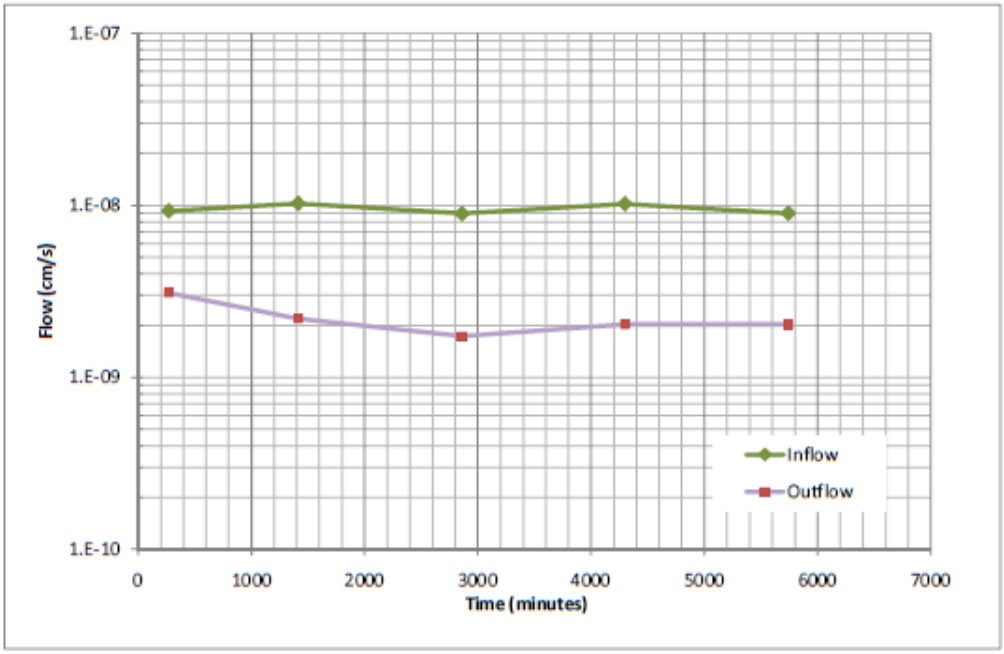

The testing services reported here have been performed in accordance with accepted local industry standards.

The results presented are for the sole use of the designated client only.

This report constitutes a testing service only. It does not represent any interpretation or opinion regarding specification compliance or material suitability.

Engineering interpretation will be provided by MDH Engineered Solutions Corp upon request.

TRIAXIAL HYDRAULIC CONDUCTIVITY TEST REPORT

Test reference: ASTM D 5084

MDH ENGINEERED SOLUTIONS

CLIENT:	University of Saskatchewan
PROJECT:	-
MDH Job No:	L2290
DATE:	10-Aug-10

SAMPLE: Shore 2 @ 186.35m Shelby specimen

Testing Summary:			Initial Water Content =	12.6 %
Total back pressure =	215 kPa		Initial Dry Density =	1969 kg/m^3
Maximum effective stress =	24 kPa		Initial Deg of saturation =	100 %
Minimum effective stress =	17 kPa		Final Water Content =	23.3 %
Hydraulic gradient =	15		Final Dry Density =	1671 kg/m^3
Initial sample diameter =	58.41	mm	Final deg of saturation =	100 %
Initial sample height =	46.55	mm	**Final Hydraulic Conductivity:**	
Permeant:	de-aired tap-water		k = 4.0 E-09 cm/s @ 31,688 minutes	

Comments:

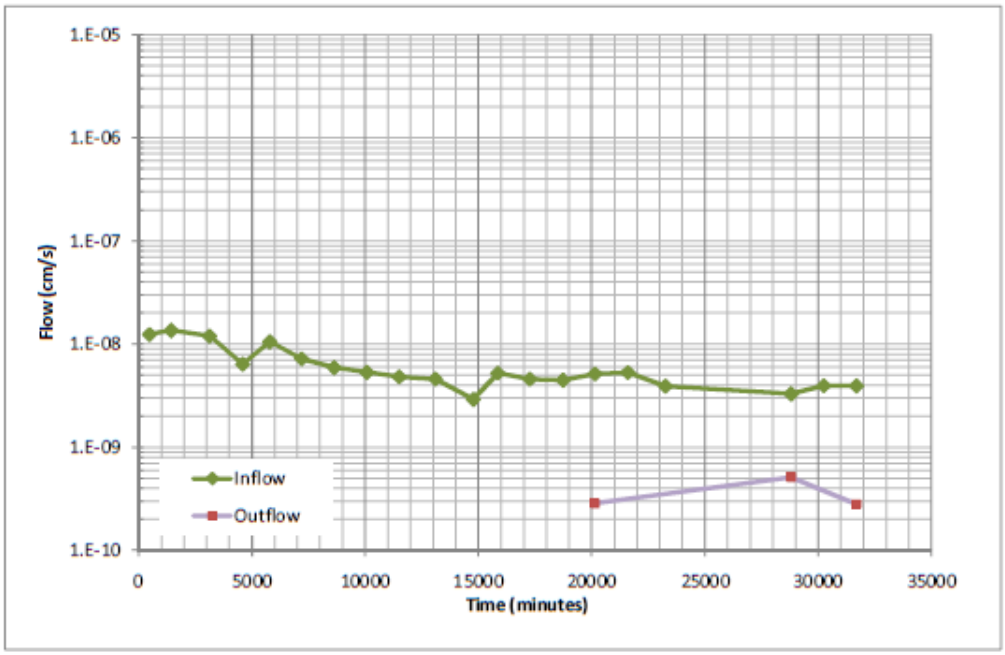

The testing services reported here have been performed in accordance with accepted local industry standards.

The results presented are for the sole use of the designated client only.

This report constitutes a testing service only. It does not represent any interpretation or opinion regarding specification compliance or material suitability.

Engineering interpretation will be provided by MDH Engineered Solutions Corp upon request.

TRIAXIAL HYDRAULIC CONDUCTIVITY TEST REPORT

Test reference: ASTM D 5084

MDH ENGINEERED SOLUTIONS

CLIENT:	University of Saskatchewan
PROJECT:	-
MDH Job No:	L2290
DATE:	16-Aug-10

SAMPLE: Shore 2 - 196m Shelby specimen

Testing Summary:			Initial Water Content =	11.4 %
Total back pressure =	215 kPa		Initial Dry Density =	2111 kg/m^3
Maximum effective stress =	24 kPa		Initial Deg of saturation =	100 %
Minimum effective stress =	17 kPa		Final Water Content =	17.1 %
Hydraulic gradient =	18		Final Dry Density =	1838 kg/m^3
Initial sample diameter =	54.07 mm		Final deg of saturation =	100 %
Initial sample height =	40.65 mm		**Final Hydraulic Conductivity:**	
Permeant:	de-aired tap-water		k = 5.0 E-09 cm/s @ 20,166 minutes	

Comments:

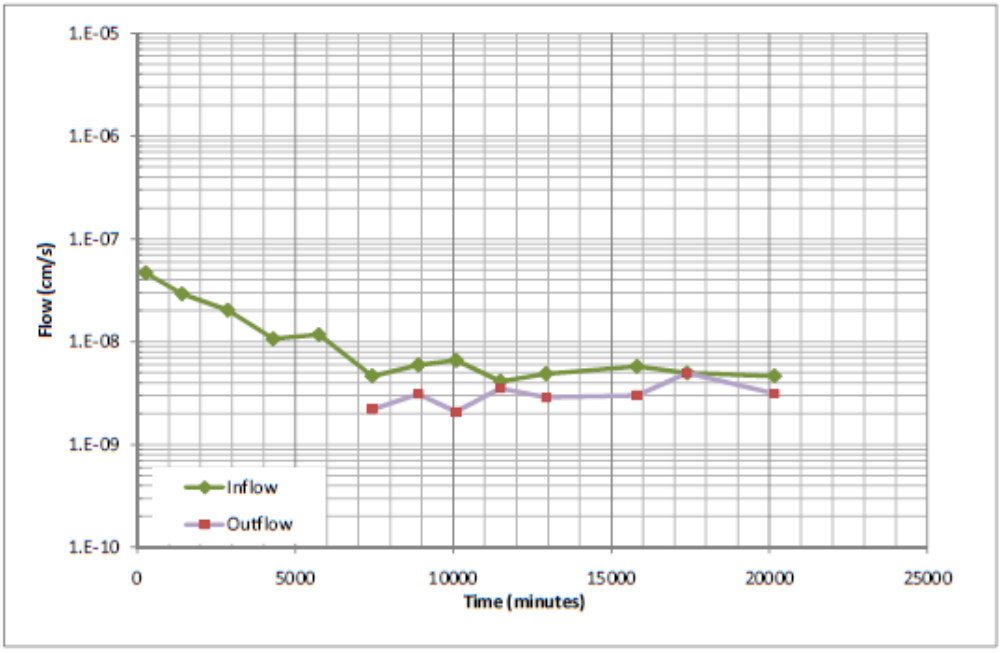

The testing services reported here have been performed in accordance with accepted local industry standards.

The results presented are for the sole use of the designated client only.

This report constitutes a testing service only. It does not represent any interpretation or opinion regarding specification compliance or material suitability.

Engineering interpretation will be provided by MDH Engineered Solutions Corp upon request.